Procédé hybride plasma-catalytique pour la méthanation du CO2

Bo Wang

PSL UNIVERSITÉ PARIS

THÈSE DE DOCTORAT
DE L'UNIVERSITÉ PSL

Préparée à Chimie ParisTech

Procédé hybride plasma-catalytique pour la méthanation du CO_2

Hybrid plasma-catalytic process for CO_2 methanation

Soutenue par

Bo WANG

Le 13 October 2020

Ecole doctorale n°391

Sciences mécanique, acoustique, électronique et robotique

Spécialité

Energétique, génie des procédés

Composition du jury:

M. Xavier DUTEN Professeur, Université Paris 13	*Président*
Mme. Catherine BATIOT DUPEYRAT Professeur, Université de Poitiers	*Rapporteur*
M. Vandad-Julien ROHANI Maître de conférences Mines ParisTech	*Rapporteur*
M. Jérôme PULPYTEL Maître de conférences Sorbonne Université	*Examinateur*
M. Patrick DA COSTA Professeur, Sorbonne Université	*Co-directeur de thèse*
Mme. Stéphanie OGNIER Maître de conférences Sorbonne Université et ChimieParisTech	*Directeur de thèse*

Chimie Paris ParisTech | PSL

Acknowledgments

This work was performed in the group “Procédés - Plasmas - Microsystèmes” (2PM) in Institut Pierre-Gilles de Gennes (IPGG) in Paris, France.

Firstly, I would like to express sincere gratitude to my supervisor: Dr. Stéphanie Ognier, for her guidance, tolerance, and insight scientific support of this project in the last three years. During the study, she has helped solving plenty of problems, this work cannot finish without her help. Her superior knowledge helps extend my vision in the scientific field. Her serious scientific attitude, and rigorous approach will inspire me in my future work. And I am also grateful for her help in the writing of the manuscript.

Also, I am deeply thankful to my co-supervisors Prof. Patrick Da Costa and Prof. Michael Tatoulian. They have given me the incentive and support to perform this research. Herein, I would like to express my sincere respect and sincere thanks to them.

Moreover, I would like also thank Prof. Simeon Cavadias and Dr. Elena Galvez. Although they are not my supervisors, they also provided a lot of ideas for my research, and offered plenty of help to my subject.

I want to thank Dr. Mengxue Zhang, who gave me special help when I just came in the lab, and help me adapt to the life of the laboratory quickly. I am also grateful for her help for my project.

Thanks also to the other permanent staff of the 2PM laboratory. Dr. Safwan Al Ayoubi, Dr. Cédric Rousseau, Dr. Frédéric Rousseau. Mr. Bruno Pelat. They have provided plenty of help during last three years so that I could enjoy my research in the lab.

I want to express my special thanks to Maria Mikhail, who is in her 2nd year of PHD. We have worked together since her master Internship. During last three years, she has helped me a lot, and offered me useful ideas to my subject.

I am grateful to work with PhD students Aurélien Lepoetre, Julien Wengler and Pierre Alexandre Royoux during my research and life. Among them, Aurélien and Julien have graduated last year, and Pierre will graduate this year. They not only gave me a lot of help in the lab, but also gave me advice for my life at Paris. I really enjoyed the game played with them.

I am very grateful to the other students in the research group that gives me a lot of help both in research and life: Gabriel Morand, Marion Gaudeau, Sandra Segondy, Elias Abedelnour, Lison Pourchet and Xinyue Hao.

I also want to express my special thanks to the students at the lab of Sorbonne University: Hongrui Liu, Hailong Zhang, Ye Wang, Chao Sun, Yutao LI, and Armando Izquierdo. I need to thank all of you for helping me so that I can complete my doctoral research.

I want to thank my friends for their constant companionship at Paris: Bin Ni, Xuan Chen, Chuanyu Zhang, Tao Zhu and Liang Zhao. We knew each other before we came to France, and they gave me a lot of help for my study and life. And I thank them for spending time in listening to me and helping me work out my problems during the difficult period of the thesis.

I want to thank the friends that helped me enjoy wonderful journey in Paris: Kun Shi, Chen Li, Ruoxin Hao, Xiaochao Zhou, Jianhua Liu, Huan Xu, Yuanyuan Zhang, Kailiang Ma, Chuang Yu…

I also want to thank all the other friends I met in Paris. It is my pleasure to know you, and I really enjoy the time with you.

I sincerely thank China and the China Scholarship Council for my scholarship to support my research at ChimieParistech/ PSL Uinversity, Paris, France.

Last my thanks would go to my beloved family for their loving considerations and great confidence in me all through these years. Thanks to my father: Linsheng Wang and mother: Baoqin Wu for giving me the best love. Thanks to my sisters: Jinli Wang and Jia Wang, who support me in all aspects. I cannot finish the PhD without their support.

Contents

Résumé de la thèse

Procédé hybride plasma-catalytique pour la méthanation du CO_2

Résumé

Ce travail se focalise sur l'étude de la mise en oeuvre de la reaction de Sabatier dans un procédé catalytique plasma à décharge à barrière diélectrique (DBD) en présence d'un catalyseur hétérogène Ni/ $Ce_{0.58}Zr_{0.42}O_2$. Il a été montré que dans un réacteur hybride plasma DBD de géométrie cylindrique, la température pour atteindre un rendement de 80 % en CO_2 est d'environ 220 °C, soit environ 130 °C de moins que celle en condition thermique. La température seuil de la réaction de Sabatier pendant le traitement au plasma a été déterminée aux environs de 116 °C sur la base des données expérimentales et de l'analyse de simulation par le logiciel COMSOL Multiphysics®. Ensuite, les rôles respectifs de la température et de la puissance plasma dans le processus catalytique plasma ont été étudiés. Il a été ainsi montré que plus la température est élevée, plus la puissance plasma necessaire est faible. L'influence de paramètres tels que la taille des particules, la vitesse spatiale horaire du gaz (GHSV) et la pression a été également étudiée dans les processus thermique et plasma. Un catalyseur avec une plus grande taille de particules s'est avéré avoir une conversion de CO_2 plus élevée dans les deux processus, peut être en raison d'une plus petite taille de particules métalliques Ni. Il a été ensuite montré que l'influence du GHSV sur la conversion du CO_2 est similaire dans les deux processus. Concernant l'effet de la pression enfin, l'augmentation de la pression à l'intérieur du réacteur entraine une légère augmentation de la conversion du CO_2 pour les deux processus étudiés et, dans le cas du processus plasma, une diminution significative de la puissance plasma consommée. Enfin, une étude prospective de la méthanation du CO_2 a été réalisée dans un milli-réacteur constitué de canaux rectangulaires. Cette étude a montré qu'en mode non isotherme un rendement de CO_2 de 72% est obtenu à une tension de 18 kV et une température de 242 °C.

1. Introduction

Les émissions anthropiques de CO_2 provenant d'un système énergétique basé sur les

combustibles fossiles sont la principale cause du changement climatique. Il est donc nécessaire de réduire ces émissions dans l'atmosphère afin d'avoir un cycle du carbone fermé. Pour cette raison, les procédés de captage et d'utilisation du carbone (CCU) ont fait l'objet d'une grande attention au cours de la dernière décennie. Plusieurs procédés pourraient contribuer à la valorisation chimique du CO_2 en produisant des produits chimiques ou des carburants synthétiques. Parmi ceux-ci, la méthanisation du CO_2, connue sous le nom de réaction de Sabatier, est un moyen prometteur de valoriser le dioxyde de carbone afin de créer une énergie renouvelable sous forme de gaz synthétique (méthane). Le méthane pourrait être en effet facilement stocké et transporté dans les infrastructures existantes, et être également utilisé pour produire des produits en aval, tels que l'éthyne, l'hydrogène et l'ammoniac.

La méthanisation ($CO_2(g)+4H_2(g)=CH_4(g)+2H_2O(g)$) est très exothermique et souffre de faibles taux cinétiques. Par conséquent, l'utilisation d'un catalyseur à haute activité et stabilité est nécessaire pour obtenir une vitesse de reaction élevée. Diverses études ont été réalisées dans la littérature pour identifier des catalyseurs performants. Le catalyseur à base de nickel a été largement étudié en raison de son bon compromis entre une activité élevée et un prix bas. Cependant, il est nécessaire dans le processus thermique de travailler à pression et température élevées, ceci afin de limiter la désactivation du catalyseur. La consequence est un coût d'opération élevé qui freine le dévelopement du procédé thermo-catalytique de conversion du CO_2 en methane.

Le procédé catalytique assisté par plasma non thermique pourrait constituer une alternative prometteuse à la voie thermo-catalytique classique pour la conversion du CO_2 en CH_4 en permettant de réaliser la reaction à basse température et à pression atmosphérique. Dans le plasma non thermique, des électrons hautement énergétiques entrent en collision avec des molécules de gaz, et produisent des espèces réactives (radicaux libres, espèces excitées, ions) capables d'initier des reactions chimiques à température ambiante. Ainsi, le procédé plasma-catalytique, qui est la combinaison du plasma non thermique et de la catalyse, est considéré comme une approche prometteuse pour convertir le CO_2 en produits chimiques à haute valeur ajoutée à basse température. Dans de précédentes études, les plasmas à décharge à barrière

diélectrique (DBD) ont été couplés avec succès à différents catalyseurs à base de Ni-zéolite, de Ni-ceria/zircone ou encore d'hydrotalcite de Ni. Plus récemment, la méthanisation du CO_2 par plasma catalytique a été testée en présence d'un catalyseur au Ni supporté par le CeZrOx et il a été montré que des rendements élevés de méthane peuvent être obtenus à pression atmosphérique et température modérée (350 °C) et qu'ils restent stables même après un temps de fonctionnement de plus de 100 heures.

Dans ce travail, la méthanisation du CO_2 en présence d'un catalyseur hétérogène Ni/ $Ce_{0.58}Zr_{0.42}O_2$ a tout d'abord été réalisée en présence d'une activation thermique puis en présence d'une activation plasma. La température seuil de la méthanisation du CO_2 dans le procédé plasma-catalytique a été étudiée en couplant expériences et simulations sur l'outil COMSOL Multiphysics®. Les rôles respectifs de la température et de la puissance du plasma dans le processus plasma-catalytique ont été également étudiés dans deux systèmes thermostatés spécialement conçus. Ensuite, l'influence de paramètres physiques tels que la taille des particules du catalyseur, la pression et la vitesse spatiale horaire du gaz (GHSV), a été étudiée dans les deux procédés thermique et plasma. Enfin, une étude prospective de la méthanisation du CO_2 dans le milli-réacteur à plasma a été réalisée.

2. Étude de l'influence de la température sur la méthanisation du CO_2 dans un procédé plasma-catalytique

2.1 Méthanisation du CO_2 par activation thermique

La Figure 1 présente la conversion du CO_2 obtenue lors de l'essai de méthanisation thermique en l'absence de décharge de plasma dans une plage de température comprise entre 200 °C et 500 °C. Selon l'équilibre thermodynamique, qui a été calculé par HSC chemistry 5, la conversion du CO_2 diminue de 98% à 68% lorsque la température augmente de 200 °C à 500 °C. Comme le montre la Figure 1, lors de l'expérience de méthanisation thermique en l'absence de décharge de plasma, la conversion du CO_2 a augmenté avec l'augmentation de la température jusqu'à 350 °C, avant de diminuer. On peut noter qu'à haute température, la valeur de conversion du CO_2 correspond à la valeur théorique, alors qu'à basse température, la conversion est

inférieure à la valeur théorique attendue, probablement en raison des limitations cinétiques. Une conversion négligeable du CO_2 peut être observée en dessous de 250 °C dans l'expérience thermique de méthanisation du CO_2, et seulement 18% de la conversion du CO_2 a été obtenue à 250 °C. La conversion maximale du CO_2 de 81% a été obtenue à 350 °C. En ce qui concerne la sélectivité du CH_4, elle a régulièrement diminué de 92% à 83% lorsque la température augmentait de 250 °C à 500 °C. Par conséquent, une température de 350 °C est nécessaire pour obtenir de bonnes performances en termes d'activité catalytique dans le processus de méthanisation thermo-catalytique, comme mentionné dans une étude précédente.

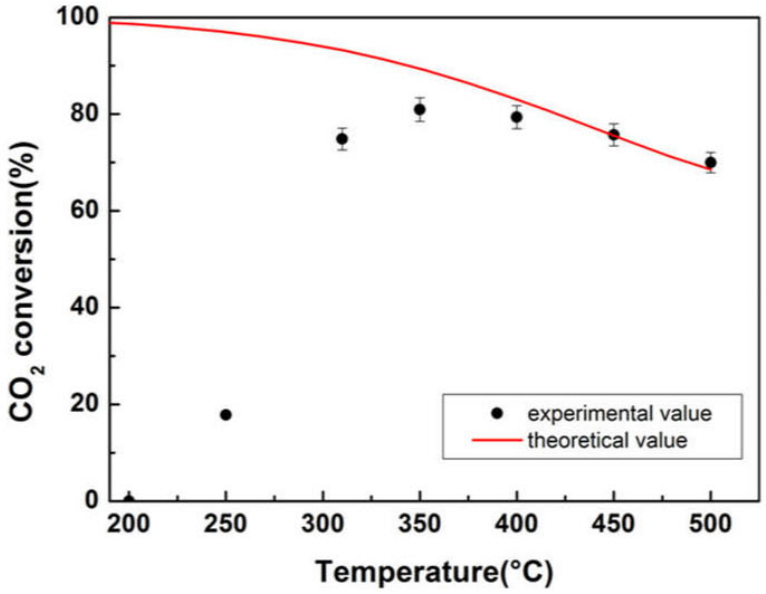

Figure 1. Conversion du CO_2 en fonction de la température dans un système thermique classique en l'absence de plasma, vitesse spatiale horaire du gaz (GHSV =46300 h^{-1})

2.2 Méthanisation du CO_2 dans un procédé plasma-catalytique avec le réacteur DBD cylindrique non isotherme

2.2.1 Processus typique de méthanisation du CO_2 dans un réacteur à plasma DBD

La Figure 2a montre l'évolution de la puissance du plasma avec l'augmentation de la tension crête à crête de 15 kV à 19 kV. Jusqu'à 18 kV, la puissance du plasma DBD généré dans le réacteur augmente linéairement de 4,8 W à 9,2 W. Dans cette plage, aucune production de CH_4 n'est observée. Le CH_4 n'est pas produit avant l'application d'une tension crête à crête de 19 kV. À cette tension, la puissance du plasma augmente fortement pour atteindre 15,1 W et la conversion du CO_2 et la sélectivité du CH_4 sont respectivement de 76% et 100%.

Comme le montre la Figure 2b, à 4,8 W (correspondant à 15 kV), la température en surface du réacteur est de 66 °C. Avec l'augmentation de la puissance, la température augmente également, et on peut observer qu'il existe une relation linéaire entre la puissance et la température du réacteur tant que la méthanisation du CO_2 ne se produit pas (15 kV à 18 kV correspondant à 4,8 W à 9 W) (cf. Figure 3-2b). Dès que la réaction de méthanisation a lieu, entraînant la conversion de 76% du CO_2, la relation linéaire entre la puissance et la température n'est plus respectée, et la température augmente fortement jusqu'à 220 °C. Cela peut s'expliquer par la forte exothermie (4 W) de la réaction de Sabatier.

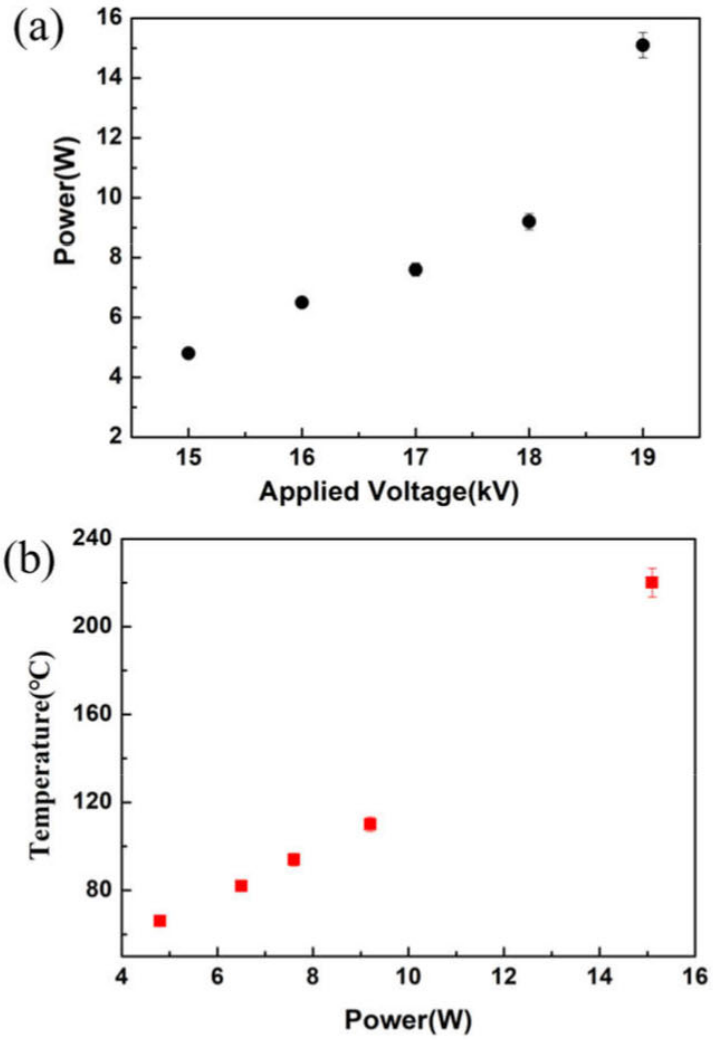

Figure 2. Puissance et température du plasma créées dans le processus de catalyse par plasma: (a) puissances de plasma DBD créées dans le réacteur sous différentes tensions appliquées (crête à crête) ; (b) températures du réacteur à différentes puissances de plasma appliquées

À partir de ces résultats, on peut seulement affirmer que la température seuil de la réaction de Sabatier utilisant l'activation par plasma se situe entre 110 et 220 °C. Toutefois, la température seuil ne peut être mesurée avec précision, en partie en raison de la forte puissance thermique libérée par la réaction.

2.2.2 Température seuil de la méthanisation du CO_2 dans des conditions de plasma DBD

La Figure 3 présente la température en surface du réacteur lorsque différents débits de mélange réactionnel H_2/CO_2 sont injectés dans le réacteur plasma-catalytique. On peut voir qu'avec la diminution du débit de 350 à 20 ml/min, la température a diminué de 255 à 130 °C en raison d'une diminution de la puissance libérée par la réaction.

Selon les données présentées dans la Figure 3, il existe une relation binomiale entre la température du réacteur et le débit du mélange de réactifs à l'entrée :

$$T=B_1x^2+B_2x+C \qquad \text{équation 1}$$

$$B_1=-8.84\times10^{-4},\ B_2=0.70,\ C=116$$

Où T est la température mesurée sur la surface externe du réacteur pendant le processus de plasma (°C), et x représente le débit du mélange gazeux du réactif d'entrée (mL/min).

En utilisant l'équation 1 et en fixant x = 0, on obtient une température de 116°C que l'on suppose être la température seuil de la réaction de Sabatier dans les conditions plasma. Dans toutes les expériences présentées jusqu'à present cependant, la température mesurée est la température à la surface du réacteur. Pour évaluer la température réelle à l'intérieur du lit catalytique, une simulation créée dans le logiciel COMSOL Multiphysics® a été réalisée comme présenté dans la partie suivante.

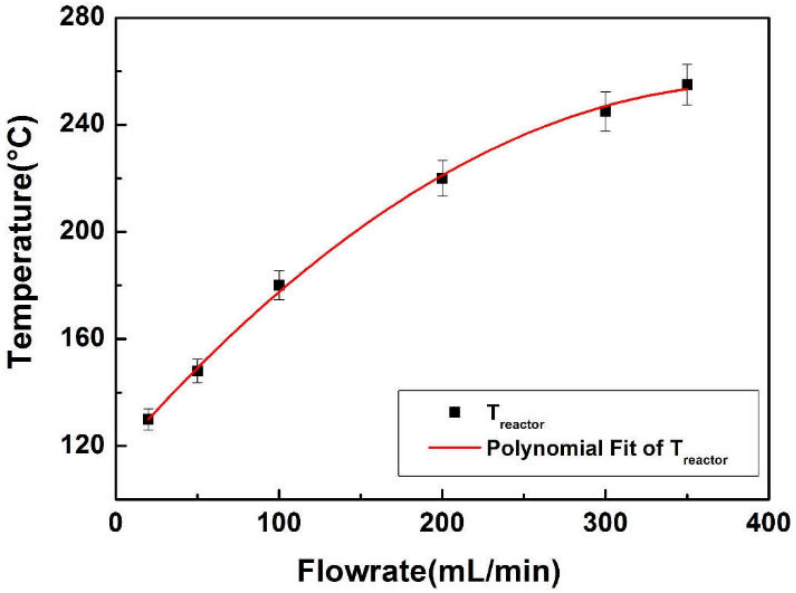

Figure 3. Températures en surface du réacteur avec différents débits du mélange de réactifs à l'entrée pendant la méthanisation du CO_2 dans le procédé catalytique au plasma

2.2.3 Simulation COMSOL de la distribution de la température dans le réacteur cylindrique

Le logiciel COMSOL Multiphysics® a été utilisé pour simuler le transfert de chaleur à l'intérieur du réacteur cylindrique. Le modèle de "transfert de chaleur en milieu poreux" a été appliqué, et "l'étude stationnaire" a été utilisée pour la détermination de la température en régime permanent.

Une étude de sensibilité a d'abord été réalisée pour déterminer la valeur de certains paramètres dont les valeurs réelles ne sont pas connues avec précision. Selon l'analyse de sensibilité, les valeurs les plus appropriées pour les quatre paramètres suivant sont : h=40 $W \cdot m^{-2} \cdot K^{-1}$; catalyseur = 20 $W \cdot m^{-1} \cdot K^{-1}$; quartz = 1,56 $W \cdot m^{-1} \cdot K^{-1}$; alumina = 20 $W \cdot m^{-1} \cdot K^{-1}$.

Les températures mesurées lors de l'expérience et calculées par la simulation sont indiquées dans la Figure 4. On peut observer que jusqu'à une puissance plasma de 9,2 W (18 kV), avant que la réaction n'ait lieu, les deux températures s'accordent très bien. En revanche, lorsque la réaction a lieu à 19 kV, il y a une différence d'environ 18 °C entre ces deux températures. Compte tenu des hypotheses considérées dans la simulation (par exemple le fait que les

propriétés des matériaux ne varient pas avec la temperature) et de la précision de la mesure de la température dans le processus de plasma, l'écart est acceptable. Finalement, la précision du modèle théorique est satisfaisante, en particulier dans des conditions de basse température.

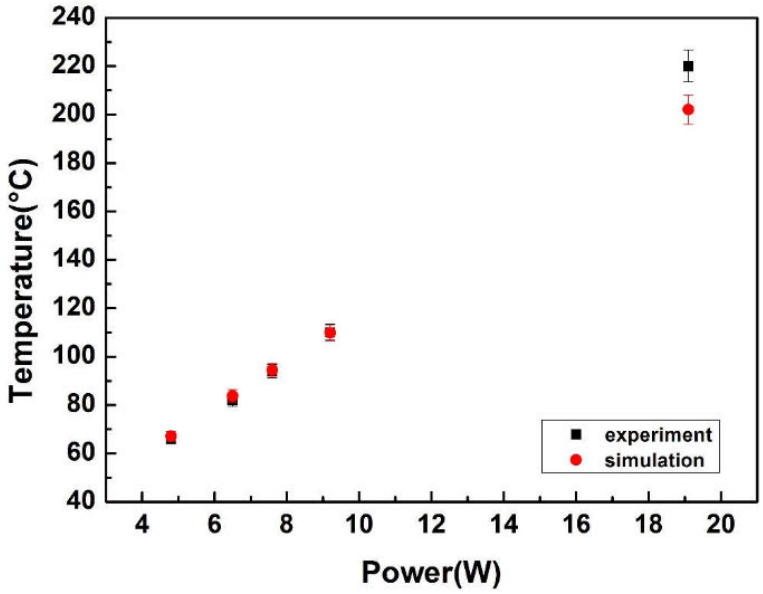

Figure 4. Comparaison entre les températures obtenues lors de l'expérience et de la simulation (200 mL/min)

La Figure 5 montre que la température la plus élevée est atteinte dans le lit catalytique. Dans l'épaisseur du lit catalytique égale à 2,5 mm, et il y a un gradient de température de 6°C lorsque le débit d'alimentation est de 20 mL/min et la puissance thermique totale générée dans le lit catalytique est de 11,2 W. Dans ces conditions, la température moyenne du lit catalytique calculée par COMSOL Multiphysics® à l'aide de la fonction "line average" est de 130 °C. A 20 mL/min, la différence entre la température moyenne du lit catalyque et la température de la surface externe n'est plus que de 2 °C. Compte tenu de la précision de la mesure de la température dans le procédé plasma, la différence de 2 °C pourrait être négligée. Par conséquent, nous pouvons considérer qu'à faible debit d'alimentation la température du lit de catalyseur est égale à la température de la surface externe du réacteur.

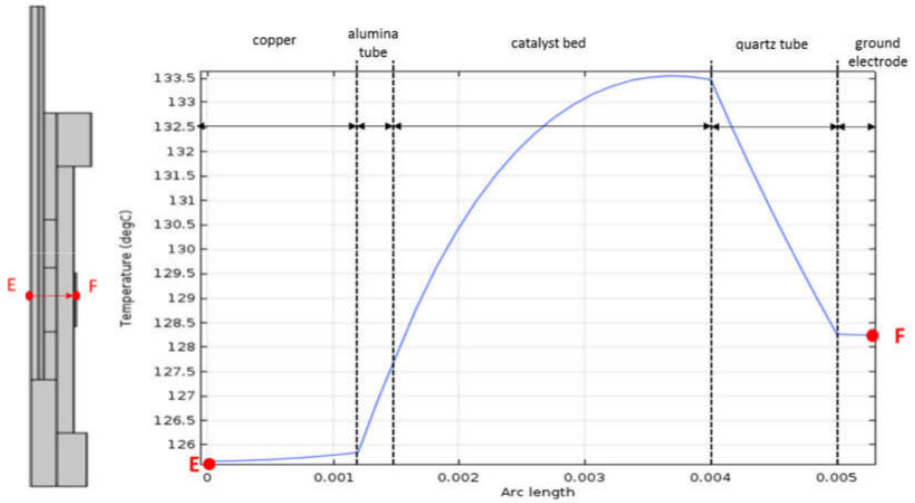

(a) (b)

Figure 5. Profil de température du réacteur (de E à F) avec une puissance de 11,2 W : (a) schéma de la ligne de coupure EF dans le réacteur ; (b) profil de température sur la ligne de coupure EF

D'après la partie 3.2, il a été estimé par extrapolation à debit nul que la réaction de Sabatier peut avoir lieu quantitativement sous exposition plasma à une température à la surface du réacteur de 116 °C. Le gradient de temperature étant négligeable à faible debit, la température seuil de la réaction de Sabatier sous conditions plasma peut être finalement évaluée à 116 °C.

2.3 Étude des rôles respectifs de la température et de la puissance du plasma

Comme mentionné précédemment, lorsque le réacteur à plasma est placé dans l'air ambiant, la chaleur produite par la décharge de plasma est majoritairement perdue par convection à la surface du réacteur et la température du lit catalytique est principalement contrôlée par la tension crête à crête (qui determine la puissance du plasma) appliquée sur le réacteur. Afin d'étudier les rôles respectifs de la température et de la puissance du plasma, de nouveaux réacteurs thermostatés permettant de contrôler la température indépendamment de la puissance du plasma appliquée ont été conçus. Les experiences ont consisté à fixer la température et à

faire varier la tension appliquée (et donc la puissance plasma injectée) dans le but de determiner la conversion optimale.

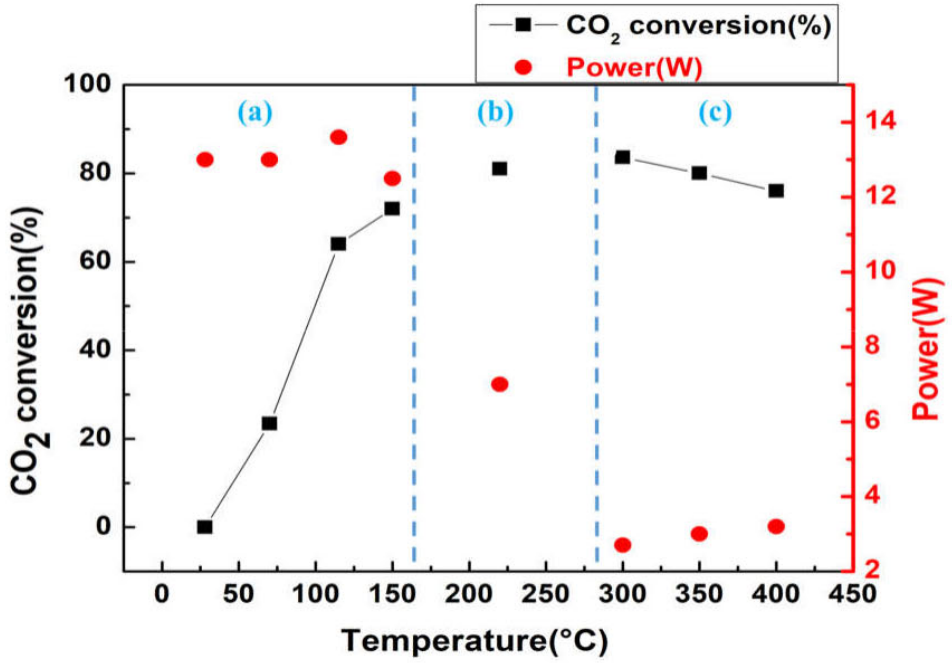

Figure 6. La conversion du CO_2 à différentes températures dans un procédé de plasma-catalyse : (a) système à basse température ; (b) dans l'air ambiant ; (c) système à haute temperature

La conversion optimale du CO_2 en fonction de la température est présentée dans la Figure 6. Il convient de mentionner que la puissance du plasma permettant d'obtenir la conversion optimale est fonction de la température (points rouges). Indépendamment de la puissance du plasma, on peut voir que dans le procédé plasma-catalytique, la conversion du CO_2 augmente avec la température jusqu'à 220 °C, puis la conversion du CO_2 diminue légèrement avec l'augmentation de la température après 300°C. En outre, la température pour obtenir la conversion maximale de CO_2 se situe entre 220 et 300 °C. Cependant, on peut également affirmer, d'après la figure, que pour que la réaction ait lieu à basse température (inférieure à 220 °C), il faut une puissance plasma supérieure à celle qui est necessaire lorsque la température est plus élevée. Par exemple, pour obtenir 23% de conversion du CO_2 à 70 °C, la puissance de plasma nécessaire est de 13 W, alors qu'à 220 °C, la consommation est seulement de 7 W de puissance pour obtenir une

conversion du CO_2 de 81%. A 300 °C, la puissance plasma nécessaire est encore plus faible, soit 3 W.

2.4 Méthanisation du CO_2 dans le réacteur à plasma pseudo-adiabatique

Dans cette partie, l'objectif est d'utiliser un réacteur mieux isolé thermiquement (comparé au réacteur cylindrique initial) afin de diminuer la puissance du plasma en profitant de l'exothermicité de la méthanisation du CO_2. La Figure 7 montre les étapes.

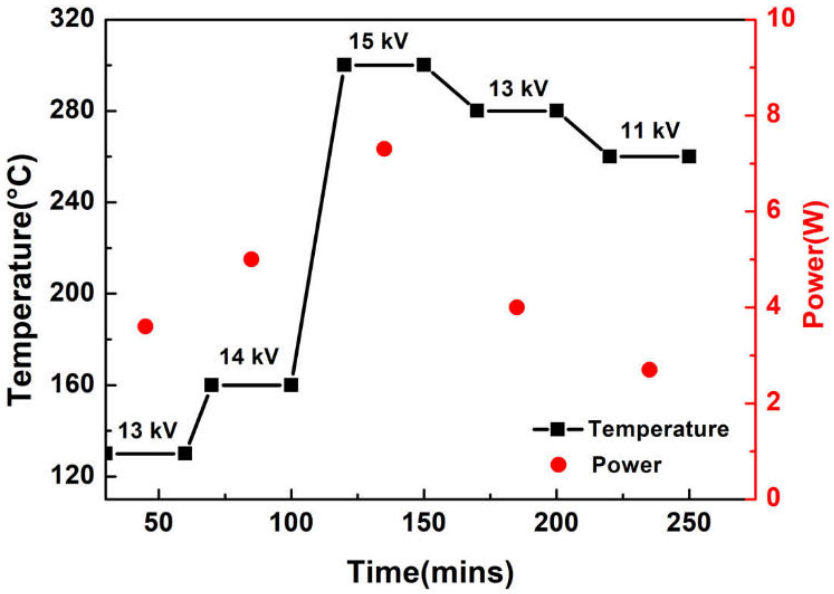

Figure 7. La procédure d'activation de la méthanisation du CO_2 dans un réacteur à plasma adiabatique (GHSV = 46300 h^{-1})

Dans ce processus, le réacteur a été isolé thermiquement pour éviter la perte de chaleur du réacteur. L'expérience a commencé à la tension de 13 kV, et la réaction n'a pas eu lieu avant 15 kV, puis la tension a été diminuée pour étudier si la chaleur dégagée par la réaction pouvait être utilisée pour maintenir la réaction. Comme le montre la figure, la réaction a eu lieu à 15 kV, mais il y avait de l'énergie supplémentaire pour l'activation de la méthanisation du CO_2 à cet état. Par conséquent, la réduction de la tension à la tension optimale pourrait aider à tirer le meilleur parti de l'énergie, ce qui répond aux besoins économiques de l'industrie. Bien que la conversion du CO_2 ait diminué avec la tension, la puissance du plasma a également diminué. Par rapport à la diminution de 4% de la conversion du CO_2 de 84% à 80% lorsque la tension

passe de 15 kV à 11 kV, la puissance du plasma passe de 7,3 W à 2,7 W, soit une diminution de 63% de la puissance. Il a été démontré que la chaleur exothermique libérée par la réaction pouvait être utilisée pour l'activation de la réaction, ce qui entraîne une diminution de la consommation d'énergie.

3. Effet de différents paramètres physiques sur la méthanisation du CO_2 dans les procédés catalytiques thermiques et plasma

Dans cette partie, l'effet de la taille des particules, du GHSV et de la pression a été étudié à la fois dans les procédés thermique et plasma.

3.1 Effet de la taille des particules du catalyseur sur la méthanisation du CO_2

Le catalyseur a été préparé avec des particules de différentes tailles et a été nommé respectivement catalyseur C1 (< 30 μm), catalyseur C2 (250-325 μm) et catalyseur C3 (> 500 μm).

L'activité catalytique pour la méthanisation du CO_2 dans le procédé thermique est présentée dans la Figure 8. On peut voir que, dans la plage de température de 200 °C à 500 °C, la conversion du CO_2 est plus élevée lorsque la taille des particules du catalyseur est plus importante. En particulier à 310 °C, les conversions du CO_2 des catalyseurs C1, C2 et C3 sont respectivement de 51%, 61% et 75%. En outre, la conversion de CO_2 optimale pour le catalyseur C3 est de 81% à 350 °C, contre 74% à 400 °C pour le catalyseur C1.

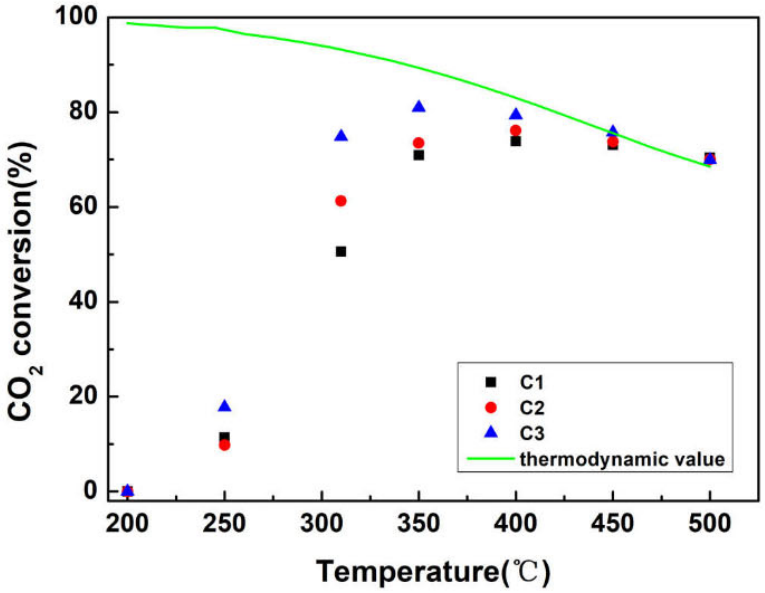

Figure 8. Conversion en CO_2 en fonction de la temperature pour des catalyseurs de différentes tailles de particules dans le procédé thermique (GHSV = 46300 h^{-1})

L'explication de l'augmentation de la conversion du CO_2 avec la taille des particules pourrait être la taille plus petite des cristallites métalliques de Ni (27 nm) des catalyseurs C3 et C2 après réduction par rapport au catalyseur C1 (32 nm). En effet, il a déjà été montré dans la littérature que les catalyseurs avec une petite taille de cristallite de Ni métallique présentent une meilleure activité catalytique.

De plus, une mauvaise répartition du flux de gaz dans le lit poreux de catalyseur pourrait également avoir une influence sur l'activité du catalyseur. Dans certaines zones, la vitesse du gaz pourraît être trop rapide en raison de la presence de chemin préférentiels, ce qui entraîne un contact insuffisant entre le mélange réactionnel et la surface du catalyseur. La mauvaise distribution pourrait être plus importante lorsque les particules sont petites, expliquant également les résultats observés.

Les performances des différents catalyseur pour la méthanisation du CO_2 à 19 kV et 20 kV dans le procédé plasma sont présentées dans le tableau 1. Ce tableau montre que la taille des particules du catalyseur affecte également la conversion du CO_2 dans le procédé hybride plasma-catalyseur. À 19 kV, le catalyseur C1 (< 30 µm) présente une conversion du CO_2 de

67,6%, tandis que les catalyseurs dont les particules sont plus grandes C2 (250-325 µm) et C3 (> 500 µm) ont une conversion du CO_2 d'environ 79%. La même tendance est également observée à 20 kV.

Tableau 1. Performance du catalyseur avec différentes tailles de particules dans le procédé de catalyse par plasma (GHSV=46300 h^{-1})

	19 kV			20 kV		
	X_{CO_2} (%)	Puissance (W)	T (°C)	X_{CO_2} (%)	Puissance (W)	T (°C)
C1	68 ± 2	14.9 ± 1	215 ± 5	66 ± 2	19.0 ± 1	235 ± 5
C2	79 ± 2	15.2 ± 1	225 ± 5	76 ± 2	20.2 ± 1	240 ± 5
C3	79 ± 2	15.9 ± 1	220 ± 5	78 ± 2	20.0 ± 1	240 ± 5

La raison pourrait être à nouveau que la taille des cristallites de Ni métallique est plus petite avec le catalyseur C3 et/ou que la distribution du flux de gaz pourrait être plus uniforme avec les particules de grande taille. De plus, une taille de particules plus grande pourrait également conduire à une meilleure homogénéité du plasma à l'intérieur du lit poreux, ce qui serait à priori favorable à la reaction de méthanisation. Nous reviendront sur l'influence de la taille des particules sur l'homogénéité du plasma dans le dernier chapitre.

3.2 Effet de la vitesse spatiale horaire du gaz (GHSV) sur la méthanisation du CO_2

L'effet de la GHSV sur la méthanisation du CO_2 dans le procédé plasma-catalytique a été étudié en faisant varier la masse du catalyseur et le débit d'entrée. Dans cette étude, la tension appliquée a été fixée à 18 kV.

Avant de présenter les résultats obtenus il convient de mentionner que le réacteur plasma-catalytique utilisé dans cette étude n'étant pas thermostaté (réacteur cylindrique non isotherme), la température n'est pas constante et augmente avec le débit du mélange réactif d'entrée en raison de l'augmentation de la chaleur dégagée par la réaction.

Dans le procédé thermique en revanche, la temperature est fixée à 350 °C et seul le débit d'entrée a été modifié pour changer la GHSV.

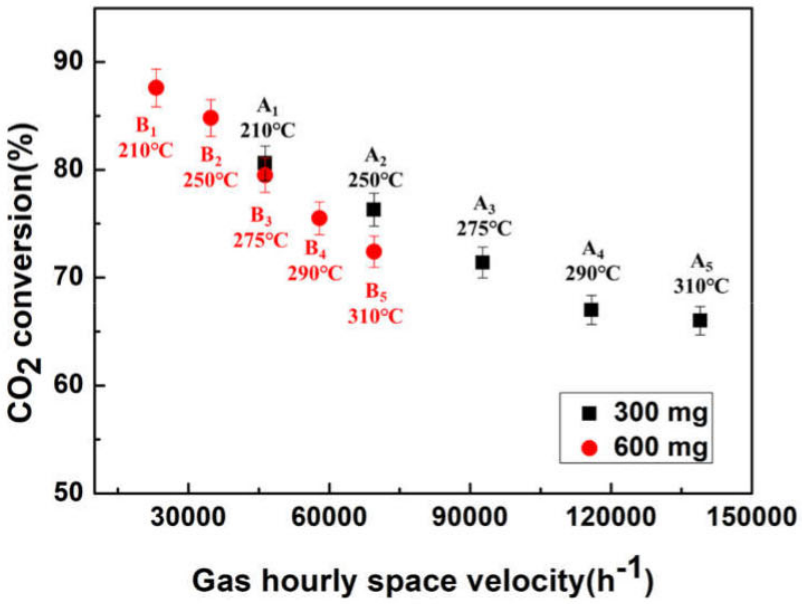

Figure 9. Effet du GHSV sur la conversion du CO_2 dans le procédé de catalyse par plasma (18 kV)

L'effet du GHSV sur la conversion du CO_2 dans le procédé plasma-catalyse est présenté dans la Figure 9. Logiquement, pour une même température, la conversion du CO_2 diminue avec l'augmentation du GHSV. Par exemple, pour une température de 275 °C, la conversion du CO_2 diminue de 79,5% à 71,4% lorsque le GHSV augmente de 46 300 à 92 600 h^{-1}.

Les résultats indiquent aussi qu'il pourrait y avoir une influence de la masse du catalyseur sur la conversion du CO_2 pour une même GHSV. Par exemple, à une GHSV de 70 000 h^{-1}, la conversion du CO_2 est plus faible dans le réacteur chargé avec 600 mg de catalyseur que dans celui chargé avec 300 mg. Cela peut cependant s'expliquer par le fait que les températures pour ces deux conditions sont différentes. Comme nous l'avons déjà mentionné, des GHSV différentes sont obtenues en faisant varier le débit qui lui même affecte la température, le réacteur n'étant pas thermostaté. Ainsi, lorsque le débit est de 300 mL/min avec 300 mg de catalyseur (point A_2), la température est de 250 °C, tandis qu'un debit de 600 mL/min avec une masse de catalyseur de 600 mg (point B_5) conduit à une température de 310 °C. Le fait qu'une température élevée ne soit pas favorable à la méthanisation du CO_2 en condition plasma

explique la meilleure conversion du CO_2 au point A_2.

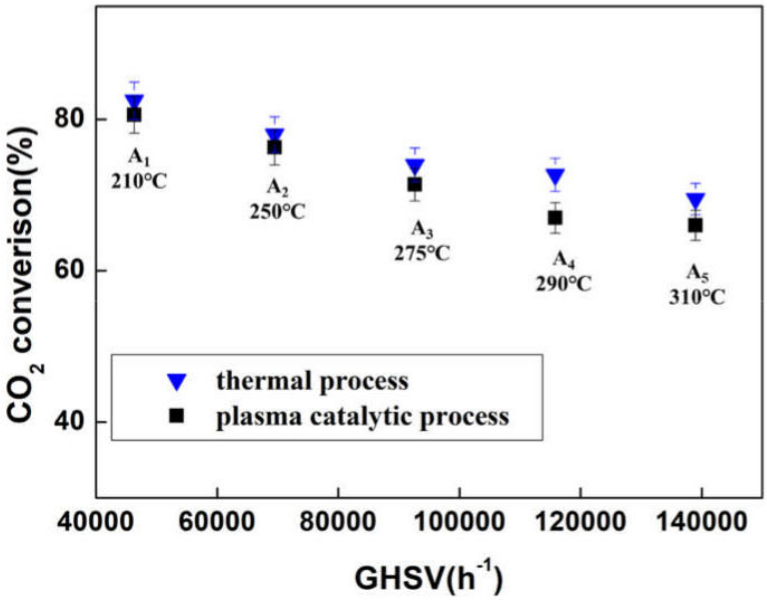

Figure 10. Comparaison de l'effet du GHSV sur la conversion du CO_2 entre le procédé thermique (350 °C) et le procédé plasma-catalytique

L'effet de la GHSV sur la méthanisation du CO_2 dans le processus thermique a été étudié en faisant varier le debit, la masse de catalyseur étant fixée à 300 mg, à une température fixe de 350 °C. La géométrie du réacteur utilisé dans le processus thermique était identique à celle du réacteur à plasma. La comparaison de l'influence de la GHSV sur la conversion du CO_2 entre le procédé thermique et le procédé plasma-catalytique est présentée dans la Figure 10. Il est observé que la diminution de la conversion du CO_2 avec l'augmentation du GHSV est remarquablement similaire dans le procédé thermique et dans le procédé plasma-catalytique. La conversion du CO_2 est sensiblement la même dans les deux procédés lorsque le GHSV est inférieur à 100 000 h^{-1}. Lorsque le GHSV est supérieur à 100 000 h^{-1}, la conversion du CO_2 dans le procédé catalytique au plasma est légèrement inférieure à celle du procédé thermique, peut-être en raison de l'augmentation de la température avec le débit (la temperature passe en effet de 210 à 310 °C lorsque le GHSV passe de 46300 à 138900 h^{-1}). En effet comme déjà souligné précédemment l'augmentation de température peut être défavorable à la méthanisation du CO_2 sous conditions plasma.

3.3 Effet de la pression sur le méthanisation du CO_2

Comme la méthanisation du CO_2 est une réaction en phase gaz, la pression peut avoir un effet important. Dans cette partie, l'influence de la pression sur le processus thermique et le processus plasma-catalytique a été étudiée.

L'influence de la pression sur la performance catalytique de la méthanisation du CO_2 dans un procédé hybride plasma-catalytique est présentée à la Figure 11. Comme le montre la figure, l'augmentation de la pression à l'intérieur du réacteur entraîne une légère augmentation de la conversion du CO_2, alors qu'aucune différence de sélectivité du CO et du CH_4 n'a été observée. À 19 kV, la conversion du CO_2 est passée de 78% à 80% alors que la pression augmentait de 0 à 0,7 bar. Dans la plage de 19 kV à 21 kV, la conversion du CO_2 a diminue avec l'augmentation de la tension sous une pression donnée, peut être en raison de l'augmentation de la température de 220 à 270 °C. Il convient de retenir l'instant de la réaction, la température à chaque tension sous une pression différente était presque la même, qui était respectivement de 220, 240 et 270 °C à la tension de 19, 20 et 21 kV.

Dans nos conditions expérimentales, l'augmentation de la pression atmosphérique à 0,7 bar n'entraîne donc qu'une légère augmentation de la conversion du CO_2. Cependant, il a été possible, à 19 kV, de diminuer la puissance du plasma d'environ 30% (de 16,6 W à 11,7 W) en travaillant à une pression plus élevée. Selon des calculs de la quantité d'électrons, la diminution de la puissance du plasma est principalement due à la diminution du nombre d'électrons, qui a diminué de 24% (de $1{,}44e^{10}$ à $1{,}10e^{10}$) lorsque la pression est passée à 0,7 bar par rapport à la pression atmosphérique. Cela signifie que le nombre d'électrons ne serait pas un critère limitant dans les conditions utilisées, expliquant pourquoi il est possible d'activer la réaction à une puissance plus faible, la tension appliquée étant maintenue à une valeur fixée.

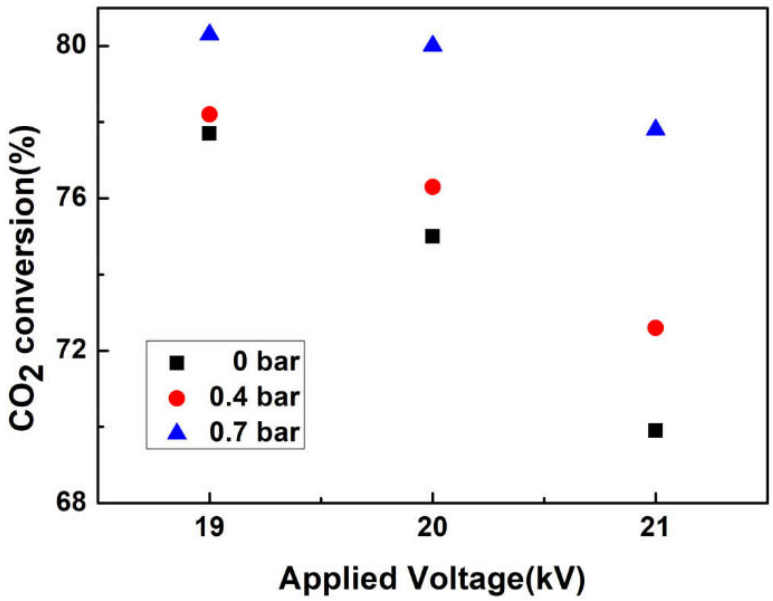

Figure 11. Conversion au CO_2 du catalyseur C3 sous différentes pressions dans le procédé catalytique au plasma (GHSV=46300 h^{-1})

À titre de comparaison, l'effet de la pression sur la méthanisation du CO_2 dans le processus thermique a également été étudié. Des pressions de 0,7 bar et 2,0 bar ont été imposes et la température a été fixée à 350 °C. Les résultats sont présentés dans le Tableau 2.

Tableau 2. Méthanisation du CO_2 sous différentes pressions dans un procédé thermique (350 °C)

Pression (bar)	**Conversion du CO_2 (%)**	**Sélectivité du CH_4 (%)**
0	74	98.5
0.7	76	99.0
2.0	79	99.0

On peut affirmer que dans le processus thermique, l'augmentation de la pression a également un effet positif sur la conversion du CO_2. Ce résultat était prévisible, la méthanisation du CO_2 étant une réaction de réduction du nombre de molécules, et l'augmentation de la pression

contribute donc à déplacer l'équilibre de la réaction vers le produit. Par rapport à la conversion du CO_2 de 74% à la pression atmosphérique, la conversion du CO_2 a augmenté respectivement à 76% et 79% lorsque la pression est passée à 0,7 bar et 2,0 bars. Il n'y a pas non plus de différence de sélectivité du CH_4 lorsque la pression change.

En conclusion, la pression a un effet positif sur la méthanisation du CO_2. De plus, dans le procédé plasma-catalytique, sous une pression plus élevée, la consommation d'énergie est significativement diminuée.

4. Étude prospective de la méthanisation du CO_2 en milli-réacteur

Une étude prospective de la méthanisation du CO_2 dans un milli-réacteur a été réalisée. La configuration du milli-réacteur a été conçue et optimisée, puis la catalyse de la méthanisation du CO_2 a été effectuée dans ce réacteur dans des conditions de plasma.

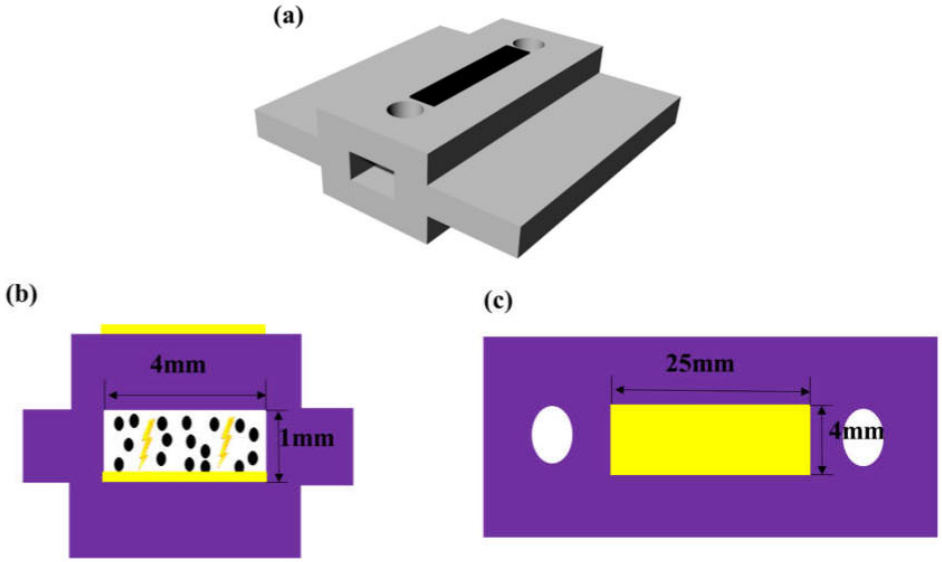

Figure 12. Configuration du milli-réacteur de plasma : (a) modèle 3D ; (b) vue de face ; (c) vue vertical

La Figure 12 représente la configuration finale du milli-réacteur à plasma. Ce réacteur est un réacteur DBD à volume asymétrique. La lame de quartz a été choisie comme matériau diélectrique et le dépôt d'or sur la lame a agi comme électrode à haute tension et électrode mise

à la terre. L'épaisseur de la lame de quartz utilisée était de 1 mm. Comme on peut le voir sur la figure, la distance entre deux électrodes était de 2 mm, et la longueur de l'électrode était de 25 mm avec une largeur d'électrode de 4 mm. Le catalyseur a été chargé à l'intérieur du réacteur et de la laine de verre a été utilisée pour fixer le catalyseur des deux côtés. La masse de catalyseur utilisée dans le milli-réacteur était de 100 mg de catalyseur C3 (500 μm), et la longueur du lit de catalyseur était de 25 mm. Le mélange de gaz d'entrée était un mélange pur de H2 et de CO2 avec un rapport de 4:1. La température était mesurée par un thermocouple de type K placé à la surface du réacteur.

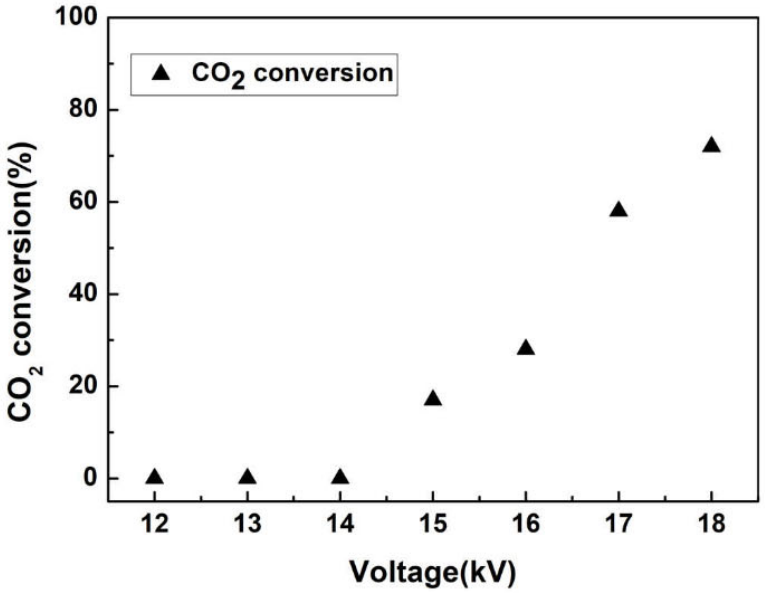

Figure 13. La conversion du CO_2 varie à différentes tensions dans le milli-réacteur

La Figure 13 montre la conversion du CO_2 à différents voltages. L'expérience a débuté avec une tension appliquée de 12 kV. La réaction ne s'est pas produite avant que la tension de 15 kV ne soit appliquée au réacteur, et la conversion du CO_2 était de 17% à la température de 188 °C. La conversion du CO_2 est ensuite passée de 17% à 72% avec une tension appliquée de 15 kV à 18 kV. Ceci est dû à l'augmentation de la température et de la puissance avec l'augmentation de la tension appliquée. La conversion maximale du CO_2 de 72% a été obtenue à 18 kV avec une

sélectivité du CH_4 de 98%, alors que la température était de 242 °C avec une consommation de 17,6W.

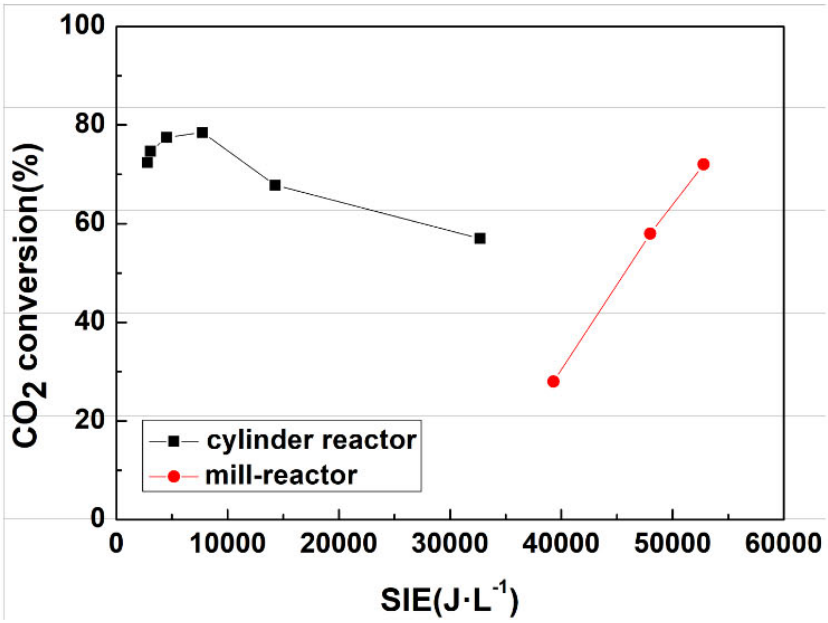

Figure 14. Comparaison de la SIE de la conversion du CO_2 en réacteur à cylindre (20-350 mL/min) et en milli-réacteur (20 mL/min) (catalyseur C3)

La Figure 14 est la comparaison de la SIE de la méthanisation du CO_2 en cylindre et en milli-réacteur. On peut voir que le SIE en réacteur cylindrique était beaucoup plus faible que le DIE en milli-réacteur. Ceci est principalement dû au fait que dans le réacteur cylindrique, le débit était différent comme mentionné précédemment, et que le SIE diminue avec l'augmentation du débit. En comparant le DIE à 20 mL/min dans les deux réacteurs, on a observé que pour avoir presque la même conversion de CO_2 de 58%, le SIE en réacteur cylindrique était de 32700 J/L, ce qui était inférieur à la valeur de 48000 en milli-réacteur.

En conclusion, la performance de la méthanisation du CO_2 en réacteur cylindrique était bien meilleure que celle en milli-réacteur. La réaction a pu avoir lieu à un degré d'isolation thermique inférieur dans un réacteur à cylindres, peut-être parce que la configuration du milli-réacteur n'est pas adaptée à cette réaction car elle nécessite une énergie et une température élevées. De plus, en raison de la configuration du cylindre et du choix du matériau de l'électrode, le réacteur à cylindre pourrait fonctionner pendant longtemps, jusqu'à ce que le réacteur soit cassé à cause

d'une mauvaise opération ou d'un accident. Au contraire, le milli-réacteur doit être remplacé après une certaine période de l'expérience, car le dépôt d'or serait lentement éliminé par le plasma créé à l'intérieur du réacteur.

En raison du temps limité pour la recherche sur la méthanisation du CO_2 dans les milli-réacteurs, de nombreuses améliorations pourraient encore être apportées pour améliorer les performances catalytiques dans les milli-réacteurs.

5. Conclusion

Ce travail s'est concentré sur le procédé plasma-catalytique pour la méthanisation du CO_2 en utilisant un catalyseur de $Ni/Ce_{0,58}Zr_{0,42}O_2$, tandis que la méthanisation du CO_2 sous activation thermique a également été effectuée pour faire la comparaison. Le procédé de catalyse au plasma a été réalisé dans le réacteur à cylindre de quartz, et une étude prospective a également été réalisée dans le milli-réacteur.

Dans la première partie, le rôle de la température dans le procédé plasma-catalytique pour la méthanisation du CO_2 a été étudié. La méthanisation du CO_2 a été réalisée respectivement dans le procédé de catalyse thermique et dans le procédé de catalyse par plasma. Dans le même GHSV de 46300 h^{-1}, pour obtenir une conversion de CO_2 d'environ 80%, la température nécessaire dans le procédé thermique était de 350 °C, alors que dans le procédé plasma-catalytique, la même conversion de CO_2 pouvait être obtenue à la température de 220 °C, ce qui est environ 130 °C de moins que la température dans le procédé thermique.

Une série d'expériences avec différents débits de mélange de gaz d'entrée a ensuite été réalisée, et il a été constaté que la température diminuait avec le débit du mélange de gaz d'entrée. Il existe une relation binomiale entre la température stable du réacteur et le débit du mélange de réactifs d'entrée. La température seuil a été déduite lorsque le débit est de 0 mL/min, soit 116 °C. Cependant, il s'agit de la température à la surface du réacteur. Pour étudier le gradient de température dans le réacteur, le logiciel COMSOL Multiphysics® a été utilisé pour simuler le transfert de chaleur à l'intérieur du réacteur. La simulation a indiqué que la différence de température entre la surface du réacteur et le lit de catalyseur était presque négligeable, la température seuil du plasma pour la réaction de Sabatier a finalement été évaluée à 116 °C.

De plus, il a été observé que la tension et la puissance de déclenchement pour l'activation de la méthanisation du CO_2 pouvaient diminuer en raison de la diminution de la convection de l'air dans le processus de plasma. Deux systèmes pouvant contrôler la température indépendamment de la puissance du plasma ont été conçus pour étudier les rôles respectifs de la température et de la puissance du plasma. On peut conclure que l'influence de la température et de la puissance du plasma sur la méthanisation du CO_2 était différente selon la plage de température. Indépendamment de la puissance du plasma, on peut voir que dans le procédé plasma-catalytique, la conversion du CO_2 augmentait avec la température avant 220 °C, et ensuite la conversion du CO_2 diminuait avec l'augmentation de la température après 300 °C. Quant à l'effet de la puissance du plasma sur la conversion du CO_2 indépendamment de la température, on peut conclure qu'à basse température (inférieure à 220 °C), la conversion du CO_2 augmente avec la puissance du plasma, mais qu'à haute température (supérieure à 300 °C) la conversion du CO_2 est plus faible à une puissance de plasma plus élevée. En outre, on pourrait également conclure que la méthanisation du CO_2 pourrait être activée dans différentes conditions: par exemple, une puissance élevée à basse température ou une faible puissance à haute température. Cela permet d'envisager différents objectifs dans le processus industriel à l'avenir.

La conversion du CO_2 a également été réalisée dans le réacteur à plasma adiabatique afin d'optimiser la consommation d'énergie. Il a été démontré que la chaleur exothermique dégagée par la réaction pouvait être utilisée pour l'activation de la réaction, et donc pour diminuer la puissance consommée du plasma pour la réaction. Par conséquent, pour atteindre une conversion de CO_2 de 80%, la puissance du plasma utilisée pourrait être réduite à 2,7 W, ce qui représente seulement 37% de la puissance du plasma consommée dans des conditions normales.

Dans la deuxième partie, différentes tailles de particules de catalyseur ont été fabriquées et leur influence sur la méthanisation du CO_2 a été étudiée. La taille et la pression des particules du catalyseur ont eu une influence positive sur la méthanisation du CO_2 dans le procédé thermique et le procédé plasma. L'augmentation de la taille des particules du catalyseur d'environ 30 μm à 500 μm pourrait améliorer de 10% la conversion du CO_2 en raison de la taille plus petite des particules métalliques de Ni après réduction. La conversion du CO_2 a diminué avec

l'augmentation de la GHSV dans le procédé catalytique thermique et à plasma, et avait une valeur similaire à la même GHSV, la conversion du CO_2 a diminué de 82,5% à 69,5%, tandis que la GHSV a augmenté de 46332 h^{-1} à 138996 h^{-1}. En outre, dans le procédé catalytique au plasma, la température dépendait du débit, et elle ne dépendait ni de la GHSV ni de la masse du catalyseur chargé dans le réacteur. La température est passée de 220 °C à 310 °C lorsque le débit est passé de 200 mL/min à 600 mL/min, ce qui est dû à l'augmentation de la puissance libérée par la réaction. En ce qui concerne l'effet de la pression, l'augmentation de la pression à l'intérieur du réacteur de la pression atmosphérique à 0,7 bar pourrait légèrement augmenter la conversion du CO_2, et elle peut également contribuer à diminuer d'environ 30% la puissance du plasma nécessaire à la réaction dans le processus de plasma.

Enfin, une étude prospective de la méthanisation du CO_2 est milli-réacteur a été réalisée. Tout d'abord, un milli-réacteur avec de l'ITO comme électrodes a été conçu pour créer un plasma DBD. Cependant, en raison de la faible conductivité de l'ITO, la tension nécessaire pour déclencher la réaction était très élevée, et le réacteur s'est cassé avant que la réaction n'ait lieu. Une optimisation du milli-réacteur a donc été effectuée, et le dépôt d'or sur la lame a été choisi comme électrode pour diminuer la tension nécessaire à la réaction, et le matériau diélectrique a été remplacé par une lame de quartz, qui pouvait fonctionner à haute tension et à haute température.

Des catalyseurs de différentes tailles de particules ont été chargés dans le réacteur, et il s'est avéré que le plasma était plus homogène dans le lit du catalyseur lorsque le catalyseur C3 (500 μm) était chargé dans le réacteur. Et on a observé que l'intensité du plasma augmentait avec le débit du mélange gazeux.

La méthanisation du CO_2 a été effectuée dans le milli-réacteur. 17% de la conversion du CO_2 a été obtenue à 15 kV avec une température de 188 °C, et la conversion du CO_2 augmentait avec la tension appliquée. La conversion maximale de CO_2 de 72% a été obtenue à 18 kV, et la température était de 242 °C. Par rapport à l'efficacité énergétique du cylindre, l'efficacité énergétique du milli-réacteur était beaucoup plus faible, et des améliorations doivent encore être apportées à ce processus.

Abstract

Anthropogenic CO_2 emissions from an energy system based on fossil fuels are the main cause of climate change. Therefore, there is a huge need to decrease these emissions in the atmosphere in order to have a close carbon cycle, the methanation reaction (CO_2 (g) + $4H_2$(g) = CH_4(g) + $2H_2O$(g), $\Delta H° = -165.3$ KJ/mol) has been considered as a promising method for this aim. The plasma-catalytic process, which is the combination of non-thermal plasma and catalysis, is considered as a promising approach to convert CO_2 to high value-added chemicals at low temperature, and has been successfully applied for the methanation of CO_2. However, what we know about the plasma-catalytic process is still limited. This work focuses on the use of a heterogeneous catalyst $Ni/Ce_{0.58}Zr_{0.42}O_2$ in order to study the Sabatier reaction using a dielectric barrier discharges (DBD) plasma catalytic process

Frist of all, the catalyst was tested in convention thermal activation and DBD plasma condition, and showed that the temperature to achieved high CO_2 conversion and CH_4 selectivity was around 220 °C, which was around 130 °C lower than that in thermal condition. This is due to the nature of the plasma that could generate chemical active species at low temperature. Then a set of experiments with different inlet flowrates is carried out in a plasma reactor to investigate the threshold temperature of Sabatier reaction. To estimate more accurately the threshold temperature of Sabatier reaction, the temperature difference between the catalytic bed and the external surface of the reactor is calculated and simulated in COMSOL Multiphysics® software. Finally, the threshold temperature of the Sabatier reaction during plasma processing is assumed to be 116 °C based on the experimental data and simulation analysis.

Then the respective roles of temperature and plasma power in the plasma-catalytic process were investigated. The results show that CO_2 methanation could take place at low temperature (<200 °C), but a higher plasma power consumption was needed. Generally, the higher is the reactor temperature, the lower is the required plasma power.

In chapter 4, ceria zirconia Ni-based catalysts with different particle sizes were prepared, characterized by SEM, XRD, BET, TPR and TPD, then tested in CO_2 methanation in a thermal-

catalysis system and a plasma-catalytic system respectively. The influence of gas hourly space velocity (GHSV) and pressure were also studied in both thermal and plasma process. Catalyst with bigger particle size was found to have higher CO_2 conversion in both processes, maybe due to a smaller metallic Ni particle size. GHSV had a similar influence on CO_2 conversion in both process, and the temperature in plasma process increase with inlet flowrate. Concerning the effect of pressure, with the increase of pressure inside of the reactor, there is a slight increase of CO_2 conversion and the power consumption decreased in plasma process.

In chapter 5, prospective study of CO_2 methanation is milli-reactor was performed. Plasma milli-reactor was designed and then various parameters were optimized for the reaction. Finally, CO_2 methanation was successfully performed in the milli-reactor. The maximum CO_2 conversion of 72% was achieved for an applied voltage of 18 kV and a plasma power of 17.6 W. In these conditions, the temperature was 242 °C.

Chapter I: State of the art

The increasing carbon dioxide concentration in the atmosphere is assumed as the main culprit for global warming. According to the measurement from Scripps Institute of Oceanography, the CO_2 concentration in the atmosphere increased from around 315 ppm in March 1958 to 391 ppm in January 2011, and close to 409 ppm in December 2018 [1]. Thus, global CO_2 emissions has been a serious concern for several decades. CO_2 actually is emitted into the atmosphere mainly by fossil fuels combustion and anthropogenic activities [2]. Until now, as a non-renewable energy, fossil fuels make up more than 85% of the world energy consumption, resulting in environmental pollution and an increasing global warming effect.

Energy generated by renewable sources has been a promising option for the use of clean energy and reduction of CO_2 emissions. However, green fuels cannot replace of fossil fuels in this moment because of the high price of its production. Efforts towards the low cost of the green energy should be further made. Carbon capture and utilization (CCU) is now considered as one of the most promising methods for the mitigation of CO_2 emissions into the atmosphere[3, 4]. Not like the storage of the CO_2 which is captured by various technologies, the aim of this method is to convert the greenhouse gas into useful chemicals[5, 6], thus diminishing the CO_2 accumulation into the atmosphere. As the long-term goal, the conversion of CO_2 could be an alternative to the petrochemistry and a promising bridging technology towards the development of sustainable renewable green energy. Among processes that contribute to the chemical valorization of CO_2, such as reverse water gas shift reaction[7], dry reforming of methane[8], hydrogenation of CO_2 to methanol[9] or dimethyl ether (DME)[10], oxidative dehydrogenation of hydrocarbons (ODH) with CO_2 [11], or production of synthetic fuels via Fischer-Tropsch synthesis from CO_2/H_2 mixture[12], CO_2 methanation or hydrogenation of CO_2 is an promising process to create new carbon dioxide based economy with respect to thermodynamics when compared to the production of other hydrocarbons or alcohols. Besides, the CO_2 methanation process could be coupled with the renewable energy process, such as wind and solar power, the electricity produced in these processes used to perform water electrolysis to generate hydrogen,

which could react with CO_2 captured from emission sources to produce methane. This coupled process could partially solve the problem of the stabilization and intermittent renewable sources of the electric grids, which account for an increasing part in electricity production. Thus, the CO_2 methanation process could be considered as a chemical storage of excess of electricity produced from the renewable resource.

In this review, a particular attention is paid to the CO_2 methanation, which involves the catalytic hydrogenation of carbon dioxide to produce methane, thus providing an alternative to the mitigation of the carbon dioxide in the atmosphere. In recent years, numerous efforts have been invested in the development of catalysts for the CO_2 methanation, and catalytic systems based on supported group VIII metals (Ru, Rh, Co or Ni) on various oxide supports (TiO_2, SiO_2, Al_2O_3, CeO_2, ZrO_2) are successfully designed[13, 14]. Among them, Ni-based catalysts have been widely studied because of its good compromise between high activity and low price[15]. Besides, various factors that influence the performance of catalysts, such as the preparation method, the nature of the support and the metal, amount of the metal and its dispersion, are presented. Moreover, the deactivation of the catalyst, which result in the decrease of the catalytic performance, is also discussed.

Due to several drawbacks in the thermal process of CO_2 methanation, such as the deactivation of the catalyst and the high reaction temperature (> 300 °C), a hybrid combination of thermal catalytic process coupled to the Dielectric barrier discharge (DBD) plasma was developed.[16-18] Thus, DBD plasma and development of the hybrid plasma catalytic process is presented here. This chapter offers a general idea about the chemical valorization of carbon dioxide and the catalytic methanation as well as the hybrid plasma-catalytic process for CO_2 methanation.

1.1 Utilization of carbon dioxide

This part is an introduction of growing concern of the control of carbon dioxide in the atmosphere, which is considered as the main culprit for climate change, as well as chemical utilization of carbon dioxide, and the promising role of Sabatier reaction process in the

mitigation of the carbon dioxide.

Global warming is a term used for the observed century-scale rise in the average temperature of the Earth's climate system and its related effects. It is a general consensus that global warming is caused by increasing concentrations of greenhouse gases (GHGs) and other human-caused emissions.

It is commonly believed that part of solar energy absorbed at Earth's surface is radiated back out to space as heat. However, greenhouse gases that in the atmosphere will absorb much of the heat as it passes through the atmosphere and back out to space. Then, they radiate the heat back to the Earth's surface, thus resulting in the increase of temperature of the Earth's climate system. The main greenhouse gases in the atmospheres of the terrestrial planets are carbon dioxide (CO_2), methane (CH_4), nitrous oxide (N_2O), and fluorinated gases (Hydrofluorocarbons-HFCs, perfluorocarbons-PFCs, fur hexafluoride-SF_6, and nitrogen trifluoride-NF_3). Moreover, as shown is Figure 1-1, CO_2 accounted for about 76% of all greenhouse gas emissions from human activities in 2010, in which 65% is produced by fossil fuel and industrial processes, while the other part is due to the forestry and other land use.

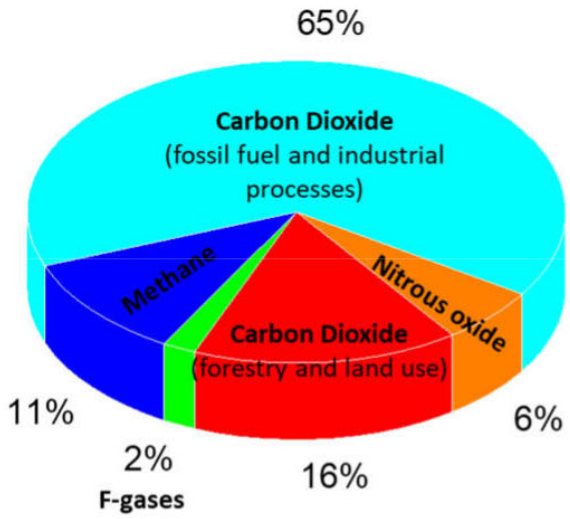

Figure 1-1. Global greenhouse gas emissions by gas[19]

From Figure 1-2, one can state that carbon dioxide has been rising in the atmosphere long before 1960. With the introduction of fossil fuels, carbon dioxide began rising at the beginning of the

Industrial Revolution around 1880. This is not direct proof that the CO_2 caused the warming. However the fact is that temperature rose faster from 1975 to now than from 1880 to 1975, and so did CO_2. It also cannot change the fact the temperature has been highest recently and so has CO_2.

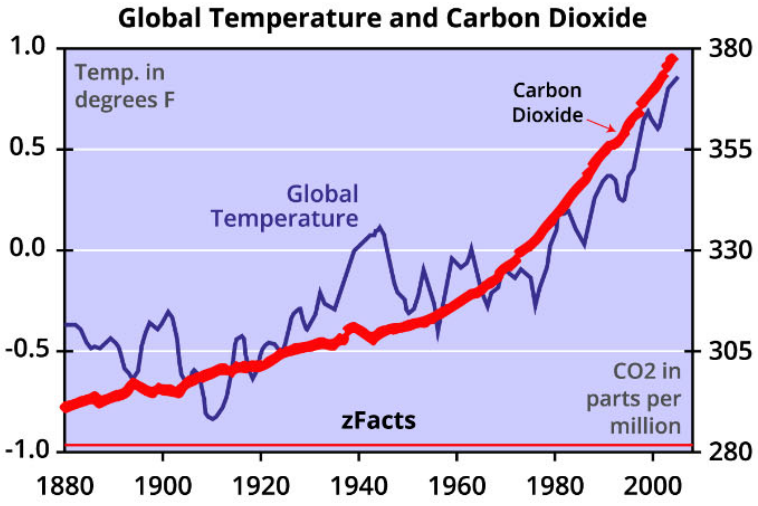

Figure 1-2. Carbon dioxide vs global temperature graph via Stephen Stoft at zfacts.com[20]

1.1.1 Sources of carbon dioxide

Carbon dioxide has always been present in the composition of our atmosphere, emitted by natural sources and anthropogenic emissions. Natural sources, which mainly include breathing, forest fires, volcanic activity, fermentation or organic decomposition. In addition to these major natural emissions, emissions from anthropogenic activity are added: agricultural and industrial sectors, waste production, reaching 33 Gt of CO_2 per year in 2019 in the atmosphere. As shown in Figure 1-3, the carbon dioxide emissions, primarily from the combustion of fossil fuels, have risen dramatically since the start of the industrial revolution, and it seems that the CO_2 emissions will continuously increase in the recent future.

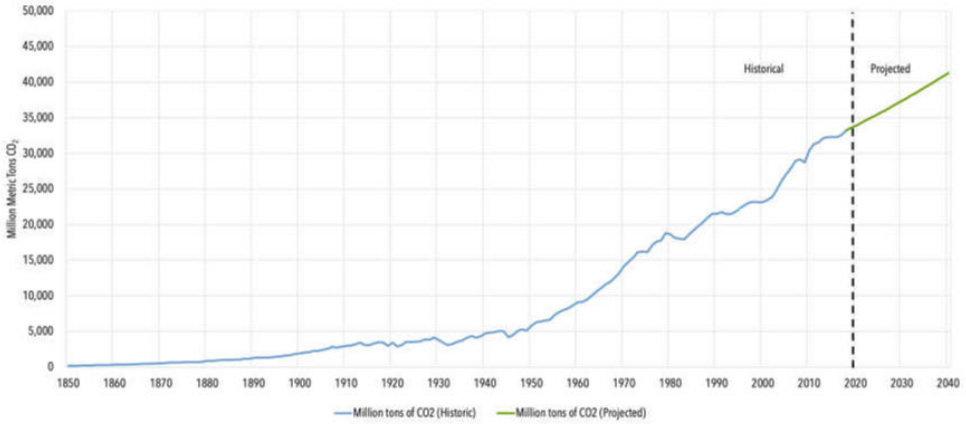

Figure 1-3. Global Carbon Dioxide Emissions from 1850 to 2040[21]

Fossil fuel combustion accounts for about 90% of total global CO_2 emissions, excluding those from forest fires and the use of wood fuel[22]. Due to the consumption of fossil fuels and cement production, over 400 billion metric tons of carbon have been released to the atmosphere since 1751. It is worth to mention that half of these fossil-fuel CO_2 emissions have taken place since the late 1980s. The 2014 global fossil-fuel carbon emission estimate, 9855 million metric tons of carbon, presents an increase of 0.8% compared to 2013 emissions. The slight increase continues a three-year trend of modest annual growth under 2% per year.

Globally, 75.1% of the emissions with consumption of fossil fuels is from liquid and solid fuels in 2014. Gas fuels (e.g., natural gas) accounted for 18.5% (1823 million metric tons of carbon) of the emissions from fossil fuels and indicates the increasing utilization of natural gas. As the main constituent of cement and the largest of non-combustion sources of CO_2 from industrial manufacturing, cement production contributing about 568 million metric tons of carbon in 2014. And this doubled in the last decade and now represent 5.8% of global CO_2 releases from fossil-fuel burning and cement production. The emission of the cement production process mainly comes from two stages: pre-heating step and the clinkerisation step. In the per-heating step, the "calcination" process, which is the decomposition of limestone $CaCO_3$ in to CO_2 and lime CaO, accounts for 60-65% of the CO_2 emission. And the clinkerisation step that includes combustion of various fuels is responsible for the additional 35-40% of CO_2 emissions. Gas flaring, which emitted roughly 2% of global CO_2 emissions during the 1970s, now releases less than 1%.

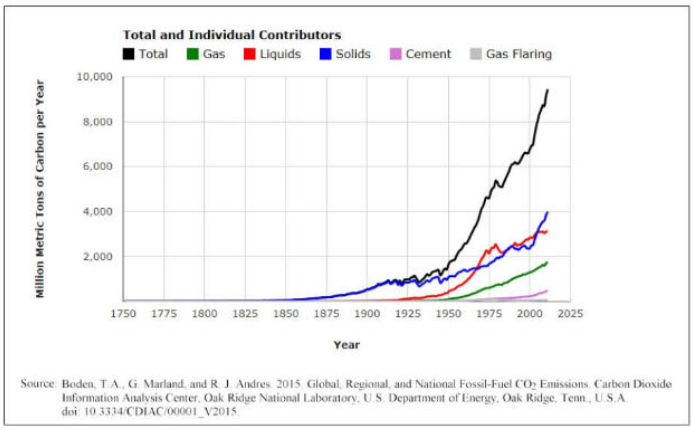

Figure 1-4. Annual global fossil-fuel carbon emissions[23]

Increased CO_2 concentration in the atmosphere contribute to an increase greenhouse effect and climatic changes. Thus, the CO_2 emission from human activity sources should be reduced. Considering the fact that almost 90% of the total global CO_2 emissions is from fossil fuel combustion for energy supply, the use of 'new' renewable energy sources, such as solar and wind energy and biofuels, could be effective. Besides, various technologies about recovery, removal and storage of CO_2 have been studied. Combination of the capture and chemical utilization of CO_2, the carbon capture and utilization (CCU) is now considered as one of the most promising methods for sustainable development.[24] Among various utilization process, the chemical utilization of CO_2 into useful and high value chemicals is of great interest.

1.1.2 Pathways of carbon dioxide utilization

The current industrial process for utilization of CO_2 as a raw material is mainly resides in the synthesis of urea, methanol, formaldehyde (CH_2O) and Dimethyl ether (DME), which accounts for 114, 8, 3.5 and 3 million tons of CO_2 utilization per year respectively.[25] Compared to today's global emissions of CO_2 around 30 billion of tons, one finds that a net unbalance towards the emission exists: the question rises if larger volumes of CO_2 can be converted into useful chemicals. Thus, more industrial process that use CO_2 as a raw material should be further research and developed.

Various possible processes for CO_2 utilization are presented in Figure 1-5. The utilization of CO_2 could be classified to physical and chemical utilization according to the mature of the

utilization.

In physical utilization, its physical properties is used, and the CO_2 remain pure or suspended in the solution without transformation. CO_2 can be used as solvent, dry ice, fire extinguisher, and refrigerant. In addition, supercritical carbon dioxide is becoming an important commercial and industrial solvent for promoting difficult chemical reactions due to its role in chemical extraction in addition to its low toxicity and environmental impact.[26] Besides, CO_2 can also be used in large-scale industries to indirectly boost a process as in the enhanced oil recovery (EOR)[27], enhanced gas recovery (EGR)[28] and enhanced geothermal systems (EGS)[29].

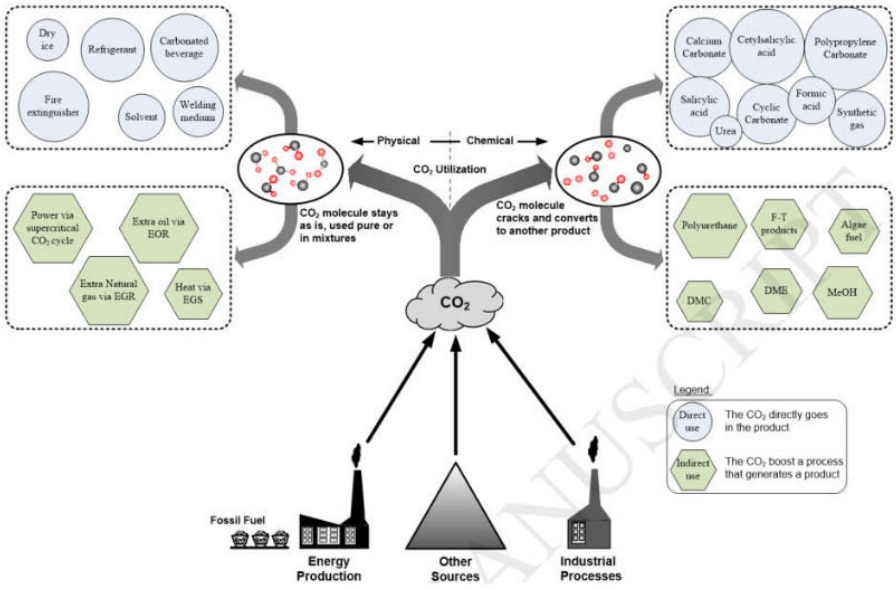

Figure 1-5. Various pathway for CO_2 utilization[30]

In chemical utilization, there is the break of CO_2 molecules bonds in reactions and eventually can be converted to various commodity chemicals, synthetic fuels, or organic intermediate for other products. As mentioned before, there is already some chemicals, mainly urea and methanol, produced in industrial process from the conversion of CO_2.

However, there exists one important lock that limit the conversion of CO_2 to other chemicals due to the kinetic and thermodynamic stability of CO_2. As we all know, CO_2 is a very stable molecule (ΔG^0= -394.3 kJ/mol), the C=O bonds in CO_2 molecules are quite stable and a lot

energy supply is needed to make their dissociation possible.

Thus, a relative high energy put and optimized parameters as well as catalyst are required to covert CO_2 into useful chemicals. The reaction in which CO_2 dissociated to CO and O_2 shows an enthalpy change (ΔH) of about 293 kJ/mol at atmospheric pressure and the temperature of 25 °C[31]. To give an example of the stability of CO_2, it is estimated that less than 2% of CO_2 could be dissociated into CO (g) and O_2 (g) at 2000 °C[32].

Main Physical and chemical properties of carbon dioxide are presented in Table 1-1.

From a thermodynamic point of view, it would be easier for the conversion CO_2 when it is used as a co-reactant with other molecules with higher Gibbs free energy.

Table 1-1. Main Physical and chemical properties of carbon dioxide

Property	Value	Unit
Heat of formation at 25 °C	-393.5	kJ/mol
Entropy of formation at 25 °C	213.6	$J \cdot mol^{-1} \cdot °C^{-1}$
Gibbs free energy of formation at 25 °C	-394.3	kJ/mol
Sublimation point at 1 atm	-78.5	°C
Triple point at 5.1 atm	-56.5	°C
Critical temperature	31.04	°C
Critical pressure	72.85	atm
Gas density at 0 °C and 1 atm	1.976	g/L
Viscosity at 25 °C and 1 atm	0.015	cp

Moreover, methane, hydrogen are some molecules that have higher (less negative) Gibbs free energy. Fox example, in the dissociation of CO_2 to CO, the ΔG of reaction where the CO_2 is used as a co-reactant with H_2 is less positive than the ΔG of the reaction where CO_2 is used as a single reactant. Moreover, the heat of the reaction is less when the CO_2 reacts with H_2 in the reaction[33].

$CO_2(g) = CO(g) + 1/2\ O_2(g)$ ΔH=+293 kJ/mol, ΔG=+257 kJ/mol equation 1-1

$CO_2(g) + H_2(g) = CO(g) + H_2O(g)$ ΔH= +51 kJ/mol, ΔG= +28 kJ/mol equation 1-2

To estimate the thermodynamic feasibility of a reaction used for the conversion of CO_2, the enthalpy change ΔH and the Gibbs free energy change ΔG values are the most important criteria. Indeed, the reaction with a negative value of ΔH indicating the reaction is exothermic is preferred for industrial process due to the economic concern. Moreover, the reaction with a negative value of ΔG is thermodynamically favorable. After analyzing the ΔH and ΔG value for some exothermic reactions involving CO_2, it was found that only a small number of reactions have both negative value of ΔG and ΔH, as presented in Table 1-2[33].

Table 1-2. Some exothermic reactions involving CO_2 with negative enthalpy and gibbs free energy changes

Eq.	Reactions	$\Delta H°$ (kJ/mol)	$\Delta G°$ (kJ/mol)
3	$CO_2(g) + 3H_2(g) = CH_3OH(l) + H_2O(l)$	-137.8	-10.7
4	$CO_2(g) + 4H_2(g) = CH_4(g) + 2H_2O(l)$	-259.9	-132.4
5	$2CO_2(g) + 6H_2(g) = CH_3OCH_3(g) + 3H_2O(l)$	-264.9	-38.0
6	$CO_2(g) + H_2(g) + CH_3OH(l) = CH_3COOH(l) + H_2O(l)$	-135.4	-63.6
7	$CO_2(g) + 3H_2(g) + CH_3OH(l) = C_2H_5OH(l) + 2H_2O(l)$	-221.6	-88.9
8	$CO_2(g) + C_2H_2(g) + H_2(g) = CH_2CHCOOH(l)$	-223.6	-115.0
9	$CO_2(g) + C_2H_4(g) + H_2(g) = C_2H_5COOH(l)$	-166.6	-56.6
10	$CO_2(g) + C_2H_4(g) + 2H_2(g) = C_2H_5CHO(l) + H_2O(l)$	-171.1	-44.4

Hydrogenation reactions of CO_2 have relatively favorable values of $\Delta G°$ because of the produce of water[33].

As mentioned before, the CO_2 molecule is very stable, so that the activation energy is relatively high. Thus, there is a kinetic limitation in the conversion of CO_2. However, the use of catalyst

makes the conversion of CO_2 to methanol, methane and longer hydrocarbon feasible. In addition, it is at a more advantage of industrialization, with the establishment of pilots demonstrating its feasibility.

Several interesting reactions for the conversion of CO_2 involving the use of catalyst are presented in Table 1-3.

Table 1-3. Catalytic process for valorization of CO_2

Process	Reaction	Temperature	Catalysts
Dry reforming of methane	$CO_2 + CH_4 = 2CO + 2H_2$	700-850°C	Rh,Ru/ Al_2O_3,TiO_2, SiO_2 ,MgO,CeO_2, Ni/TiO_2, Ni/MgO
Partial oxidation of methane	$CH_4 + 1/2O_2 = CO + 2H_2$	500- 900°C	Ni/La_2O_3, Ni/CeO_2
Methanol production	$CO_2 + 3H_2 = CH_3OH + H_2O$	220-300°C	Cu-ZnO/Al_2O_3 ZrO_2, Ga_2O_3, SiO_2
Reverse water-gas shift	$CO_2 + H_2 = CO + H_2O$	>350°C	Fe/Al_2O_3,TiO_2,SiO_2
Methanation	$CO_2 + 4H_2 = CH_4 + 2H_2O$	200-500°C	Ni/CeO_2, Al_2O_3

1.1.3 Methanation of carbon dioxide

CO_2 methanation, also called Sabatier's reaction, is the hydrogenation of CO_2, which produce CH_4 and H_2O from the mixture CO_2 and H_2.

$$CO_2 + 4H_2 = CH_4 + 2H_2O \qquad \Delta H = -165 \text{ kJ/mol} \qquad \text{equation 1-4}$$

This reaction is highly exothermic, and take place at high temperatures with the presence of catalysts (Ni, Ru[34]). During this temperature range (200-500 °C), some side reactions could also occur simultaneously other than CO_2 methanation, resulting in some side products, as shown in Table 1-4.

Table 1-4. Possible reactions that could take place in the CO_2 methanation[35]

No.	Reaction	$\Delta H_{298\ K}$ (kJ/mol)	Reaction type
R1	$CO + 3H_2 = CH_4 + H_2O$	−206.1	CO methanation
R2	$CO_2 + 4H_2 = CH_4 + 2H_2O$	−165.0	CO_2 methanation
R3	$2CO + 2H_2 = CH_4 + CO_2$	−247.3	Inversed methane CO_2 reforming
R4	$2CO = C + CO_2$	−172.4	Boudouard reaction
R5	$CO + H_2O = CO_2 + H_2$	−241.2	Reverse water-gas shift
R6	$CH_4 = 2H_2 + C$	74.8	Methane cracking
R7	$CO + H_2 = C + H_2O$	−131.3	Carbon monoxide reduction
R8	$CO_2 + 2H_2 = C + 2H_2O$	−90.1	Carbon dioxide reduction
R9	$nCO + (2n+1)H_2 = C_nH_{2n+2} + nH_2O$		
R10	$nCO + 2nH_2 = C_nH_{2n} + nH_2O$		

The equilibrium constants (K) of the first eight possible reactions (Table 1-4) occurring in the methanation process as a function of temperature using minimization of the Gibbs free energy method is presented in Figure 1-6. K is calculated below by the Van't Hoff equation:

$$\frac{\mathrm{d}\ln K}{\mathrm{d}T} = \frac{\Delta_r H_m}{RT^2} \qquad \text{equation 1-11}$$

One can state that all exothermic reactions are inhibited as temperature increases except for the endothermic reaction of methane cracking (R6). Main side reactions that could take place during the CO_2 methanation process are R1, R3, R4, and R7 due to their high K values in the temperature range 200–500 °C.

Moreover, the carbon deposition will mainly come from the Boudouard reaction (R4) because its equilibrium constant is much larger compared to R6, R7, and R8. In addition, all these reactions may simultaneously occur during the methanation process, so that the selectivity of the product should be paid more attention.

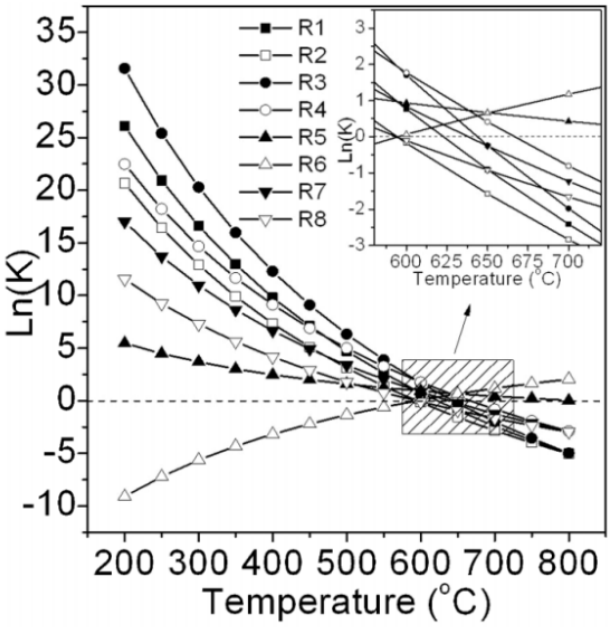

Figure 1-6. The calculated K values of the reactions involved in methanation[35]

Figure 1-7 shows the effect of temperature on equilibrium product composition for a molar mixture of H_2 and CO_2 to be 4:1 at 1 atm. It is clear that low operating temperature (200-250 °C) favor a high conversion of CO_2 and high selectivity of CH_4. However, this requires sufficiently catalysts with high active at low temperature, which is the challenge for developing catalysts. As the reaction is highly exothermic, increasing temperature is unfavorable for the reaction. The concentration of side product CO will increase when the temperature is higher than around 450 °C, due to the reverse water gas shift reaction in which the CO and H_2O are produced by the reaction between CO_2 and H_2. The reverse water gas shift reaction dominates as the temperature is higher than 550 °C, leading to a decrease of mole fraction of CO_2, and the increase of CO fraction in the meantime.

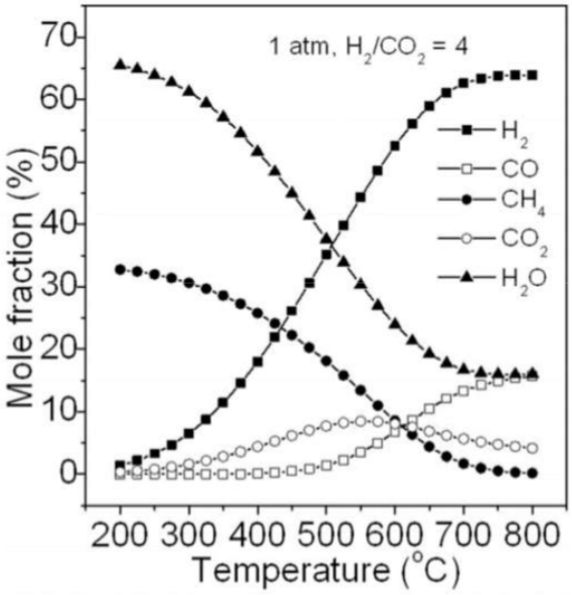

Figure 1-7. The effect of temperature on equilibrium product composition at 1atm[35]

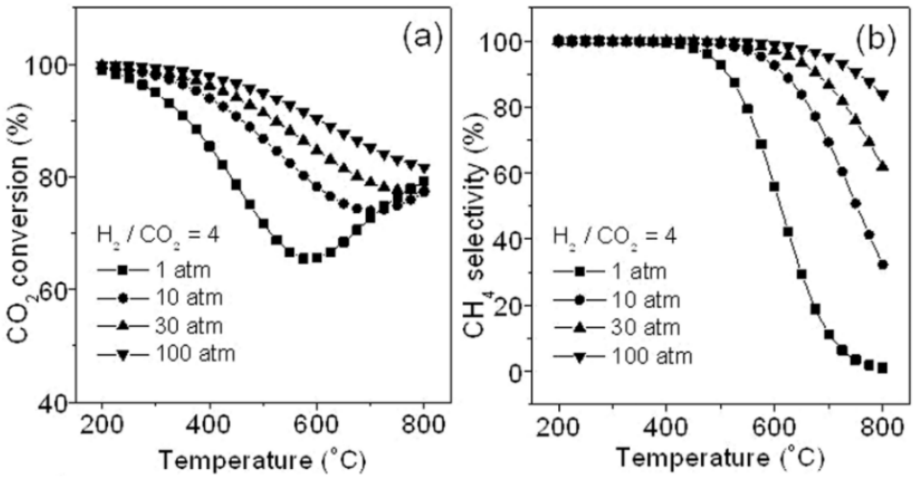

Figure 1-8. Effects of pressure and temperature on CO_2 methanation: (a) CO_2 conversion, (b) CH_4 selectivity[35]

Figure 1-8 shows the effects of pressure and temperature on CO_2 methanation performance with a mole ratio of H_2 and CO_2 at 4:1. It can be seen that in Figure 1-8a, a high pressure leads to a higher CO_2 conversion at the same reaction temperature as CO_2 methanation is a reaction with volume reduced. It can be seen that a high CH_4 yield can be achieved at low temperature and

high pressure. As a conclusion, high pressures and low temperature are favorable for CO_2 methanation. Several researchers got the similar calculation results for CO_2 methanation.[36, 37] These calculations were confirmed by some experiment results.[38, 39]

As mentioned before, the CO_2 methanation is highly exothermic and favorable at low temperature, so there exist two main challenge in methanation process: the development of active catalyst at low temperature and the temperature controlling. In contrary to the calculation, the CO_2 conversion exhibit a low value at low temperature (200-300 °C) because of the kinetic limitation even with the presence of the catalyst. Thus, high active catalysts towards CO_2 methanation should be further developed. In addition, the combination of plasma and catalysis, allows a high CO_2 conversion and high CH_4 selectivity at low temperature (around 220 °C), which is investigated in this thesis. Another challenge for the process is the control of the temperature. The reaction will release plenty of heat as the reaction take place, which will result in the increase of the temperature, thus leading to a decrease of reaction efficiency. So it is a problem of the temperature controlling strategy of the system: how to active the reaction at the beginning and remove the heat released from the reaction during the process.

Furthermore, CO_2 methanation offers an interesting route to produce synthetic natural gas using CO_2 as raw material, which is one of the cheapest and most abundant carbon-containing raw materials in the world. And this reaction could be used to mitigate the CO_2 emission in the atmosphere in order to reduce the greenhouse effect. Exhaust gases from power plants could be used as feed gas for CO_2 methanation[40]. Besides, the CO_2 methanation process could be coupled with the renewable energy process, such as wind and solar power, the electricity produced in these process used to perform water electrolysis to generate hydrogen, which could be used in the CO_2 methanation process. This process offers a “power to gas” approach to utilize excess energy from renewable electricity generation. This coupled process could partially solve the problem of the stabilization and intermittent renewable sources of the electric grids, which account for an increasing part in electricity production. In a word, the CO_2 methanation process could be considered as a chemical storage of excess of electricity produced from the renewable resource.

1.2 CO_2 methanation: A catalytic process

The CO_2 methanation process offers a promising route to convert greenhouse CO_2 to useful chemical CH_4, and this process could be coupled to the industrial process for the production of syngas and the formation of natural gas. Besides, for the long-terms goal, this process has been investigating by the National Aeronautics and Space Administration (NASA) for manned space colonization on Mars.[41] It is possible to convert the CO_2 in the atmosphere of Martian into methane and water for fuel and astronaut life-support systems.[42] However, the CO_2 molecule is very stable, there is significant kinetic limitations in the CO_2 methanation process, thus a highly active catalyst is required to achieve acceptable rates and selectivities.[43] Extensive studies have been conducted to find optimal catalysts for methanation of CO_2 to methane. In this sub-chapter, metal-based heterogeneous catalysts were mainly discussed.

1.2.1 Main characteristics of the catalysts

On the effect of transition or noble metal

CO_2 methanation has been investigated using a number of catalytic systems based on Group VIII metals (e.g., Ru and Rh). The notable catalytic performance is attributed to its unique thermal and structural stability as well as a large BET surface area. Takayuki et al developed a catalyst with Ru nanoparticles loaded on a TiO_2 support ($Ru/TiO_2(B)$), which was prepared by employing a "dry" modification method using a barrel-sputtering instrument, and this catalyst showed high performance for CO_2 methanation. A 100% yield of CH_4 was obtained at 160 °C and the methanation reaction proceeded a reaction rate of 0.04 mmol min^{-1} g^{-1} at room temperature.[44] . Kowalczyk et al. also found that, under a temperature of 220 °C and gas composition (4000 ppm CO_x), the reaction rates of $Ru15/Al_2O_3$ are about 10 times as high as the rates obtained for the Ni-based system in CO_2 hydrogenation.[45] Ruthenium, although more active for CO_2 methanation than nickel, its high cost makes it less attractive for the industrial process. Nickel based catalysts are wildly studied due to its relative high activity and low price. However, the Ni based catalysts deactivated at low temperatures mainly due to the loss of metallic surface, which came from the mitigation of nickel sub-carbonyl ad-species formed

during the reaction.[46] Ni-based catalysts with high stability would be further developed.

The metal loading of a catalyst not only influence the interaction between the metal and the support, but also the nickel dispersion on the support, which further influence the catalytic performance for CO_2 methanation. In general, the number the active sites increase with the metal loading, while the dispersion of the metal decrease with the increase of the metal loading due to the formation of large metallic particles. However, for a Ni-based catalyst, the optimal amount of the Ni loading is dependent on the type of support used.[47-50]

On the effect of support

Although unsupported meatal catalysts exist in some industrial process, for example, Raney nickel used for the hydrogenation of glucose to sorbitol, there are many advantages for the use of support in supported metal catalysts. First of all, the small amounts of the active metal (often expensive) could have a high dispersion on the support. The use of a support could increase the available metal surface area which may result in the increase of catalytic performance. The support provides a structural framework and stabilizes the active species (small metal particles) versus sintering, making the catalyst more mechanically robust. In some cases, the support used in the catalyst could create new active sites (acidic or basic or both) to the system, In a word, the support has a significant influence on the interaction between active metal and support, thus determining CO_2 conversion, CH_4 selectivity in the CO_2 methanation process.[51]Typical support materials include high-surface area, porous, metal oxides (e.g., Al_2O_3, SiO_2, TiO_2, ZrO_2, and CeO_2), zeolites, and carbons.

Amorphous silica extracted from rice husk ash (RHA) has been reported as an active support for Ni catalysts due to its high specific surface area (125–132 m^2g^{-1}), melting point, and porosity.[52, 53] Hydrogenation activity of nickel nanoparticles supported on amorphous silica is better than those on silica gel.[53] Silica-alumina composites were also used as supports for the Ni catalyst.[51, 54] The Ni/RHA–Al_2O_3 had a higher catalytic activity than Ni/SiO_2–Al_2O_3 because of its better metal dispersion and higher chemical reaction rate.

Zeolite and TiO_2 are also wildly used as the supports for Ni catalysts in CO_2 methanation. High

catalytic activity of sorption catalysts based on Ni/zeolite was because of the properties of zeolites, which are chemically active nanostructures and have space for enhancing the sorption properties of the catalysts.[55] Ni nanoparticles (NPs) on a TiO_2 support were synthesized through a deposition precipitation method. The Ni NPs (2.2 nm) had a high dispersion on the TiO_2 surface, with a low Ni–Ni coordination number.[56] Besides, the catalyst with a Ni loading of 15 wt% shows excellent catalytic performance for CO_2 methanation (CO_2 conversion: 96%; CH_4 selectivity: 99%) at a low temperature of 260 °C. The good dispersion of Ni NPs with large unsaturation facilitates a high exposure of active sites is responsible for the enhanced low-temperature catalytic performance.

Tada et al. has studied the influence of various supports (CeO_2, α-$Al2O_3$, TiO_2 and MgO) on Ni catalysts for methanation of CO_2. And the catalyst supported on CeO_2 presented high CO_2 conversion, especially at low temperatures, due to the surface coverage by CO_2-derived species on the CeO_2 surface and the partial reduction of CeO_2 surface.[57] Recently, ceria–zirconia mixed oxides supported catalysts shows high catalytic performance for the CO_2 methanation due to their high oxygen storage capacity and properties to activate CO_2.[58, 59] Ocampo et al. studied $Ce_{0.72}Zr_{0.28}O_2$ supported on Ni catalysts for the conversion of CO_2 to methane.[60] The high oxygen storage capacity of $Ce_{0.72}Zr_{0.28}O_2$ and its ability to enhance nickel dispersion lead to the high catalytic performance. Rauf et al obtained a CO_2 conversion higher than 95% and a CH_4 selectivity of 99% at 400 °C on the ZrO_2−CeO_2-supported catalyst prepared with coprecipitation method.[61] The high performance of this catalyst can be attributed to better metal−support interaction, higher active metal reduction, and an improved crystalline structure.

On the effect of catalyst promotion

In most industrial applications, addition of a second metal to the catalyst has been attempted to enhance catalytic performance, which is called promoter of a catalyst. For example, Fe, Zr, Co, La, Y, and Mg could be used to as a promoter to increase the catalyst activity for CO_2 methanation. The use of a promoter in the metal-based catalyst had a variety of advantages compared to the original catalyst.[62] The addition of MgO into Ni/SiO_2 catalyst played an

important role in increasing the capacity of CO_2 adsorption and accelerating the activation of CO_2.[63] SrO modification enhanced the catalytic activity of Ni/SiO_2, and increased the catalyst stability because of the inhibition of the metallic Ni sintering, while CaO addition negligibly affected the catalyst activity.[64] Appropriate Co metal addition into $Ce_xZr_{1-x}O2$-supported Ni nanosized catalyst can improve catalytic stability of catalysts significantly.[65]

Hwang et al investigated the influence of different promoters on the nickel –alumina xerogel catalyst (35Ni5MAX) for CO_2 methanation.[66] And they found promoters increased the CH_4 yield in an order: 35Ni5FeAX >35Ni5ZrAX > 35Ni5NiAX > 35Ni5YAX > 35Ni5MgAX. 35Ni5FeAX catalyst shows best catalytic performance because it retained the most optimal CO dissociation energy and the weakest metal–support interaction.

La_2O_3 was used to modificate Ni/SiC catalyst as reported by Zhi et al.[62] The addition of La_2O_3 showed several advantages compared to Ni/SiC system. First, CO_2 methanation over Ni–La/SiC begins at 150 °C, which is 50 °C lower than the temperature in Ni/SiC. And the CH_4 yield in Ni–La/SiC is higher at the same temperature with a better stability, due to the effect that the presence of La_2O_3 could restrain the growth of NiO nanoparticles, improve the dispersion of NiO and strengthen the interaction between NiO and SiC.

On the influence of the catalyst synthesis

The choices of preparation method and pretreatment conditions are important in determining the performance of the catalyst.

These parameters are directly related to catalyst activity, selectivity, and stability. Therefore, the preparation method should be carefully chose to produce catalysts with high performance.

Lu *et al.* has reported the influence of preparation method of heat treatment (HT) and conventional solvent impregnation (SI) on the catalytic performance of NiO/SBA-15.[67] The dispersion of NiO particles location was different with low NiO loading, while there was no difference with high NiO loading. In both preparation method, the conversion increase with NiO loading, the location of NiO particles did not influence methanation activity. However, the preparation method influences the temperature to achieve the maximum conversion. In addition,

NiO/SBA-15 had high thermal stability under methanation when prepared by HT method, while NiO/SBA-15 prepared with SI method only showed high thermal stability under high NiO loading.

Zhang *et al.* studied the influence of preparation method on Ni/SiO2 catalysts. They found that the plasma treatment could improve remarkably the dispersion of active components and enhance the reactivity of Ni/SiO_2 catalysts compared to the impregnation method.[68] The conversion of CO_2 and the space–time yield of CH_4 were higher over the catalyst prepared by plasma treatment.

Cai *et al.* reported a simple, low-cost hydration method for the synthesis of $Ce_xZr_{1-x}O2$ with the goal of Ce and Ni enriched on the surface.[69] The impregnation method makes the Ni enriching on the surface of products which enhances the efficiency of active component. These catalysts exhibit significantly high catalytic performance.

1.2.2 Nickel based catalysts

Noble metal, although more active for CO_2 methanation than nickel, its high cost makes it less attractive for the industrial process. Nickel based catalysts are wildly studied due to its good comprise of high activity and low price. In this part, we will show some works using Ni-based catalyst for CO_2 methanation.

Various support has been studied for Ni-based catalyst for the conversion of CO_2 to CH_4, for example CeO_2, ZrO_2, Al_2O3, zeolite, SiO_2, TiO_2, USY, SBA-15. There are some catalysts used for the methanation of CO_2 in Table 1-5.

Table 1-5. Ni-based catalyst for CO_2 methanation in thermal condition

Catalyst	Preparation method	T [°C]	X_{CO_2} [%]	Stability test
5wt% Ni–$Ce_xZr_{1-x}O_2$[69]	Hydration-impregnation	420	75.66	Decreased by 15% after 60 h
5wt% Ni/ $Ce_xZr_{1-x}O_2$[58]	Pseudo sol–gel	350	67.9	Decreased by 15% after 90 h
5wt% Ni–$Ce_xZr_{1-x}O_2$[59]	Pseudo sol–gel	350	80	Decreased by 18.8% after 140 h
10wt% Ni/CeO_2[57]	Impregnation	350	93	-
5wt% Ni/2 wt% CeO_2-Al_2O_3[70]	Co-impregnating boehmite with metal solutions	300	70	Stable after 120 h
12wt% Ni/ZrO_2-Al_2O_3[71]	Impregnation-precipitation	360	69.8	Decreased by 1.6% after 100 h
10 wt% Ni/β-zeolite[72]	Impregnation	360	97	
20 wt% Ni/H–Al_2O_3[73]	In situ reduction of a hierarchical $Ni^{II}Al^{III}$-LDH precursor at 400 °C	300	99	Decreased by 7% after 252 h
20 wt% Ni/γ-Al_2O_3[74]	Impregnation	350	78	Stable after 10 h
35 wt% Ni/5 wt% Fe/ Al_2O_3 xerogel [66]	Single step sol–gel	220	63.4	
15 wt% Ni–La/SiC[62]	Impregnation	360	85	Stable after 70 h
Ni/SiO2[68]	Impregnation method and treated by glow discharge plasma (H_2 atmosphere)	250	90	Decreased by 15.54% after 100 h
15 wt% Ni/TiO2[56]	Precipitation–deposition	260	96	Decreased by 2.9% after 81 h
14 wt% Ni/USY[75]	Impregnation	400	65.5	Stable after 10 h
70 wt% Ni/SBA-15[67]	Heat treatment	300–450	99.2	High thermal stability

1.2.3 CO_2 methanation reaction mechanisms

Although CO_2 methanation is a comparatively simple reaction and has been studied for several decade, there are still arguments on the nature of the intermediate compound formed during the reaction and on the methane formation scheme. There is still no consensus on the kinetics and

mechanism for the reaction. According to literature, the reaction mechanisms could be classified into two main categories: in the first path, CO_2 is first converted to CO as an intermediate, then follows the same mechanism as CO methanation.[76, 77] The other reaction mechanism involves the direct methanation from CO_2 to CH_4, without the formation of CO in the mechanisms, but involves the formation of carbonates and formats during the process.[58] It has been proposed that the rate-determining step is either the formation of the CHxO intermediate and its hydrogenation or the formation of surface carbon in CO dissociation and its interaction with hydrogen.[58, 78, 79]

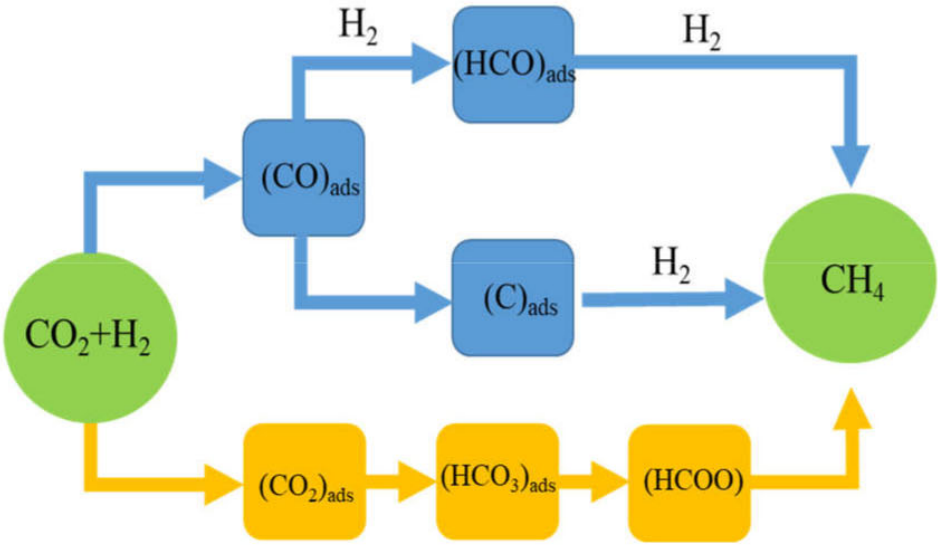

Figure 1-9. Reaction mechanisms of CO_2 methanation[80]

Mechanism involving CO as the intermediate

The mechanism of CO_2 methanation is difficult to determine due to the nature of the catalyst. According to some research, the CO is a important intermediate for the methanation of CO_2. The CO_2 is first converted to CO as the described equation 1-2, and then CO is transferred to CH_4 through the CO methanation route, which is shown in equation 1-4.

$$CO_2 + H_2 = CO + H_2O \qquad \text{equation 1-7}$$

$$CO + 3H_2 = CH_4 + H_2O \qquad \text{equation 1-1}$$

The presence of CO as a key intermediate in CO_2 methanation has been proven by steady-state

transient (SST) studies on a Ru/TiO2 catalyst ,[81] while formate species is fixed on the support, in equilibrium with an active formate species on the interface metal-support. A reaction mechanism is proposed including the formation of the formate through a carbonate species:

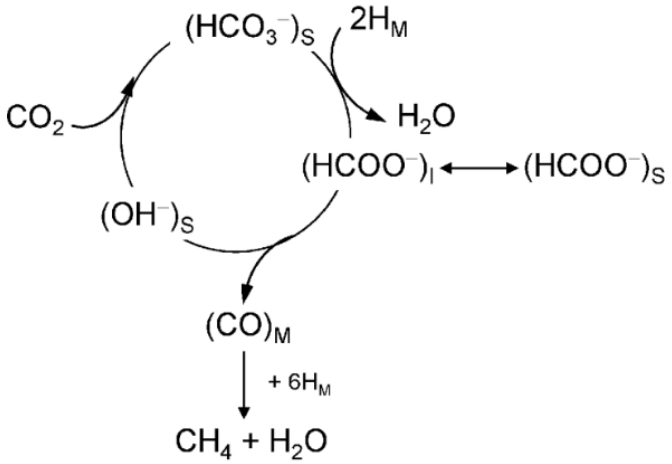

S: the support; M: the metal; I: the metal-support interface.

Figure 1-10. Reaction mechanisms of CO_2 methanation involving CO as the intermediate

Ni single crystals experiments have been performed to demonstrate the presence of CO during the CO_2 methanation. Peebles *et al*. studied the methanation on Ni(100) and found that the activation energy and absolute rates for CH_4 formation directly from CO_2 are very close to the values seen from CO under the same conditions.[82] Moreover, the activation energy for CH_4 formation from CO_2 over a Ni(100) single crystal surface is 21.2 kcal mol^{-1}, and rapid formation of large amounts of CO was observed when the activation energy applied ranges from 17.4 to 19.7kcal mol^{-1}. These results support the mechanism that CO_2 is firstly converted to CO and subsequently to carbon before hydrogenation.

Choe et al. investigated the CO_2 methanation on a Ni(111) surface in a detailed manner using the ASED-MD (atom superposition and electron delocalization-molecular orbital) theory,[83] and the elementary reaction steps considered are:

$$CO_{2,ads} - CO_{ads} + O_{ads} \qquad \text{step (1)}$$

$$CO_{ads} - C_{ads} + O_{ads} \qquad \text{step (2)}$$

$$2CO_{ads} - C_{ads} + CO_{2,gas} \quad \text{step (3)}$$

$$C_{ads} + H_{ads} - Ch_{ads} \quad \text{step (4)}$$

$$CH_{ads} + H_{ads} - CH_{2,ads} \quad \text{step (5)}$$

$$CH_{2,ads} + 2H_{ads} - CH_{4,g}as \quad \text{step (6)}$$

They proposed that CO2 for methanation is converted to CO and then to Cads before hydrogenation. And there are two mechanisms in the CO2 methanation: the carbon formation and the carbon methanation. For carbon formation mechanism, the activation energies for dissociation of CO_2, CO, and 2CO are 1.27 eV, 2.97 eV and 1.93 eV, respectively. As for carbon methanation mechanism, the calculated activation energies are 0.72 eV for methylidyne, 0.52 eV for methylene and 0.50 eV for methane, respectively. Moreover, the calculated activation energy of CO dissociation is higher than that of 2CO dissociation, so the dissociation of CO is assumed as the rate-determining step in the CO_2 methanation process.

Mechanism involving CH_xO as the intermediate

Another mechanism proposed for the methanation of CO_2 is to consider a CH_xO (x=1, 2) as the intermediate, which is then converted to CH_4 without the existence of CO during the reaction route[58, 84].

Aldana *et al*. studied CO_2 methanation on Ni/CeO_2-ZrO_2 catalyst with the use of IR operando spectroscopy, and revealed that the main mechanism does not require CO as reaction intermediate.[58] A proposed mechanism is shown in Figure 1-11.

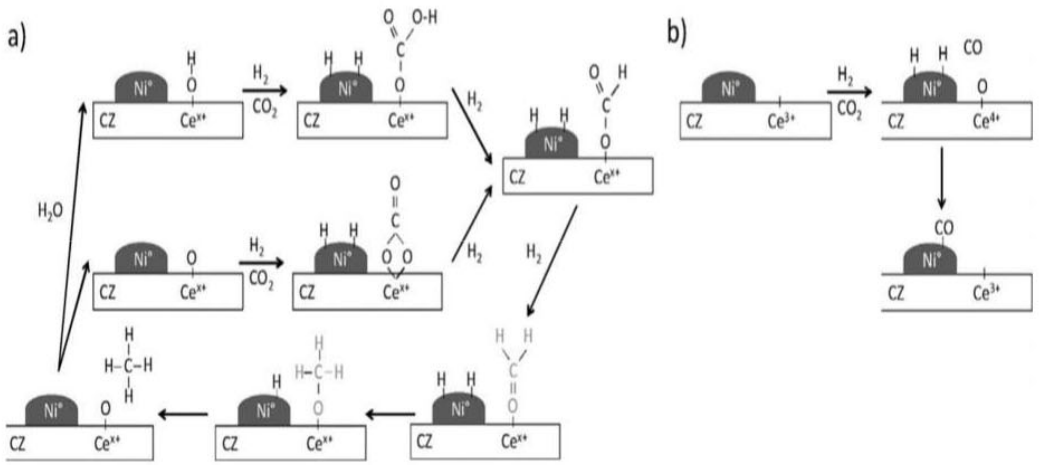

Figure 1-11. Reaction mechanisms proposed on Ni/CeO_2-$ZrO_{2\ sol\text{-}gel}$ catalyst: (a) CO_2 methanation; (b) CO formation

In this mechanism, there is any evidence of the existence of CO as an intermediate (Figure 1-11a). CO_2 is firstly adsorbed on the mild basic sites to form covalent carbonates, hydrogen carbonates and then bidentate carbonates. These species are further reduced and hydrogenated by H atoms formed by dissociation of hydrogen at the surface of Ni_0 particles to form formate species and then probably formaldehyde-type and methoxy species (not observed) and to finally produce CH_4. This mechanism involves weak basic sites of the support for the adsorption of CO_2 and implies a stable metal-support interface. Besides, they proposed that a parallel pathway may exist (Figure 1-11b) where CO is formed by a redox cycle on reduced ceria.

Moreover, Mikhail *et al.* studied the CO_2 methanation on NiCeZr catalyst in plasma conditions, and proposed a mechanism, as shown in Figure 1-12.[84] The CO_2 is chemisorbed on the surface of the support, and activated in its bent configuration, leading to the formation of monodentate and bidentate carbonates. At the same time, the dissociation of H_2 takes place on the metallic Ni-sites.

From these sites and upon oxygen transfer yielding NiO and two electrons, it can migrate to the vicinity of the carbonate-occupied sites on the support, forming first hydrogeno-carbonates, then formate species, and finally methane and water, the reaction products.

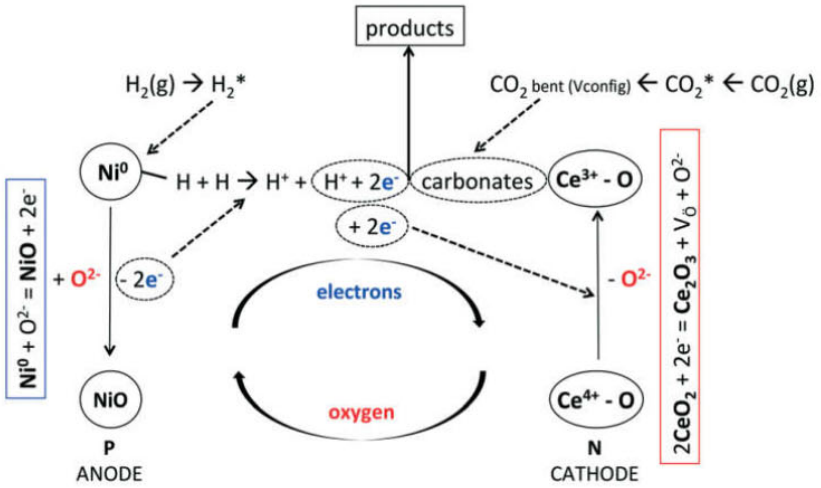

Figure 1-12. General schema of the plasma-catalytic cycle proposed for CO_2 methanation on the NiCeZr catalyst.

1.3 The Plasma

1.3.1 What is a plasma?

Plasma is considered as the fourth state of matter, and was first described by chemist Irving Langmuir in the 1920s.[85] Plasma could be seen as a partially or wholly ionized gas, therefore plasma could be created by any gas while a large amount of energy is applied (by heating or subjecting the gas to a strong electromagnetic field), resulting in charged ions and electrons. In spite of the existence of the charged particles, plasmas as a total are neutral. However, compared with the gas, plasma is more active in chemical reactions due to a combination of active spices. As mentioned before，plasma could be partially or fully ionized gas based on the energy applied. Neon signs and lightning are examples of partially ionized plasmas. The Earth's ionosphere is a plasma and the magnetosphere contains plasma in the Earth's surrounding space environment. The interior of the Sun is an example of fully ionized plasma, along with the solar corona and stars.

Plasma could be divided into two main categories in terms of electron temperature: thermal plasma and non-thermal plasma (NTP), which are also known as equilibrium and non-equilibrium plasma, respectively. The main characteristics of plasma are presented in Table 1-

6.[86] In thermal plasma, inelastic collisions between electrons and heavy particles create the plasma reactive species, while elastic collisions heat the heavy particles (the electrons energy is thus consumed). The difference in non-thermal plasma is that heavy particles are slightly heated by a few elastic collisions ,and this is why the electrons energy remains very high.[87]

Table 1-6. Main characteristics of plasma

(T_0-gas temperature, T_i -ion temperature, T_r-rotational temperature, T_v-vibrational temperature, T_e-electron temperature)

Properties	**Thermal plasma**	**Non-thermal plasma**
Temperature	$T_0 \approx T_i \approx T_r \approx T_v \approx T_e \leq 2\times10^4$K	$T_0 \approx T_i \approx T_r < T_v << T_e \leq 10^5$K
Density	High electron density: 10^{21}~10^{26} m^3	Low electron density $<10^{19}$ m^3

Thermal plasma

Thermal plasma, which is also called hot plasma, achieve a local thermodynamic equilibrium, mainly because electron temperature is similar to the gas temperature in a high-temperature plasma. Normally, the energy is firstly transferred to electrons over acceleration by a heating or an applied electric field, then transferred to heavy particles through collisional process. With an equilibrium temperature determined by collisions processes, could be assumed as the single temperature of the thermal plasma. Indeed, for thermal plasma, the electron temperature along with energy content is very high and equals to heavy particle (neutrons, protons, etc) temperatures. Thermal plasma is also characterized by higher power and higher density as well as low selectivity for chemical process.[88] The relationship of the particle temperature in thermal plasma is shown in Table 1-6. Moreover, the ionization degree, which is the ratio of charged species density in the plasma (equation 1-12), is very high in thermal plasma, that is to say, the thermal plasma is almost complete ionized.

$$X=n_e/(n_e+n_0) \qquad \text{equation 1-12}$$

n_e : number density of electrons, $1/m^3$

n_0 : number density of neutrals, $1/m^3$

Non-thermal plasma

Non-thermal plasma is also named as cold plasma, and is characterized by different temperature related to various plasma species. The plasma dose not reach the thermal equilibrium because the electron number density is not high enough when compared with heavy particle to achieve sufficient energy transfer between them. The temperature order of species in non-thermal plasma is presented in Table 1-6. Generally, in non-thermal plasma, the electron temperature is about 11600 K (1 eV), while the gas temperature is usually around room temperature (300-2000 K).[86, 88]

Non-thermal plasma contains ionized and excited states of atoms and molecules and radicals not normally present at thermal equilibrium at ambient temperatures, it possesses reactive properties that are only seen in combustion systems and thermal discharges at much higher temperature (> 1000 K). Thus non-thermal plasma has a promising potential for chemical process performed at low temperatures, which is not normally possible in a conventional thermal equilibrium system.[89]

The plasma studied for the utilization in chemical process is commonly recognized as weakly ionized with an ionization degree around 10^{-7}~10^{-4}. The DBD plasma used in this research in also weakly ionized.[90]

Based on the generation mechanism, there are several types of non-thermal plasma, from example: dielectric barrier discharge plasma, corona discharge plasma, glow discharge plasma, radio frequency discharge plasma, microwave discharge plasma and so on.

The nature of plasma makes it electrically conductive, internally interactive and strongly sensitive to electromagnetic.[91] There are several major advantages for the utilization of plasma: first of all, the plasma could create very high temperature and high density compared with the conventional chemical process. Besides, there are high concentration of energetic and

chemically active species in the plasma condition, such as radicals, ions, electrons, atoms and photos. Moreover, in the plasma condition, the gas temperature could be lower as room temperature while providing lots of chemical active species.

1.3.2 Utilization of plasma for CO_2 utilization

In recent years, various type of plasmas have been successfully applied to convert CO_2 into value-added chemicals or fuels,[92] such as gliding arc (GA) plasma,[93] microwave (MW) plasma,[94] and dielectric barrier discharge (DBD) plasma.[95]

The MW and GA discharges are typical 'warm plasma', which operates at the boundary of both thermal and non-thermal plasma, and therefore shares their properties. The MW and GA discharges are non-equilibrium discharges, and they can not only provide (re)active species, but also offer some controlled level of translational temperature. Of course, this translational gas temperature is still much lower than the electron temperature, however it is a lot higher than room temperature and can easily reach up to 2000–3000 K. As a result, these warm plasmas can take the advantage of a non-equilibrium condition, and they can also influence the chemical kinetics of the reaction due to the high gas temperature in the meantime, so that they are promising plasmas for the conversion of CO_2.[96]

DBD plasma is a typical example of a non-thermal plasma. In the DBD plasma, the gas temperature is more or less at room temperature, while the electrons are heated to temperatures of 2–3 eV (20 000–30 000 K) by the strong electric field in the plasma.

Gliding arc plasma

Gliding arc (GA) plasmas are potential plasma sources for gas conversion[97, 98] because they offer benefits of both thermal and non-thermal discharges. The plasma is weakly ionized and characterized by the lack of local thermodynamic equilibrium since the energy of the electrons is markedly higher than that of the heavy species. Moreover, they are characterized by a better energy efficiency than other types of plasmas due to the efficient vibrational excitation of the molecules provided in these plasmas, which is seen as the most energy-efficient way to split

CO_2 molecules.

G.M.El-Aragi *et al.* created a GA discharge at high atmospheric pressure, the system consists of two electrodes, one of which connected to the ground and the other connected to the high voltage power supply, as shown in Figure 1-13.

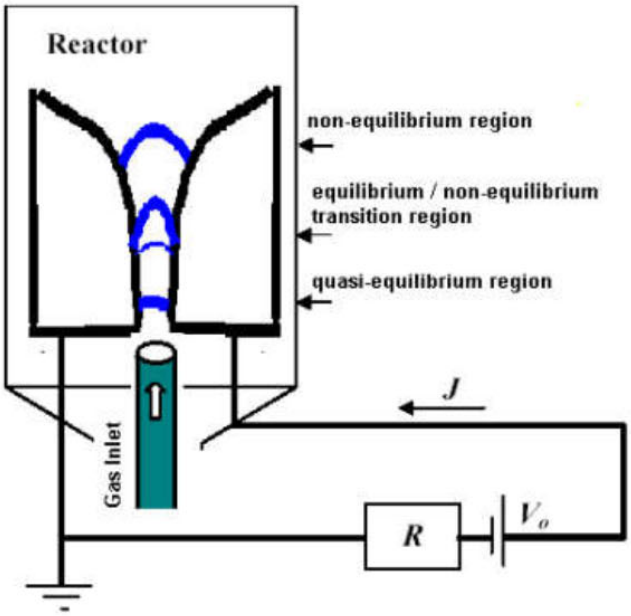

Figure 1-13. A scheme of gliding arc discharge operating in atmospheric pressure air[93]

The performance of CO_2 decomposition via gliding arc plasma at atmospheric pressure was studied by Antonius *et al.*[99] N_2, O_2, air, and H_2O were used to study the dilution effects on CO_2 conversion. The main product was CO and O_2. The conversion of CO_2 increased with an addition of N_2, while water in the plasma reaction decreased CO_2 conversion.

A combined gliding arc plasma experimental and 2D modelling approach research was studied by Wang *et al.* for the conversion of CO_2 to CO and O_2.[100] Compared with classical thermal conversion, as well as other plasma-based technologies for CO_2 conversion reported in literature, they demonstrate the non-equilibrium character of the gliding arc, because the electron temperature is much higher than the gas temperature, and the highly energetic electrons can induce several different chemical reactions. Thus, indicating that the gliding arc is a

promising plasma technology for CO_2 conversion.

To gain an insight into conversion of CO_2 in GA-based warm plasma, a magnetically driven GA plasma was created by Liu *et al.* to study GA characteristics and reaction mechanism.[101] The maximum rate towards the production of CO was achieved at the stoichiometric ratio ($H_2/CO_2 = 1$), and this is 10 times higher than that in pure CO_2 case.

Microwave plasma

Microwave (MW) plasma is mostly used for the conversion of CO_2 into value-added chemicals or fuels because of the high energy efficiencies reported under some conditions.[86, 102-104] The conversion of CO_2 have been studied in pure CO_2,[105] or in combination with CH_4[94, 106] (i.e., dry reforming), H_2O,[107] or an inert gas.

Silva et al. studied microwave pulsed discharge used for dissociation of CO_2,[105] and are characterized by several non-intrusive plasma characterization methods based on optical emission spectroscopy. It is confirmed that the vibrational excitation caused by electron impact is a key factor in the CO_2 dissociation process in this type of plasma. The CO_2 is first converted to CO and O ground state species formation, as well as to a possible further excitation of these species through the secondary electron impact.

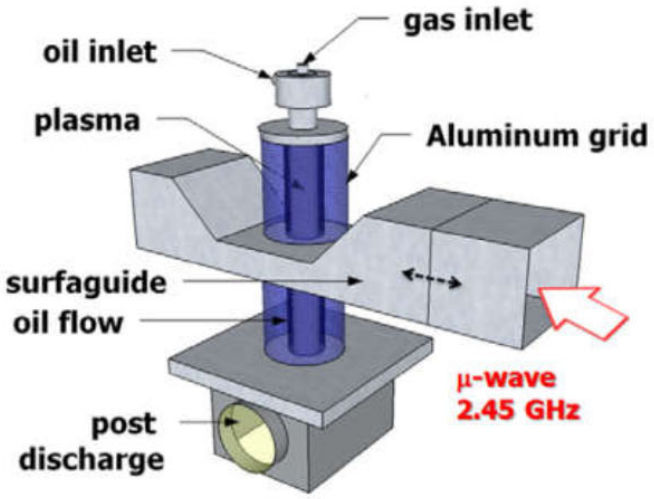

Figure 1-14. A scheme of microwave pulsed discharge for the conversion of CO_2[105]

The study of conversion of CH_4 and CO_2 in a pulsed microwave plasma under atmospheric pressure is performed by Zhang *et al*,[94] and demonstrate that this type of plasma is useful for oxidative coupling and reforming of CH_4 with CO_2 in C1 chemistry. Under the flow rate of 200 mL/min (CH_4/CO_2=1.5:1) with a peak microwave power consume of 120 W and pulse duty factor of 100/100 ms, conversions of CH_4 and CO_2 are 70.8% and 68.8%, respectively, and with selectivities of CO, C_2H_2, C $_2H_4$ are 75%, 17.8% and 4.1%, respectively. Besides, there is no carbon deposits in the reaction. Ratio of H_2/CO in the product increases with the CH_4 concentration in the feed gas, and the H_2/CO ratio of 2 could be achieved at a ratio 2:1 of CH_4 to CO_2, which is acceptable for Fischer-Tropsch and other synthesis processes. The energy efficiency of the pulsed microwave plasma is found obviously improved.

Dielectric barrier discharge (DBD) plasma

Dielectric barrier discharge (DBD) plasma is the widely used for the conversion of CO_2.[95, 108, 109]. Some research are concentrated on the CO_2 pure splitting,[95, 110] while in other research, a co-reactant, such as CH_4[111], H_2O[112], and H_2[72], is used together with CO_2 to convert it to other useful chemicals.

Paulussen *et al.* studied the conversion of carbon dioxide to value-added chemicals in atmospheric pressure dielectric barrier discharges.[95] The discharge obtained in CO_2 is characterized as a filamentary mode with a micro-discharge zone in each half cycle of the applied voltage. And they found the CO_2 conversion and CO yield are both higher at low flow rate. The maximum CO_2 conversion of 30% is obtained at a flow rate of 0.05 L /min, with a power density of 14.75 $W \cdot cm^{-3}$ and a frequency of 60 kHz. The most energy efficient conversions are achieved at a flow rate of 0.2 L/min, a power density of 11 $W \cdot cm^{-3}$ and a discharge frequency of 30 kHz.

The DBD plasma-catalytic process for methanation of CO_2 was investigated by Jwa *et al* using Ni/zeolite pellets.[72] In the plasma-assisted condition, a CO_2 conversion of 96% was observed at 260 °C, which is 100 °C lower than the temperature in conventional process to obtain the same CO_2 conversion value. They proposed that the reactive species generated in the plasma

condition could help to speed up the rate determining step of the catalytic hydrogenation. In their hypothesis, the CO_2 was first converted to CO as an intermediate on the active site, and the dissociated species react with hydrogen to produce CH_4. Moreover, the conversion of CO_2 was found to be less than 1% in the absence of Ni (bare zeolite), implying that the zeolite support together with the plasma cannot efficiently convert CO_2 into CH_4.

Other types of plasma

Besides the above three main discharge types for CO_2 conversion, some other plasma discharge are also applied for this aim. These include radio frequency (RF) impulse discharge[109], , several different atmospheric pressure glow discharges (APGD), corona discharges, spark discharges and nanosecond pulsed discharges.

Corona discharges occur near sharp points edges or thin wires (used as an electrode) when a sufficiently large electric field is applied. An advantage of corona discharges compared to DBDs is their ease of establishment, however, their performance in CO_2 conversion processes is quite similar.[96] Guo *et al.*[113] applied a negative DC corona discharge for the reaction of CO_2 and H_2O, varying the water vapor content and the pressure. The CO_2 conversion decreased with the increase of gas flow rates (hence decreasing SEI) and water content. The main products in this process were ethanol and methanol, in roughly a 3 : 1 ratio, and the maximum CO_2 conversion was 16% at 1bar, while H_2 and CO were also detected in the product. Besides, increasing the pressure had a positive influence on the methanol and ethanol yields.

When a streamer is able to connect two electrodes, without the presence of a pulsed power supply or the presence of a dielectric, the current will further develop as a spark discharge. Spark discharges have been applied for DRM, but the developments are rather new and limited to date.[114-119] A pronounced increase in total conversion with the SEI was found in the literature. Besides, the energy consumed is between 3 and 10 eV per molecule, while the best performance (a total conversion of 85%) was obtained at an energy cost of barely 3.2 eV per molecule.[114] In addition to H_2 and CO, C_2H_2, C_2H_4 and C_2H_6 were also formed in the product stream.[115] Higher conversions were reported when the pressure was increased, i.e. up to 2.5 bar, or when

the interelectrode distance rise from 3 to 9 mm.[116]

The atmospheric pressure glow discharges (APGD) has some similarities with DBD and corona discharges. The main advantage of APGDs is the absence of vacuum conditions compared to with regular glow discharges, and also operating without elevated temperatures. This discharge is interesting for DRM due to its high electron density and proper plasma temperature for vibrational excitation. The highest obtained conversions

are respectively 99% and 90% for CH_4 and CO_2, while the main products are H_2 and CO.[120] According to the research available,[96] the best performance was achieved at an energy cost of only 1.2 eV per molecule, whereas a total conversion of 89% was obtained. Moreover, there was a clear trend that both the conversion and energy cost show a clear increasing trend with the SEI.

1.3.3 Introduction to dielectric barrier discharge (DBD) plasma

Dielectric barrier discharge (DBD) plasma is also called 'silent discharge', have been studied for more than 100 years. The first experimental investigations for the application of DBD plasma were reported by Siemens in 1857 to generate ozone.[121]

DBD plasma is strongly non-thermal plasma, and can be created at atmospheric pressure. The voltage is supplied by a sinusoidal AC voltage with the frequency range from 0.05-500kHz, and DBD plasma could be created under various gases at relatively high discharge powers.[90] The discharge type created depended on the gas composition, the voltage and frequency excitation, and could be filamentary or glow discharges.[122] DBD plasma could create high density active species (radicals, electron and ions) while has a moderate gas temperature, which is a promising technology for the conversion of CO_2.

The configuration of DBD plasma consists of two plane-parallel or concentric metal electrodes, and it contains at least one dielectric barrier (e.g. glass, quartz, ceramic material or polymers) in between the electrodes.[123] And the normally used dielectric barrier materials are glass, quartz, ceramic material and polymers. The use of the dielectric barrier could restrict the electric current, and thus to prevent the formation of sparks and/or arcs inside the reactor.[87] The

(discharge) gap between dielectric barrier can typically vary from 0.1 mm (e.g. in plasma displays), to over 1 mm (e.g. for ozone generators) to several cm (e.g. in CO_2 lasers).[123, 124] Some typical planar (top) and cylindrical (bottom) DBD configurations are presented in Figure 1-15.

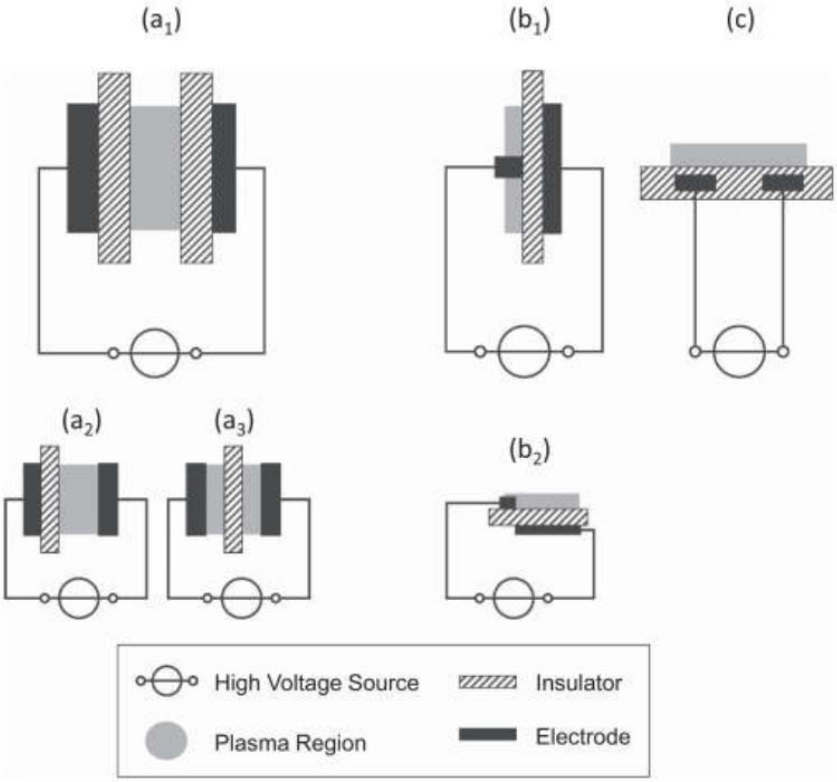

Figure 1-15. Typical DBD configurations[125]

To ignite the plasma, an electric field high enough needs to be applied to cause breakdown in the gas. This breakdown voltage (Vb) can be calculated according to Paschen's Law, and is a function of the pressure (p) and the gap distance (d).

$$V_b = \frac{D \cdot pd}{\ln\left(\frac{C \cdot pd}{\ln(1/\gamma)}\right)} \qquad \text{equation 1-13}$$

where C, D and g are the gas (or mixture) specific parameters.

It is stated that the in the DBD plasma, the gas is partially ionized. And the plasma volume accounts for about 1–10% of the total gas volume[126, 127]. The rest of the gas is not ionized and serves as background reservoir to absorb the energy dissipated in the micro-discharges and to

collect and transport the long-lived species created in the micro-discharges.[121]

As mentioned before, the DBD plasma could be applied to the conversion of the CO_2 to useful chemicals. This part is more concentrated on the conversion of CO_2 through CO_2 methanation process. However, due to the kinetic limitation of this reaction, an active catalyst is always combined with DBD plasma, so called plasma-catalytic process, to increase the CO_2 conversion and CH_4 yield.

An example of DBD plasma for the CO_2 methanation was performed by Nizio *et al*,[128] they investigated the CO_2 methanation process in a packed-bed DBD with Ni-$Ce_xZr_{1-x}O_2$ catalysts for a stoichiometric H_2/CO_2 ratio of 4:1. They found the CO_2 methanation could not take place under lower temperature in DBD plasma (in absence of catalyst), while a CO_2 conversion of 78% with a CH_4 selectivity of 99% was achieved when adding the active catalyst at the same condition. This demonstrated that in plasma-catalytic systems, CO_2 methanation could take place at low temperature (Tg <260 °C), and there is the chance to increase both CO_2 conversion and CH_4 selectivity for CO_2 methanation in this system.

More details about the plasma-catalytic system for the methanation of CO_2 is presented in following part.

1.4 Hybrid plasma-catalytic process for CO_2 methanation

1.4.1 Plasma-catalysis system

As described before, catalysis and plasma are effective technologies for the conversion of CO_2 to useful chemicals. To overcome the drawbacks of these technologies, their combination, called plasma-catalysis, has been studied by plenty of researchers. Plasma-catalysis is an emerging technology at the interface of various disciplines, such as physical chemistry, material science, nanotechnology, catalysis, plasma physics and plasma chemistry. The objective is to enhance the plasma reaction by adding an active catalyst in the system and vice versa.

In the conventional thermal catalysis process, reactant molecules are dissociatively absorbed on the surface of the catalyst with energy supplied with heat. However, in the plasma-catalysis

process, molecules are activated by the plasma due to excitation, ionization or dissociation by electrons in the gas phase or on the catalyst surface.

There are two main configurations between plasma and catalyst, as presented in Figure 1-16. The first one is called two-stage configuration (Figure 1-16b), in this system, the plasma zone and catalyst are spatially separated from each other, and the main configuration is that the catalyst is at downstream of the plasma zone. The second configuration is one-stage configuration, and the catalyst is placed in the plasma zone. The main difference of these two configurations is the type of the species that react on the surface of catalyst. In the two-stage configuration, only the products and long-lived intermediates created in plasma zone will interact with the catalyst, while in the one-stage configuration, catalyst can not only interact with products and long-lived intermediates, but also interact with all the short-lived species, for example excited species, radicals, photons and electrons. Besides, in this configuration the catalyst and plasma could have an effect on each other, as will be described in the following part. Moreover, there are also a few research studies on multi-stage plasma catalysis process,[129, 130] in which several different catalysts could be placed to treat different components of the gas stream.

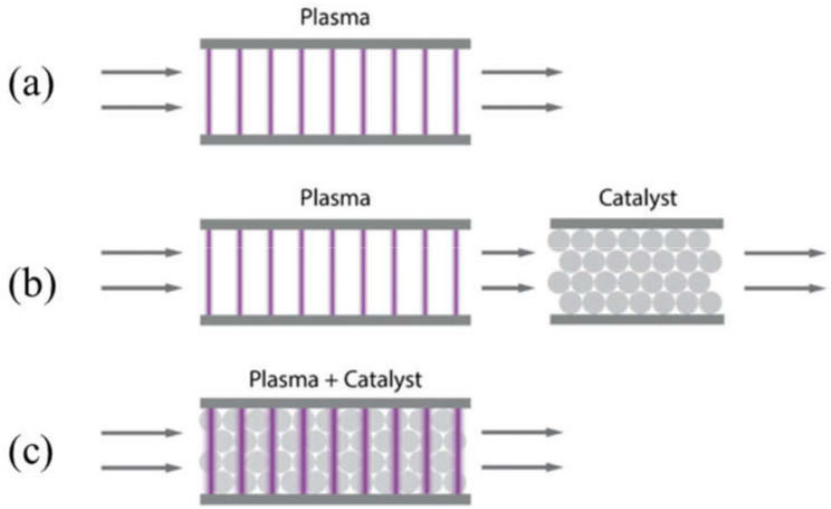

Figure 1-16. Schematic of the different plasma-catalysis configurations: (a) plasma alone without a catalyst, (b) catalyst at the downstream of the discharge, and (c) catalyst directly inside the discharge zone[96]

The advantage of one-stage configuration makes it interesting for the conversion of CO_2. In this configuration, the catalyst is placed in the plasma zone. The catalyst could be introduced in the discharge in the form of pellets, (fine) powders, foams, honeycomb monoliths, various electrode materials and electrode coatings. The ease of adding the catalyst into the discharge zone greatly varies depending on the type of plasma reactor used. In general, the combination of a catalyst with DBD reactor is very interesting, because it is easy to add the catalyst into the reactor due to the simple geometry, and this system could work at a temperature even lower as room temperature.

1.4.2 Plasma catalyst interaction

In the case of DBD plasma, catalysts are usually used as powders and placed between the electrodes. This is a very simple configuration and it is easy to put catalyst in the plasma reactor. And it has been noted in the case of dry reforming of CH_4 with CO_2 that the particle size, the amount used, and the way of catalyst packed in the reactor have a significant effect on the performance of the plasma-catalyst processing.[131] However, main drawbacks of this DBD plasma-catalysis reactor are the difficulty to scale-up and the pressure drop due to the packing. Some other types of plasma reactor have the particular problem on introducing the catalyst in the plasma zone, especially for the case of gliding arc discharge reactor. Schmidt-Szaloskwi *et al.*[132] came up a novel method including the use of a sprouted bed to solve this problem. In this reactor, the catalyst powers are lifted to the discharge region by the gaseous reagents introduced from the bottom of the reactor.

The interaction between plasma and catalyst for the conversion of CO_2 often results in improved process in terms of conversion, selectivity, yield and energy efficiency. The complex interaction could be divided into two categories: effects of catalyst on plasma, and *vice versa*, effects of plasma on catalyst. Moreover, it is important to distinguish the type of the effect: physical and chemical effects. Besides, the physical effects are responsible for the better energy efficiency, while the chemical effects mainly result in a higher selectivity toward the preferred products.

Possible synergisms in plasma-catalysis system are presnented in Figure 1-17. Effects of catalyst on plasma when adding the catalyst have been reported: (i) an enchancement of electric

field through the geometric distortion and surface roughness; (ii) the formation of micro-discharges inside the pores of the catalyst material, because of the very strong electric field inside the pores; (iii) the change in discharge type, due to the the presence of insulating surfaces, which could promote the development of surface discharges; (iv) the adsorption of species on the catalyst surface, and this influence the concentration and reation performance due to a longer residence time.

Besides, the effects of catalyst on plasma could be considered as physical effects, while the effects of plasma on catalyst are physical and chemical effects. And these effects are: (i) Changes in the physico-chemical properties, for example, a higher adsorption probability at the catalyst surface, a higher catalyst surface area, a changed catalyst oxidation state, the reduction of metal oxide catalysts to their metallic form, reduced coke formation on the surface and a change in the catalyst work function; (ii) The formation of hot spots on the surface due to the formation of strong micro-discharges in the reactor; (iii) Catalyst activation by photon irradiation emitted by the excited plasma species; (iv) Lower activation barriers because of the existence of more reactive vibrationally excited plasma species and therefore a greater possibility for non-adiabatic barrier crossings; (v) Changes in the reaction pathways due to the presence of a wide variety of (re)active species.

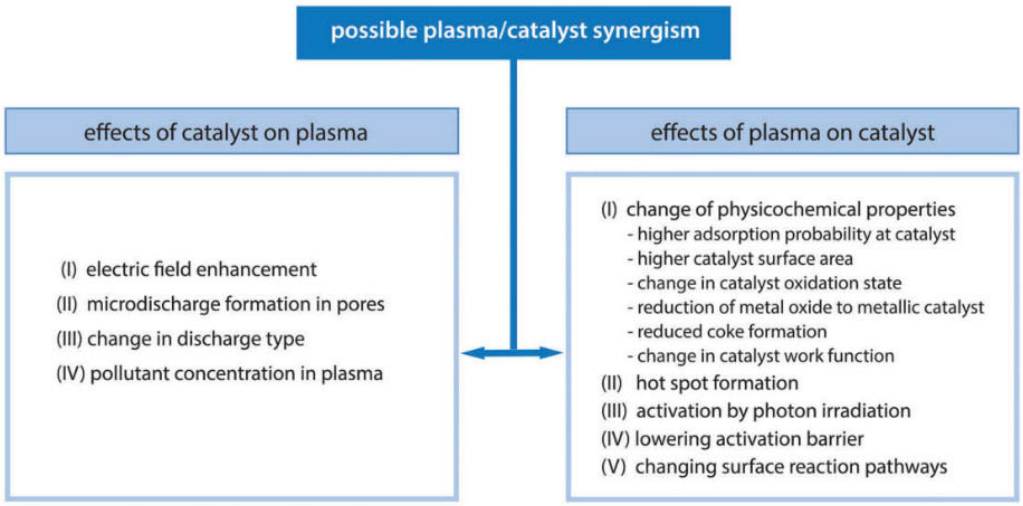

Figure 1-17. Possible synergism in plasma-catalysis system[96]

1.4.3 Plasma-catalytic process for CO_2 methanation

As discussed before, plasma-catalytic process have several advantages for the gas purification, and is a promising technology for the mitigation of CO_2 in the atmosphere. Various Ni-based catalysts have been coupled with plasma for CO_2 methanation, as shown in Table 1-7.

Table 1-7. Plasma-catalytic process for CO_2 methanation in the literature

Catalyst	Plasma type	T (°C)	Power (W)	X_{CO_2} (%)	S_{CH_4} (%)
Ni/USY zeolite[133]	Glow discharge	-	-	60	<1
Ni/Zeolite-Ce[134]	DBD	-	25	76	98
Ni/zeolite [72]	DBD	260	-	96	-
Ni-$Ce_{0.58}Zr_{0.42}O_2$[128]	DBD	100	-	80	100
Ni-Ce-Zr-HT [16]	DBD	230	-	80	65
Ni/Mg/Fe/Al-HT[135]	DBD	-	18	75	-

Azzolina-Jury and Thibault-Starzy[133] studied the mechanism of CO_2 methanation under glow discharge plasma conditions at low pressure over a Ni/USY zeolite catalyst by Operando time-resolved FTIR spectroscopy. In the plasma condition 60% of CO_2 conversion was achieved while CO was the main product with a selectivity of 99%. A relatively low amount of CH_4 was generated in gas phase, but a proper catalyst could enhance CH_4 selectivity. They supposed that CO_2 was first dissociated into CO under plasma condition, and then carbonyls generated from adsorption of CO molecules as well as from formate species are consecutively hydrogenated to form CH, CH_2 and CH_3 species on nickel, which were precisely detected using FTIR. Finally, CH_4 and H_2O are formed and desorbed from the nickel surface.

DBD plasma-assisted CO_2 methanation using zeolite-based catalysts was performed by Bacariza et al.[134] The influence of plasma on the performances of Ni based Cs-USY zeolites

with different Si/Al ratios (3 and 38) and also containing Ce were evaluated. It was observed that in plasma process, higher Si/Al zeolites led to lower affinity to water, decreasing the inhibition effect of H_2O on the CO_2 methanation activity, and plasma was responsible for the removal of the H_2O from the surface of catalyst. Moreover, the addition of Ce as a promoter enhanced the catalytic performances, especially under plasma conditions, enhanced activation of CO_2 over CeO_2 species.

Jwa et al studied the performance of Ni/zeolite for the CO and CO_2 methanation in DBD plasma catalytic process.[72] It was demonstrated that conversions of CO_2 into CH_4 could be promoted in the presence of plasma as compared with the results that obtained in the thermal activation of Ni/zeolite only. In plasma-catalytic process, a CO_2 conversion of 96% could be achieved at 260 °C, while in thermal condition, the temperature to obtain the same conversion was high as 360 °C. And the CO_2 conversion increased when Ni loading increased from 2.5% to 10%. It is presumed that reactive chemical species created in plasma can change the rate-determining-step of the catalytic hydrogenation. Moreover, the phenomenon that Ni particles were dispersed more uniformly after the plasma reaction was also observed.

Nizio et al performed CO_2 methanation in the plasma catalytic process with a Ni based catalyst.[128] And it was clearly demonstrated that the hybrid plasma catalytic process is active at low temperature ($T < 260$ °C) on the conversion of CO_2 into CH_4. Three catalysts were prepared using 15 wt% of Ni loading over ceria-zirconia mixed oxides having different Ce/Zr ratios. Among them, the catalyst 15NiCZ5842 presented enhanced methanation performance because of the presence of low and medium strength basicity together with a better dispersion of Ni-species, at high ZrO_2 contents on the mixed oxide support. Moreover, the activity of Ceria and Zirconia-promoted Ni-containing hydrotalcite-derived catalysts was also performed in a hybrid plasma-catalytic process for methanation of CO_2 at low temperatures and in the presence of the dielectric barrier discharge (DBD) plasma by them.[16] High methane yields, around 80%, were measured under hybrid plasma-catalytic conditions, even at very low temperatures (110 °C, adiabatic conditions). It was observed that the addition of Ce and Zr did not result in a noticeable improvement of the catalytic activity.

Chapter II: Catalysts Synthesis, Materials and Methods

2.1 The preparation of the ceria-zirconia supported catalyst

The catalyst used in this study was chosen because it already showed very promising results in plasma-methanation process.[16, 84, 128, 136]

This catalyst was prepared by a conventional wet impregnation method, commercial ceria-zirconia mixed oxide $Ce_{0.58}Zr_{0.42}O_2$ (Rhodia Solvay) was used as a support. The support was impregnated with an aqueous solution of nickel nitrate hexahydrate ($Ni(NO_3)_2 \cdot 6H_2O$, Aldrich) as a metal precursor. The nickel loaded for the catalyst was fixed as 15 wt%. After the impregnation, the catalyst was dried overnight at 80°C and subsequently calcined at 550°C for 4 h in air.

Three catalysts in different particle sizes were then made in following procedure: First, original catalyst powers were pressed into a tablet with a mold, and then the tablet was crushed into small pieces, finally catalyst particles were separated into different sizes with several meshes (250μm, 325μm, 500μm), finally, three types of catalytic particles were obtained: C1 with particle size below 30 μm (original size), C2 with particle size between 250 μm and 325 μm, and C3 with particle size above 500 μm.

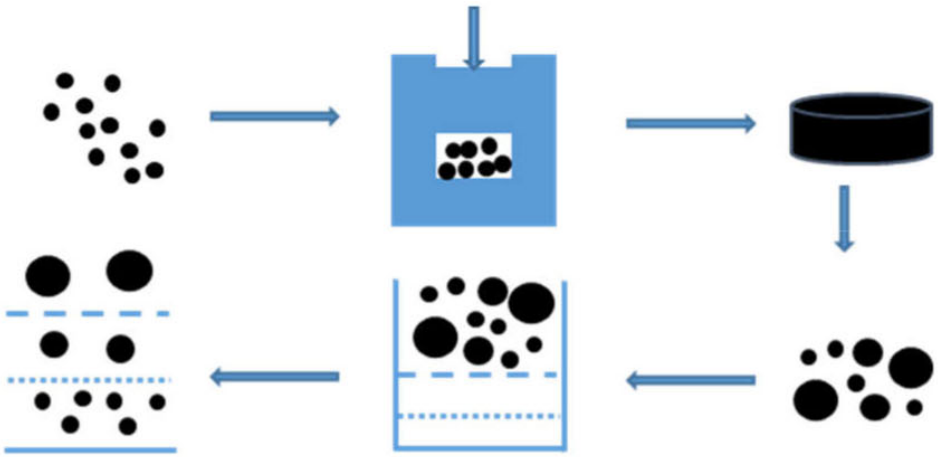

Figure 2-1. The process to make different sizes of catalyst particles

2.2 Characterization of catalyst

Several physico-chemical characterizations, presented below, were carried out in order to verify the textural and structural properties of the catalyst.

Surface Area measurement by Brunauer-Emmett-Teller (BET) technique

Textural properties were studied in using N_2 adsorption–desorption method. First, the sample was pretreated at 200 °C for 2 h under vacuum conditions before measurement. Then the test was performed in a Belsorp Mini II apparatus (BEL Japan) instrument under liquid nitrogen temperature (−196 °C). The specific surface area was calculated based on the Brunauer–Emmett–Teller (BET) method, and the pore volume and diameter were calculated using the Barrett–Joyner–Halenda (BJH) method.

X-Ray Diffraction (XRD)

X-Ray diffraction (XRD) was performed in order to check the X-Ray patterns of Ni0 and Ni° over Ceria-Zirconia samples. It was carried out on a Panalytical X'Pert pro diffractometer with an incident-beam Ge monochromator in order to study the structural properties. The apparatus was equipped with Cu Kα radiation source. The data was recorded over a 2θ range of 10° to 80° with a scan step size of 0.05°. The crystallite size of the metallic Ni was calculated by using the Debye-Scherrer equation.

$$\mathbf{D} = \frac{K \cdot \lambda}{\beta \cdot cos\theta} \qquad \text{equation 2-1}$$

D : the mean size of the ordered (crystalline) domains;

K : a dimensionless shape factor, with a value close to unity. The shape factor has a typical value of about 0.89;

$\boldsymbol{\lambda}$: the X-ray wavelength;

$\boldsymbol{\beta}$: the line broadening at half the maximum intensity (FWHM);

$\boldsymbol{\theta}$: the Bragg angle.

Temperature-Programmed Reduction (TPR)

In order to check the reducibility of the catalyst, hydrogen Temperature programmed reduction was carried out (Figure 2-2). Temperature programmed reduction plots were obtained with a BELCAT-M apparatus from BEL Japan, equipped with a thermal conductivity detector (TCD). The catalyst (70 mg) was first treated at 100 °C for 2 h under argon, and then heated up to 900 °C using a mixture of 5% hydrogen in argon at the heating rate of 10 °C/min.

Temperature-Programmed Desorption (TPD)

The basicity of reduced catalysts was analyzed according to the temperature programmed desorption in CO_2, using the BELCAT-M apparatus from BEL Japan. After TPR-H_2 measurement, the catalyst was put in helium for purification. Then a mixture of 10% of carbon dioxide in helium was fed for 1 h at a set temperature of 80 °C. Subsequently, a flow of helium was applied for 15 mins to clean the weakly adsorbed CO_2. Then, the catalyst was heated up at 10 °C/min under a gas flow of helium. The result obtained were plotted into profiles and fitted into three peaks (weak, middle and strong basic sites).

The set-up for temperature-programmed reduction (TPR) and temperature-programmed desorption (TPD) is shown in Figure 2-2.

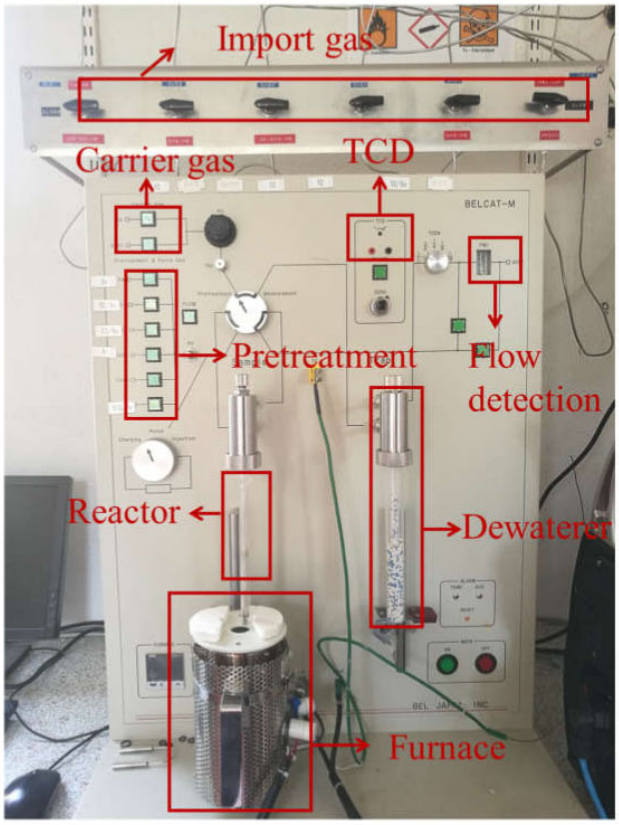

Figure 2-2. The set-up for Temperature-Programmed Reduction (TPR) and Temperature-Programmed Desorption (TPD)

Scanning Electron Microscopy (SEM)

A scanning electron microscope (SEM) is a type of electron microscope that produces images of a sample by scanning the surface with a focused beam of electrons. In this research, the surface morphology of the samples was investigated by scanning electron microscopy (SEM). This was performed on a Proxima 100-Micromecha machine in a field emission gun scanning electron microscope (FEG-SEM ZEISS LEO1530) operating at 20 kV and a NORDIF EBSD camera.

2.3 Experiment set-up for CO_2 Methanation

2.3.1 Thermal analysis system

The thermal activation process was studied in the U reactor shown in Figure 2-3. The U reactor loaded with 150 mg of catalyst was put in an oven. The temperature of the oven was controlled by a regulation system allowing to set the temperature from 200 °C to 500 °C. A K-type thermocouple was placed close to the catalytic bed to measure the temperature (Figure 2-3). The inlet gas was composed of a mixture of H_2, CO_2 and Ar, with flow rates of 60 mL/min, 15 mL/min, and 25 mL/min, respectively as already reported in the literature.[128] Before the experiment, the catalyst was reduced in-situ in the presence of 50 vol%. H_2/Ar mixture at 470 °C for 2 h. At the outlet of the reactor, the gas product was processed through a condenser to remove the water vapor from the mixture. The outlet flowrate was measured with a bubble flowmeter, and the composition of the mixture was analyzed by a gas chromatograph (Agilent 490 Varian MicroGC) to calculate the conversion of CO_2 and the selectivity of CH_4.

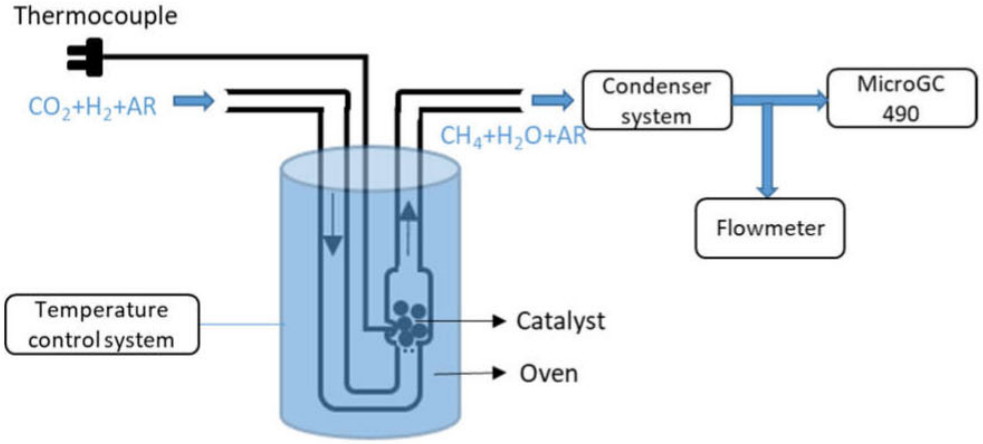

Figure 2-3. Schematic diagram of the set up for the thermal activation process

2.3.2 Plasma-catalytic hybrid system for Cylinder reactor

The schematic diagram of the plasma-catalytic reactor for cylinder reactor is shown in Figure 2-4. The dielectric barrier discharge (DBD) plasma reactor consists of two coaxial tubes (quartz and alumina tubes). Between the outer quartz tube (10 mm outer diameter, 1 mm wall thickness)

and the inner alumina tube (3 mm external diameter, 0.6 mm wall thickness), the discharge is sustained in a gap of 2.5 mm between two tubes. The high voltage electrode is a polished copper rod placed in the alumina tube with a steel wire wrapped around the outer surface of the quartz tube acting as the ground electrode. The temperature was measured by a K-type thermocouple placed on the outer surface of the quartz tube, in the middle of the grounded electrode.

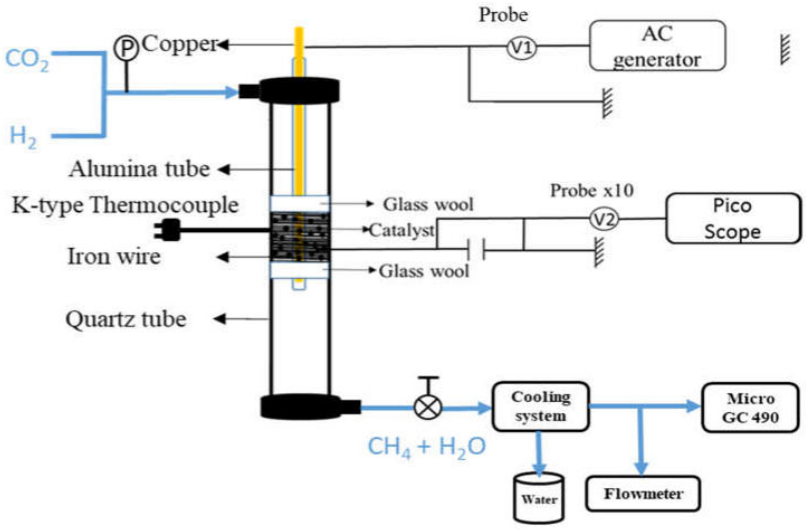

Figure 2-4. Schematic diagram of the hybrid plasma-catalytic process set-up for cylinder

The reactor was loaded with 300 mg of catalyst, with a length of catalyst packed bed of 6 mm. Glass wool was placed on both sides of the catalyst-bed in order to immobilize the catalyst powders. In this research, the feed gas was a mixture of pure hydrogen and carbon dioxide with a fixed H_2/CO_2 stoichiometric ratio of 4:1. Before the experiment, the catalyst was reduced in-situ in the presence of 160 mL/min H_2 at an applied voltage of 20 kV for 30 min, and the temperature used during the reduction process was around 200 °C.

A valve was put at the outlet of the plasma reactor to adjust the pressure inside the reactor to investigate its influence on the CO_2 methanation in the plasma-catalytic process. A bourdon pressure gauge was put at the inlet of plasma reactor to measure the pressure created inside the plasma reactor.

2.3.3 Plasma-catalytic hybrid system for milli-reactor

Plasma-catalytic hybrid process for CO_2 methanation was also performed in milli-reactor, and the scheme set-up is presented in Figure 2-5. The temperature of the reactor was measured by a K-type thermocouple, which was glued on a metal slide to have a better precision of measurement of temperature because of the better heat transfer between the quartz slide and metal slide. The reactor was loaded with 100 mg of catalyst, with a length of catalyst packed bed of 25 mm.

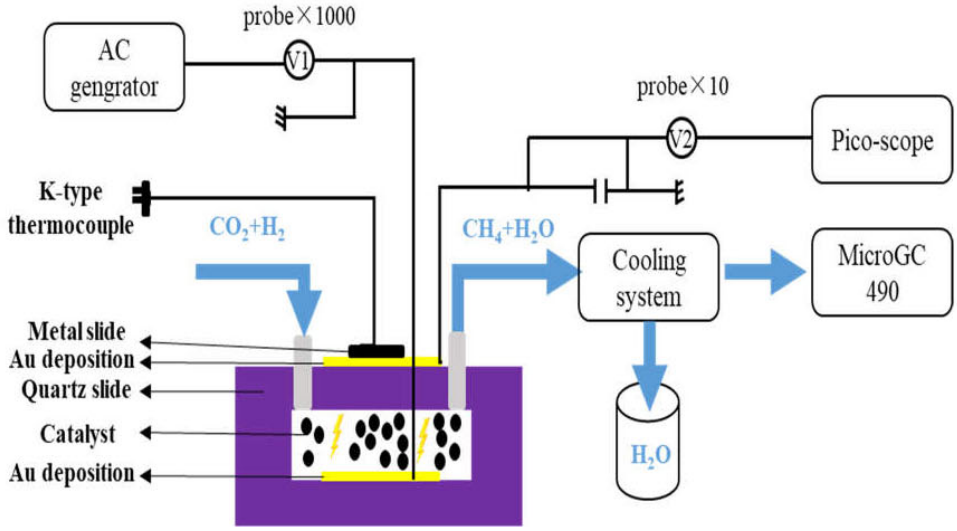

Figure 2-5. Schematic diagram of the hybrid plasma-catalytic process set-up for milli-reactor

The glass slides used in this research was from VWR Internationale. And the quartz slide (Fisher Scientific) was chosen as the dielectric material due to its ability to work at high temperature. The Au deposition on the quartz slide was act as the high voltage electrode and grounded electrode, and the deposition was performed on the machine Edwards Auto 500 system. In the deposition, 40g 99.99% pure gold bars produced by Neyco S.A, and chromium in fragments, purity 99.95%, was produced by Neyco S.A.

The ITO deposition used as electrode was doped by gold in the middle of the layer to increase the conducitivty, and was did on hybride HSPT520 (Plasmionic Inc). ITO alloy used in the deposition was from a target composed of In_2O_3 and SnO_2, 90/10% m, purity 99.99%, produced by Kurt J. Lesker Company Ltd. Gold was from a 99.99% pure gold target, produced by Neyco

S.A.

In the plasma-catalyst hybrid process in cylinder reactor and milli-reactor, the energy was supplied using a high voltage Calvatron SG2 (41 kHz), and applied voltages ranged from 15 kV to 19 kV (peak-to-peak). The applied voltage was measured by a digital picoscope (series 3000, PicoTechnology) with a probe (ELDITEST GE 3830). A capacitor (2.15 nF) was inserted between the reactor and the grounded electrode to measure the power provided to the plasma reactor by the Q-V Lissajous method, as described in following part. The outlet flow was analyzed by a gas chromatograph (Agilent MicroGC 490) equipped with a thermal conductivity detector (TCD). Its flowrate was measured with a bubble flowmeter.

Finally, for both thermal and plasma assisted reactions, the conversion of CO_2 and selectivity of CH_4 was calculated by the following equations:

$$X_{CO_2}\ (\%) = \frac{F_{CO_2\,in} - F_{CO_2\,out}}{F_{CO_2\,in}} \times 100 \qquad \text{equation 2-2}$$

$$S_{CH_4}\ (\%) = \frac{F_{CH_4\,out}}{F_{CO_2\,in} - F_{CO_2\,out}} \times 100 \qquad \text{equation 2-3}$$

Where $F_{CO_2\,in}$ is the CO_2 flow rate in the fed mixture, $F_{CO_2\,out}$ is the CO_2 flow rate in the product, and $F_{CH_4\,out}$ is the CH_4 flow rate in the product.

The details about measurement of plasma power by Q-V Lissajous method and gas concentration by micro-GC 490 was described in following part.

2.4 Plasma Diagnostics

2.4.1 Q-U lissajous method

In this study, the plasma power created in the reactor was measured by Q-U lissajous method introduced by Manley in 1943, and scheme of measurement set-up is shown in Figure 2-6. This method is now considered as the most precise method for DBD power measurement, and the capacitance of the reactor could also be measured by this method.[137]

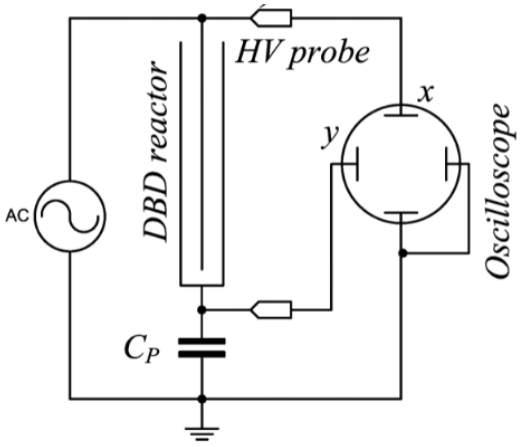

Figure 2-6. Scheme of set-up for Q-V Liassajous method

In this method, an additional capacitor (C_P) is placed in series with the reactor. This capacitor accumulates the charge from the current flowing through the reactor, and can be obtained by measuring the voltage on the capacitor (Uc) as equation 2-4:

$$\mathrm{Q(t)} = I_C \cdot \mathrm{t} = C_P \cdot U_C(t) \qquad \text{equation 2-4}$$

The current pass through the capacitor is given by equation 2-5:

$$I_C = \frac{dQ(t)}{dt} = \frac{C_P \cdot dU_C(t)}{dt} \qquad \text{equation 2-5}$$

As the capacitor is in series with the reactor, so that the current pass through the reactor I_R is equal to the current flowing over the capacitor I_C:

$$I_R = I_C \qquad \text{equation 2-6}$$

And the Ug is the voltage at the terminal of the generator, the voltage at the terminal of the reactor U_R is given by equation 2-7, and because $Ug \gg Uc$, then Ug is approximately equal to U_R.

$$U_R = Ug - Uc = Ug \ (Ug \gg Uc) \qquad \text{equation 2-7}$$

Then the instantaneous power dissipated in the reactor is presented in equation 2-8:

$$\mathrm{P}_i = U_R \cdot I_R = Ug \cdot \frac{C_P \cdot dU_C(t)}{dt} \qquad \text{equation 2-8}$$

Therefore, the average power can be obtained by:

$$P = \frac{1}{T}\int_0^T Ug(t) \cdot \frac{C_P \cdot dU_C(t)}{dt} dt = f \cdot C_P \cdot \oint U_g(t)\, dU_C \qquad \text{equation 2-9}$$

The value of plasma power was obtained by the following equation 2-10:

$$P = f \cdot E = f \cdot \oint U(t) \frac{dQ}{dt} dt = f \cdot C_P \cdot \oint U(t)\, dU_P = f \cdot \oint U(t)\, dQ(t) \qquad \text{equation 2-10}$$

Thus, by plotting the charge versus high voltage, the Q-U Lissajous figure could be obtained, as shown in Figure 2-7. The discharge power dissipated in the reactor is then equal to the area of Q-U Lissajous figure. The advantage of this method is that the charge is stored in the capacitor, so that it does not require a fast-transient digitizer to record the charge. The area of the figure is calculated by the rectangle's method using a Python program, as shown in equation 2-11.

$$P = f \cdot \sum_{k=1}^{n} \frac{(U_{k+1}+U_k)}{2} \cdot (Q_{k+1} - Q_k) \qquad \text{equation 2-11}$$

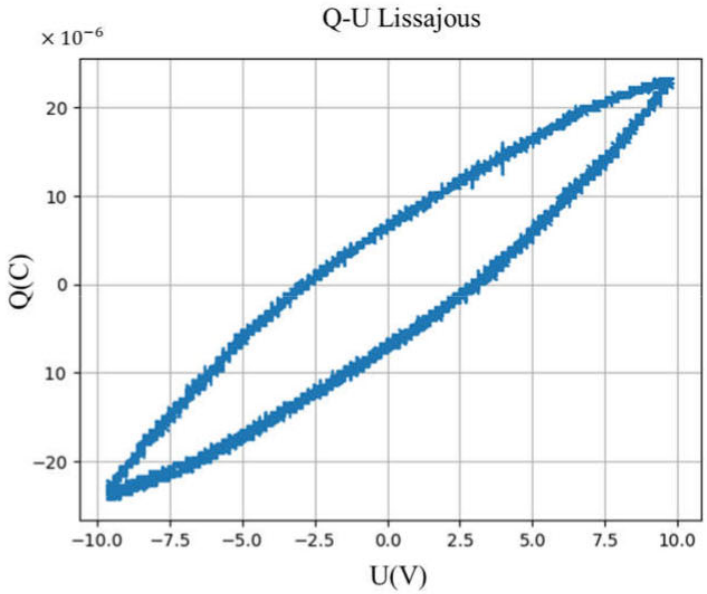

Figure 2-7. A typical Q-U Lissajous figure of the cylinder reactor in plasma-catalytic process

Moreover, this method could also be used to measure the capacitance of the reactor. Indeed,

when the applied voltage is lower than breakdown voltage, the minimum voltage for which a plasma is generated in the reactor, there is no plasma discharge created inside the reactor, and the area of the Lissajous plot is zero. The figure will be a straight line, and the values of capacitance of the reactor c_R could be determined by the slope the line.

The charge accumulated in the capacitor could be determined by equation 2-12:

$$\mathrm{Q(t)} = C_P \cdot U_C \qquad \text{equation 2-12}$$

As the capacitor is in series with the reactor, so the charge in the reactor is equal to the charge in the capacitor. Besides, the voltage of reactor could be determined by the voltage of the capacitor and the generator, as shown below:

$$\mathrm{Q(t)} = C_R \cdot U_R \qquad \text{equation 2-13}$$

$$U_R = Ug - Uc \qquad \text{equation 2-14}$$

From equation above, the relationship between the capacitance of the reactor and capacitor could be obtained as equation 2-15:

$$U_g = Uc \cdot (1 + \frac{C_P}{C_R}) \qquad \text{equation 2-15}$$

Therefore, by plotting the voltage of the capacitor versus the voltage of the generator, the capacitance of the reactor could be obtained from the slope. A typical figure is shown in Figure 2-8.

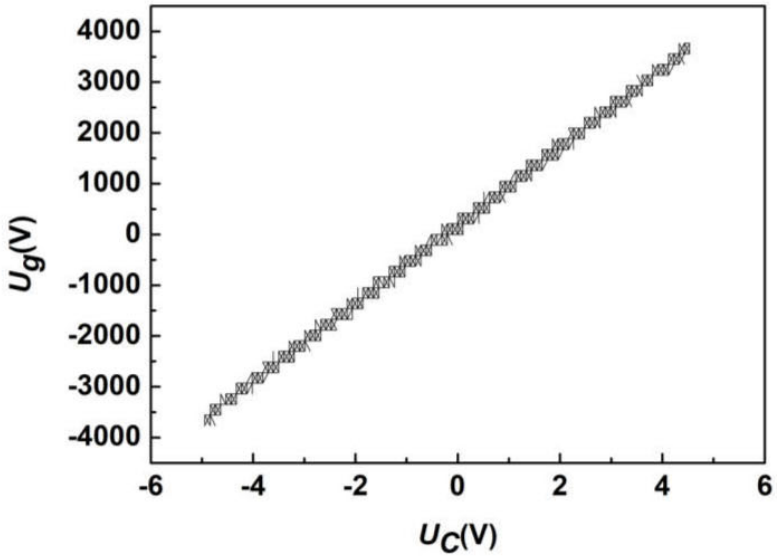

Figure 2-8. A typical figure for the calculation of the capacitance of the reactor

2.4.2 Gas phase analysis by MicroGC 490

The gas composition of the product is determined by the Agilent micro-GC 490 equipped with TCD detector. The gas sample is injected manually with a syringe, 5 mL of gas sample is taken from the gas collector for every injection. There are two channels in the GC, H_2, CH_4 and CO are detected in the first channel with the carrier as of Argon, while CO_2 and CH_4 are detected in the second channel with the carrier gas of helium. Although CH_4 could be detected in both channels, its quantitative determination is based on the data on channel 2.

The typical gas chromatogram is presented in Figure 2-9.

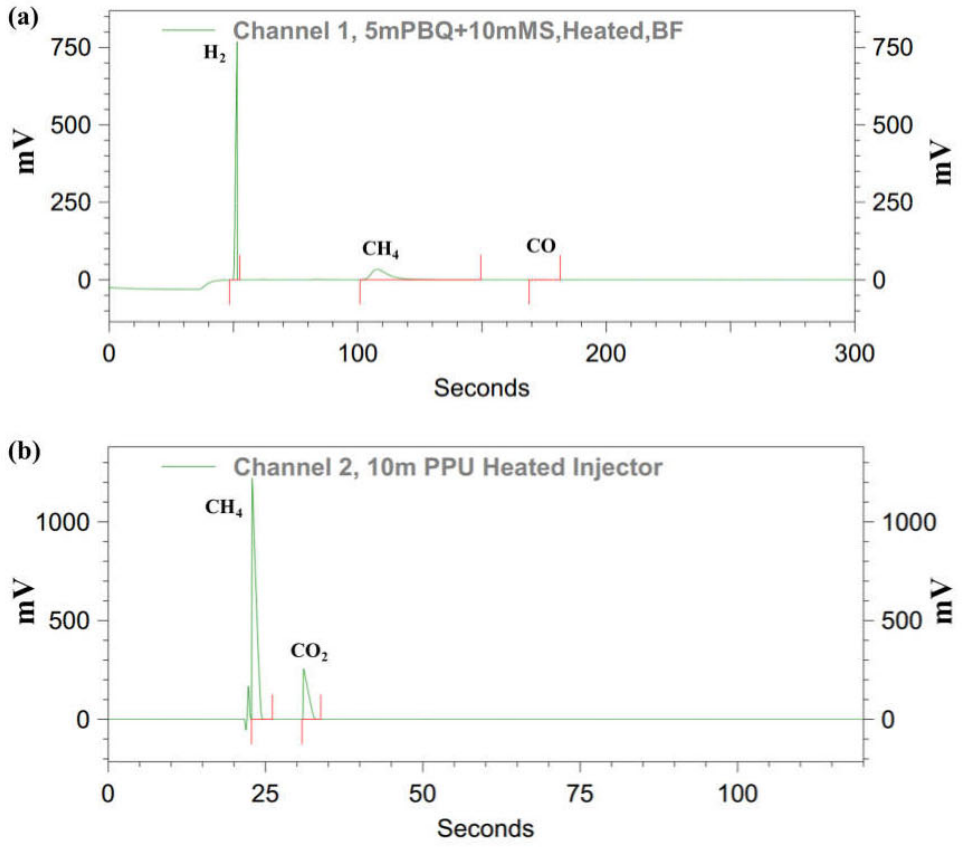

Figure 2-9. Gas chromatogram of the product stream: (a) channel 1for the detection of H_2, CH_4 and CO; (b) channel 2 for the detection of CH_4 and CO_2.

The method used for the detection of the product is shown in Table 2-1.

Table 2-1. Micro-GC method for the detection of the product stream

Channel 1		**Channel 2**	
Inject temperature	90 °C	Inject temperature	90 °C
Column temperature	50 °C	Column temperature	50 °C
Initial pressure	150 kPa	Initial pressure	150 kPa
Backflush time	35 s		

The regenation process of column was performed at the temperature of 180 °C once a week to maintain. And this process of was performed overnight to have a fully regenation of the column.

The calibration of gas composition was using the external standard method. For example, for the calibration of a certain gas, several samples with different gas concentration is injected into the micro-GC, then different area of the peak could be calculated for corresponding gas concentration. Then by plotting the gas concentration versus the peak area, the calibration could be obtained. A typical calibration of gas is shown in Figure 2-10. Therefore, an equation of the relationship between the gas concentration and area could be obtained by linear fitting of the data. In the experiment, putting the value of area into the specific equation, the gas concentration of the product stream could be obtained, and then the conversion and selectivity could be calculated from these results.

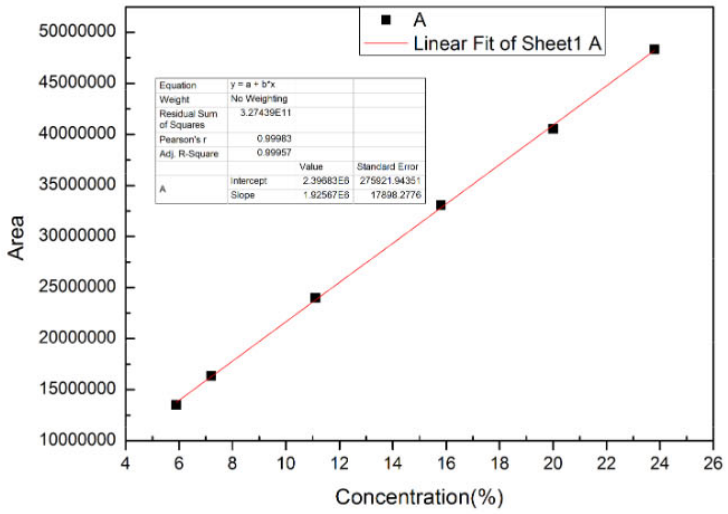

Figure 2-10. A typical calibration of gas using external standard method

2.5 COMSOL simulation of the reactor

The software COMSOL Multiphysics® 5.3 was used in order to calculate the temperature inside the catalytic bed. "Heat transfer in porous media" model was applied, and the "Stationary study" was used for the steady-state research for the temperature. A 2D axisymmetric geometry model of the reactor was created to study the temperature (Figure 2-11).

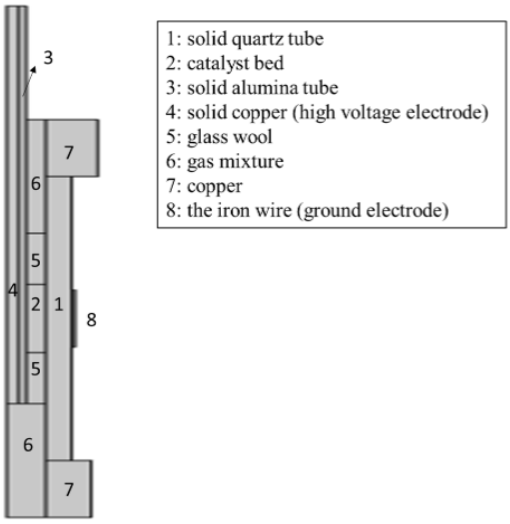

Figure 2-11. 2D axisymmetric geometry model of the reactor used for the simulation

The heat generated per unit of time in the catalytic bed was designed as a heat source in the reactor. The value of this power was estimated as a sum of the power created by the discharge plasma and the power created due to the exothermicity of the reaction using the equation below:

$$P = P_{discharge} + \Delta Hr^{\circ} \times X_{CO_2} \times (F_{CO_2\,in}) \qquad \text{equation 2-16}$$

Where $P_{discharge}$ is the plasma discharge power measured by the Q-V Lissajous method, ΔHr° is the enthalpy of Sabatier reaction, X_{CO_2} represent the CO_2 conversion value in the process, and $F_{CO_2\,in}$ is the inlet flowrate of CO_2.

The heat transfer at the external surface of the glass tube was designed as a heat flux by radiation and natural convection. The velocity of the gas mixture in domains 2, 5, and 6 was calculated using the inlet mixture flowrate. Concerning the properties of the gas mixture, heat capacity at constant pressure ($Cp_{mixture}$) and heat capacity at constant volume ($Cv_{mixture}$) were estimated as the following formulas:

$$Cp_{mixture} = m_1 \times Cp_{CO_2} + m_2 \times Cp_{H_2} \qquad \text{equation 2-17}$$

$$Cv_{mixture} = m_1 \times Cv_{CO_2} + m_2 \times Cv_{H_2} \qquad \text{equation 2-18}$$

Where m_1 and m_2 are the mass fractions of CO_2 and H_2, respectively, in the mixture.

Chapter III: Temperature investigation of CO_2 methanation in plasma-catalytic process

3.1 Introduction

According to literature, the combination of catalysis and plasma processing can lead to synergistic effects,[138, 139] and had been proven to be a successful technology for gas purification.[140] In the case of the CO_2 methanation process, hybrid plasma-catalytic reactors were developed.[96, 133, 136, 141] In these systems, numerous studies showed that high CO_2 conversion and CH_4 selectivity were obtained at a lower temperature compared with the conventional thermal process.[16, 72] To explain this, Whitehead pointed out that the presence of a plasma could contribute to a more effective adsorption of the different reactive species on the catalyst surface, lowering adsorption energy barriers and increasing the number of active sites.[142] Other authors suggested that the mechanism could be an electrocatalytic one.[141]

Within our research team, a hybrid DBD plasma-catalytic process coupled with $Ni/Ce_{0.58}Zr_{0.42}O_2$ catalyst has been successfully established, and the optimization of the process considering the effect of different parameters such as voltage, Gas Hourly Space Velocity (GHSV), catalyst mass and discharge length was studied.[136] A more recent study performed by Mikhail *et al.* showed that the high CO_2 conversions and high methane yields obtained under DBD plasma conditions, can be maintained with time-on-stream over 100 h of operating time.[84] To the best of our knowledge, the "plasma threshold temperature", defined as the minimum temperature at which the Sabatier reaction takes place under plasma conditions, has never been determined. And there are few researches about the respective role of plasma and temperature in the plasma-catalytic process. In this chapter, the objective is therefore to determine the plasma threshold temperature of the Sabatier reaction when a stoichiometric ratio of 4:1 mixture of H_2 and CO_2 is in contact with a catalyst under plasma exposure and the effect of temperature on the process.

A hybrid plasma-catalytic process for CO_2 methanation using a nickel-based catalyst with

ceria-zirconia mixed oxide as support (15 wt% of nickel on $Ce_{0.58}Zr_{0.42}O_2$) was used. This system has already been studied elsewhere for thermal catalysis and plasma catalysis reactions.[58, 128] The temperature at the reactor surface was measured using a K-type thermocouple directly located on the external grounded electrode, and an experimental method based on the decrease of the flowrate of the feed mixture was carried out to determine the minimum surface temperature at which the Sabatier reaction takes place quantitatively. A simulation model was created in COMSOL Multiphysics® software to determine the temperature difference between the external surface of the plasma reactor and the inside of the catalytic bed, and therefore provide a precise estimation of the threshold temperature of the Sabatier Reaction with plasma activation. Then to study of the respective role of temperature and power in the process, two systems were respectively designed for the investigation at low temperature and high temperature due to the technical restrictions. Finally, the CO_2 methanation was studied in the adiabatic plasma reactor to reduce power consumption.

3.2 CO_2 methanation under thermal activation

The thermal CO_2 methanation was performed in the U reactor that was placed in an oven in order to control the reactor temperature, as shown in chapter 2. The temperature of the oven was set in the range of 200 °C to 500 °C. The mass of catalyst loaded in the reactor was chosen as 100 mg, and the inlet gas was composed of a mixture of H_2, CO_2 and Ar, with flow rates of 60, 15, and 25 mL/min, respectively. The flowrate is fixed to have the same gas hourly space velocity (GHSV) as in the plasma-catalytic process to make the comparison.

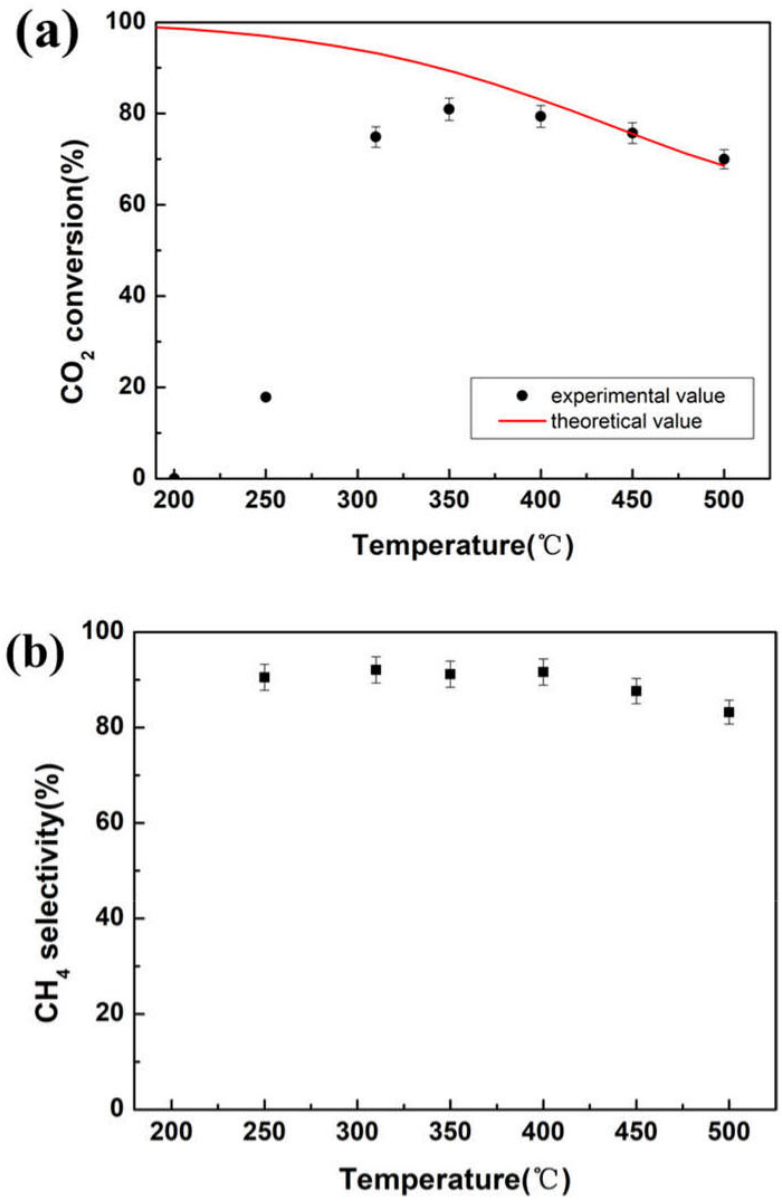

Figure 3-1. CO_2 conversion (a) and CH_4 selectivity (b) versus temperature over the conventional thermal system in the absence of plasma, Gas hourly space velocity (GHSV) =46300 h^{-1}

Figure 3-1 presents the CO_2 conversion and CH_4 selectivity obtained in the thermal methanation

test in the absence of plasma discharge within a temperature range from 200 °C to 500 °C. According to the thermodynamic equilibrium, which was calculated by HSC chemistry 5, the CO_2 conversion decrease from 98% to 68% when the temperature increases from 200 °C to 500 °C. As it is presented in Figure 3-1a, during the thermal methanation experiment in the absence of plasma discharge, the CO_2 conversion increased with the increase of the temperature up to 350 °C, before decreasing. On can note that at high temperature, the CO_2 conversion value fits the theoretical value, whereas at low temperature, the conversion is lower than the theoretically expected value due to the kinetic limitations. Negligible CO_2 conversion can be observed below 250 °C in the CO_2 methanation thermal experiment, and only 18% of CO_2 conversion was obtained at 250 °C. The maximum CO_2 conversion of 81% was achieved at 350 °C. Concerning the CH_4 selectivity, it regularly decreased from 92% to 83% when the temperature increased from 250 °C to 500 °C, which is in agreement with thermodynamics and which can be explained by the reverse water-gas shift reaction (RWGS reaction) that produces CO from CO_2 and H_2. Therefore, a temperature of 350 °C is needed to have good performance in terms of catalytic activity in the thermo-catalytic methanation process, as mentioned in a previous study.[16]

3.3 CO_2 methanation in plasma-catalytic process with the classical DBD reactor

3.3.1 Typical process of CO_2 methanation in DBD plasma reactor

Sinusoidal peak-to-peak voltage from 15 kV to 21 kV was applied to create plasma in the cylinder reactor. The power supplied in the reactor was measured by the Q-V Lissajous method. In this study, the feed gas mixture was fixed at 200 mL/min, and a stoichiometric ratio of H_2: CO_2 corresponding to 4:1 was used.

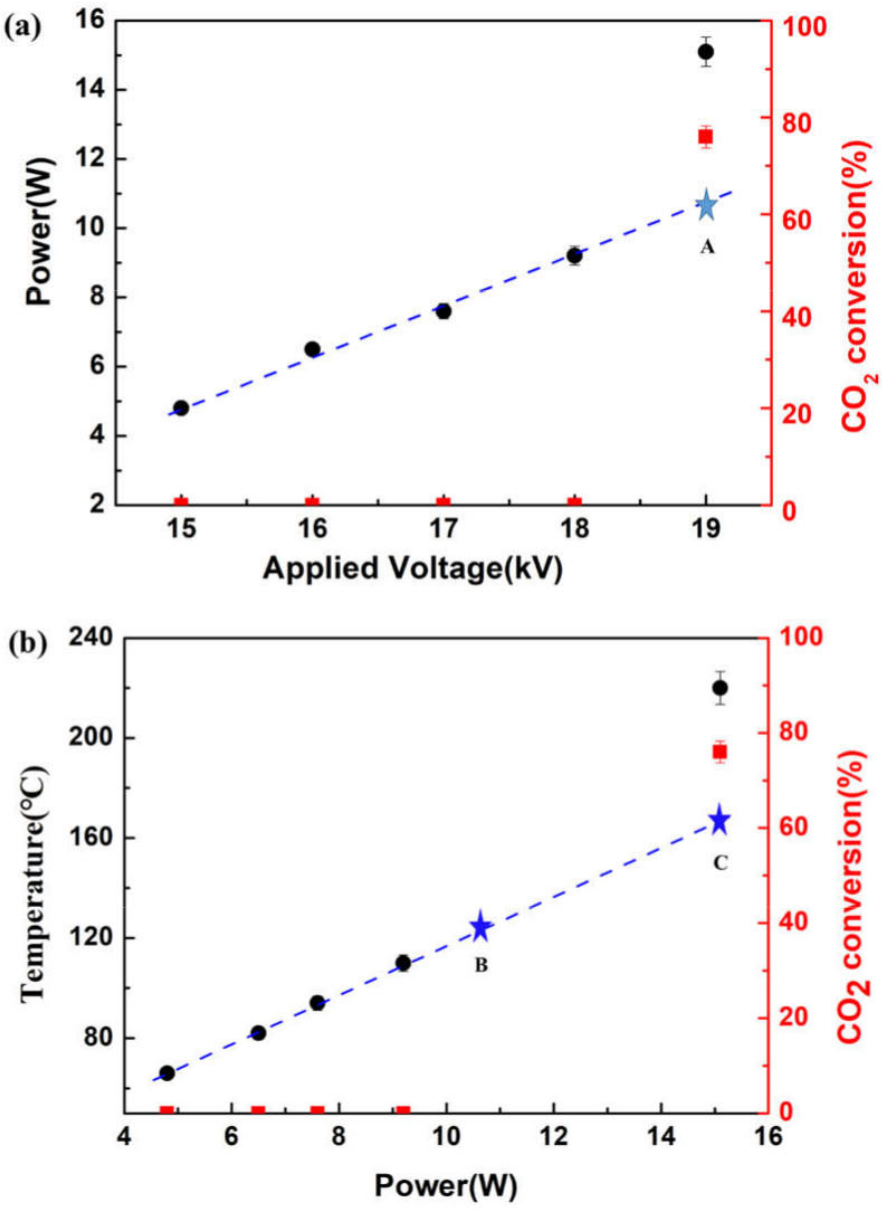

Figure 3-2. Plasma power and temperature created in the plasma-catalytic process: (a) DBD plasma powers created in the reactor under different applied voltages (peak-to-peak); (b) temperatures of the reactor at different applied plasma powers

Figure 3-2 presents the plasma power and the temperature measured at the surface of the plasma reactor for different applied voltages. Figure 5a shows the plasma power with the increase of peak-to-peak voltage from 15 kV to 19 kV. Up to 18 kV, the power of the DBD plasma generated in the reactor increased linearly from 4.8 W to 9.2 W. In this range, no CH_4 production was observed. The CH_4 was not produced until a peak-to-peak voltage of 19 kV was applied. At this voltage, the plasma power increased sharply to 15.1 W, and the CO_2 conversion and CH_4 selectivity were respectively 76% and 100%. This increase of power can be explained by the fact that when the reaction takes place, the composition of the gaseous mixture will change. For a given applied voltage indeed, the plasma power is a function of the gaseous composition.

Temperatures of plasma reactor at different plasma powers are shown in Figure 3-2b. At 4.8 W (corresponding to 15 kV), the reactor was heated to 66 °C. Following the increase of power, the temperature increased as well, and it can be observed that there is a linear relationship between the power and the temperature of the reactor as long as the CO_2 methanation does not occur (15 kV to 18 kV corresponding to 4.8 W to 9 W) (cf. Figure 3-2b). As soon as the methanation reaction takes place, resulting in 76% of CO_2 conversion, the linear relationship between power and temperature is no longer respected, and there is a sharp increase of the temperature to 220 °C. This can be explained by the high exothermicity of the Sabatier reaction. At 19 kV, the exothermic heat from the reaction is 4 W, which contributes to the increase of the temperature.

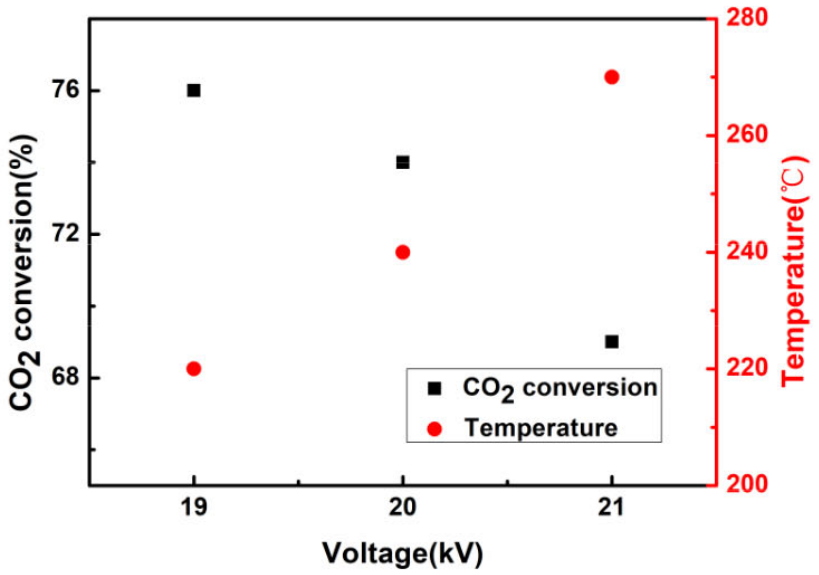

Figure 3-3. CO_2 conversion and temperature in the plasma-catalytic process (19 kV to 21 kV)

Besides, as the reaction toke place at 19 kV, the voltage was increased to 21 kV with a step of 1 kV to study its influence on the CO_2 methanation, and the CO_2 conversion and temperature under different voltages are presented in the Figure 3-3. It can be seen from the figure that CO_2 conversion decreased with the increase of voltage, the CO_2 conversion decreased from 76 % to 69 % while the applied voltage increased from 19 kV to 21 kV. This was due to the increase of temperature and the plasma power increased with voltage. As shown in the figure, the temperature increased from 220 to 270 °C, this increase of temperature maybe not favorable for the reaction. Besides, the plasma power increased from 15.1 W to 23 W and 32 W when the applied voltage increased from 19 kV to 20 kV and 21 kV respectively, which is also the reason for the decrease of CO_2 conversion because when the plasma power (or more precisely the SIE) is too high for the reaction, there could be a destruction of the product of CH_4 due to impacts between electrons and CH_4 in the gas phase.

Moreover, after mathematical analysis of the data in Figure 3-2, it could be state that before the reaction took place (in the range of 15kV to 18kV), there was an approximate linear function between the applied voltage and plasma power, and there was also the linear function between plasma power and reactor temperature, as shown in equation 3-1 and 3-2 respectively:

$$P = 1.45 \times V - 16.87, R^2 = 0.991 \quad \text{equation 3-1}$$

$$T = 9.99 \times P + 17.79, R^2 = 0.999 \quad \text{equation 3-2}$$

P: generated plasma power in the reactor, W;

V: applied voltage (peak to peak), kV;

T: reactor temperature, °C.

From these two equations, it could deduced that what was the plasma power (point A) and temperature (point B) at 19 kV if the reaction did not occur, as shown in the Figure 3-2. It could be obtained from equation 3-1 that the plasma power was 10.7 W at the voltage of 19 kV if the reaction did not take place. And put this power value in equation 3-2, the reactor temperature of 124.7 °C could be achieved. Thus, what happened at 19 kV could be assumed as follows:

Step 1: As the voltage of 19 kV was applied in the reactor, a plasma power of 10.7 W was generated in the reactor, and then the reactor temperature was 124.7 °C.

Step 2: As the reactor temperature excessed the threshold temperature of CO_2 methanation, the reaction occurred. And then the composition of the gaseous mixture changed, as a result, the plasma power was increased to 15.1 W, and the temperature was increased to 220°C at the stable state.

It has to be mentioned that this process finished in a very short time, and it was too difficult to observe this phenomenon by the measurement of power and temperature. Moreover, putting the measured plasma power of 15.1 W at 19 kV in equation 3-2, the reactor temperature could be obtained as 168.6 °C if there was no compensated heat from the reaction, as point C shown in the Figure 3-2b. And this temperature was far lower than the real temperature of 220 °C measured in the experiment. This phenomenon further demonstrated that the stable reactor temperature was a combination result of plasma power and exothermicity of the reaction

From these results, it can be asserted only that the threshold temperature for the Sabatier reaction using plasma activation is between 110 and 220 °C. Indeed, when the temperature of the catalyst reaches the threshold temperature, the reaction is triggered, and then the temperature increases sharply because of the increased plasma power and the exothermicity of

the reaction. It is therefore apparent that under these conditions, the threshold temperature cannot be measured precisely. This is partly because using an inlet flowrate of 200 mL/min, the heat released from the CO_2 methanation is high (4 W) and causes therefore a sharp increase of the temperature.

3.3.2 Threshold temperature of CO_2 methanation under DBD plasma condition

Considering the results presented in 3.2.2, it was decided to decrease the inlet flowrate in order to reduce the influence of the power released by the reaction on the reactor temperature. Several experiments were performed at different flowrates of inlet gas mixture with the same H_2: CO_2 stoichiometric ratio as previously. The applied voltage was fixed at 19 kV. For each condition, the temperature at the surface of the reactor was measured at steady state. Table 3-1 summarizes the CO_2 methanation results with the different flowrates of inlet gas mixture studied.

Table 3-1. Experimental results of CO_2 methanation with different flowrates in the plasma process

Flowrate [mL/min]	CO_2 conversion [%]	CH_4 selectivity [%]	T [°C]	GHSV [h^{-1}]	Plasma power [W]	Released power from reaction [W]
20	57.0	94.9	130	4630	10.9	0.3
50	67.8	98.0	150	11575	11.9	0.9
100	78.5	98.1	180	23150	12.9	2.0
200	77.5	95.1	220	46300	15.1	4.0
300	74.7	96.7	245	69450	15.4	5.8
350	72.4	96.3	255	81025	16.2	6.5

As expected, the results indicated that the use of smaller flowrates allows decreasing the heat power released by the Sabatier reaction and therefore decreasing the temperature measured at the reactor surface at steady-state. The plasma-assisted catalytic CO_2 methanation can then be performed at different temperatures from 130 °C to 255 °C in this study.

According to the results presented in Table 3-1, the CO_2 conversion increased with flowrates

ranging from 20 mL/min to 100 mL/min, and after 100 mL/min, the CO_2 conversion decreased with a further increase of the flowrate. This could be explained by that temperatures were not the same at these flowrates. In spite that the Gas hourly space velocity (GHSV) increase from 4630 h^{-1} to 23150 h^{-1}, the CO_2 conversion increased with the flowrate from 20 mL/min to 100 mL/min because the temperature increased from 130 °C to 180 °C. In this range, the effect of temperature on CO_2 conversion predominates. From 100 mL/min, the CO_2 conversion decreased with the increase of the flowrate. For example, the CO_2 conversion decreased from 78.5% to 72.4% with the increase of flowrate from 100 mL/min to 350 mL/min. Again, this could be explained by the increase of temperature. Indeed as discussed in 3.1, too high temperatures do not favor the Sabatier reaction. However, the increase of GHSV may also be responsible for the decrease of CO_2 conversion. Indeed, an increase of GHSV means a decrease of the residence time of the reactant mixture inside the catalyst bed, which results in the decrease of CO_2 conversion. It is worth to mention that the CO_2 conversion decreased only 6.1% (from 78.5% to 72.4%) with the increase of flowrate from 100 mL/min to 350 mL/min.

Finally, the main result is that under plasma conditions and with a GHSV of 4630 h^{-1}, 57% of CO_2 conversion and 94.9 % of CH_4 selectivity can be obtained even if the temperature at the reactor surface was only 130°C. Even if the GHSV is ten times lower compared to the ones usually used, it is evident that it would not be possible to obtain these performances at such a low temperature in conventional operating conditions. Thus, with a Ni-based catalyst and at atmospheric pressure, it was not possible to have the reaction under 200°C even with a low GHSV of 2400 h^{-1} in the conventional thermal heating process. Therefore, it can be stated from these experiments that with the use of plasma conditions, the threshold temperature of the Sabatier reaction is even lower than 130°C.

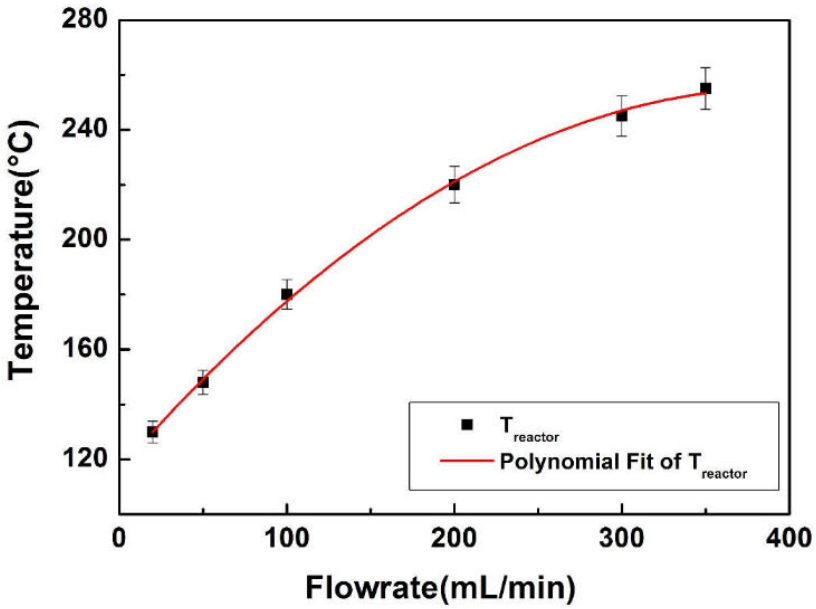

Figure 3-4. Stable temperatures of the reactor with different flowrates of the inlet reactant mixture during the CO_2 methanation in plasma catalytic process

According to the data presented in Figure 3-4, there is a binomial relationship between the stable reactor temperature and the flowrate of the inlet reactant mixture:

$$T=B_1x^2+B_2x+C \qquad \text{equation 3-3}$$

$$B_1=-8.84\times10^{-4},\ B_2=0.70,\ C=116$$

Where T is the temperature measured on the external surface of the reactor during the plasma process, °C, and x represents the flowrate of the inlet reactant gas mixture.

The external temperature of the reactor decreased with the decrease of the flowrate. The stable temperature with a flowrate of 0 mL/min could be derived from equation 3-3, which is 116 °C. And this could be the threshold temperature of Sabatier reaction under plasma conditions. In all the experiments presented until now, the temperature measured is the temperature on the reactor surface. To evaluate the true temperature inside the catalytic bed, a simulation created in COMSOL Multiphysics® software was carried out in the following part.

3.3.3 COMSOL simulation of the temperature distribution in the cylinder reactor

COMSOL Multiphysics® software was used to simulate the heat transfer inside the reactor.

"Heat transfer in porous media" model was applied, and the "Stationary study" was used for the determination of the temperature at steady-state.

3.3.3.1 Sensitivity analysis and model validation

A sensitivity study was first performed to determine the value of some parameters whose true values are not known precisely. These parameters are the thermal conductivity of quartz λ_{quartz}, the thermal conductivity of alumina $\lambda_{alumina}$, the thermal conductivity of the catalyst $\lambda_{catalyst}$, and finally the convective heat transfer coefficient at the surface of the reactor h. In this optimization, four parameters in three scales were chosen: the thermal conductivity of quartz ($W \cdot m^{-1} \cdot K^{-1}$): 1.3, 1.56, 1.8; the thermal conductivity of alumina ($W \cdot m^{-1} \cdot K^{-1}$): 10, 20, 30; the thermal conductivity of catalyst ($W \cdot m^{-1} \cdot K^{-1}$): 10, 20, 30; h of the heat flux of air ($W \cdot m^{-2} \cdot K^{-1}$): 30, 40, 50.

Table 3-2 is the sensitivity study of simulation of the surface temperature of reactor. T_1, T_2, and T_3 is the temperature from the simulation with a power at 4.8 W, 7.6 W, and 9.2 W respectively, and f(x) is the function to evaluate the optimization:

$$f(x)=(T_1-66)^2+(T_2-94)^2+(T_3-110)^2 \qquad \text{equation 3-4}$$

Table 3-2. Sensitivity study of the simulation of the surface temperature of reactor

	λ_{quartz} [$W \cdot m^{-1} \cdot K^{-1}$]	$\lambda_{alumina}$ [$W \cdot m^{-1} \cdot K^{-1}$]	$\lambda_{catalyst}$ [$W \cdot m^{-1} \cdot K^{-1}$]	h [$W \cdot m^{-2} \cdot K^{-1}$]	T_1 [°C]	T_2 [°C]	T_3 [°C]	f(x)
1	1(1.3)	1(10)	1(10)	1(30)	78	111	129	794
2	1(1.3)	2(20)	2(20)	2(40)	67	94	110	1
3	1(1.3)	3(30)	3(30)	3(50)	61	85	99	227
4	2(1.56)	1(10)	2(20)	3(50)	66	93	110	1
5	2(1.56)	2(20)	3(30)	1(30)	70	99	116	77
6	2(1.56)	3(30)	1(10)	2(40)	67	94	109	2
7	3(1.8)	1(10)	3(30)	2(40)	70	99	115	66
8	3(1.8)	2(20)	1(10)	3(50)	65	91	106	26
9	3(1.8)	3(30)	2(20)	1(30)	69	97	113	27
K_1	1022	861	822	898				
K_2	80	104	29	69				
K_3	119	256	370	254				
R	942	757	793	829				

K_1, K_2, and K_3 are the sum of the f(x) at the same scale of one parameter, respectively. For a parameter, a scale with the lowest K value means this scale is the most proper value among these three values. R is the range of K_1, K_2, and K_3. A higher R means that the parameter has a bigger influence on the simulation.

For example, as for the sensitive study of thermal conductivity of alumina, K_1 is the sum of value f(x) while putting scale 1(10 $W \cdot m^{-1} \cdot K^{-1}$) in the model, which is the f(x) value of experiment 1, 4 and 7. In this case, the value of f(x) is 794, 1 and 66 respectively for experiment

1, 4 and 7, therefore K_1 is the sum of three value, that is 861. And the K_2 is the sum of f(x) of experiment 2 (f(x)=1), 5 (f(x)=77) and 8 (f(x)=26), which is 104, while K_3 is 256. Moreover, the R is the range of K_1, K_2, and K_3, which is the difference of K_1 and K_2, that is 757.

As we can observe from Table 3-2, the range R of four parameters is 942, 757, 793, and 829. Among these values, the λ_{quartz} has the highest R-value (R=942), which means it has the most critical influence on the simulation of the temperature. And the order of the effect of parameters on the simulation is: $\lambda_{quartz} > h > \lambda_{catalyst} > \lambda_{alumina}$. For one certain parameter, the minimum value represent the most optimal level for the simulation. According to the value of K, the most suitable value of four parameters in three scales are: $h=40\ W\cdot m^{-2}\cdot K^{-1}$; $\lambda_{catalyst} = 20\ W\cdot m^{-1}\cdot K^{-1}$; $\lambda_{quartz} = 1.56\ W\cdot m^{-1}\cdot K^{-1}$; $\lambda_{alumina} = 20\ W\cdot m^{-1}\cdot K^{-1}$.

Temperatures obtained in the experiment and simulation are shown in Figure 3-5. Thus, it can be observed that up to 9.2 W (18 kV) before the reaction takes place, the two temperatures fit very well. On the contrary, when the reaction takes place at 19 kV, the power obtained from the Q-V Lissajous method is 15.1 W, and the power released from the reaction is 4.0 W, so the total power in the reaction is 19.1 W with a temperature of 220 °C. However, with a power value of 19.1 W input to the model, the temperature is 202 °C, there is around 18 °C difference between these two different temperatures. The reason might be that in the model, the values of all physical properties of materials are those at 20 °C. This is however not true, and the values of some parameters will likely change a little when the temperature increases from ambient temperature to around 220 °C. For example, the thermal conductivity increases with temperature in alloys, and also the physical parameters of the gas mixture will change with temperature. Considering that the difficulty and precision of the measurement of the temperature in the plasma process, the deviation is acceptable. Finally, the precision of the theoretical model is satisfying, especially at low-temperature conditions.

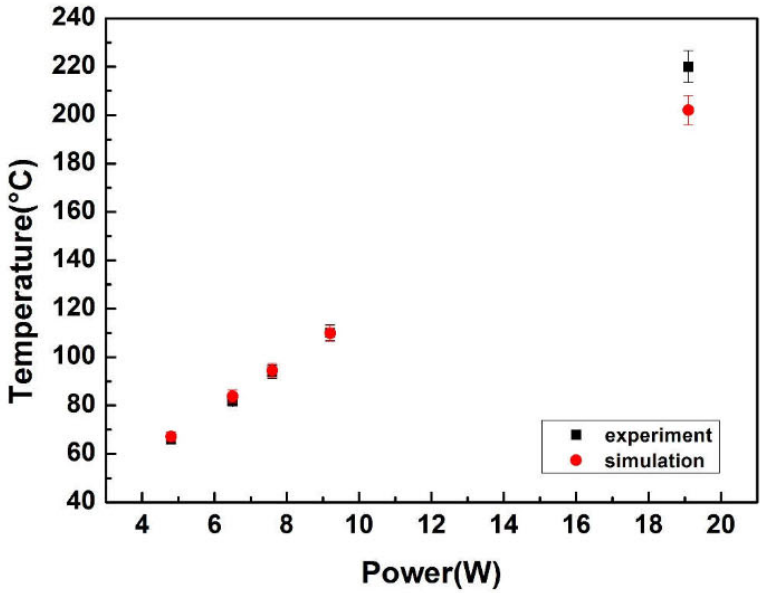

Figure 3-5. The comparison between temperatures obtained in the experiment and the simulation (200 mL/min)

3.3.3.2 Threshold temperature of the catalyst in the plasma-catalytic process

As discussed before, using a lower flowrate of 20 mL/min, the threshold temperature of Sabatier reaction could be approximately at around 116 °C, but this is the external temperature of the reactor surface. The objective in this part is to use the model previously developed to study the temperature distribution of the reactor and the temperature difference between the reactor surface and the catalyst. The temperature distribution at low flowrate was then simulated by using a heat source of 11.2 W in the catalytic bed and by calculating the new fluid velocity at the reactor inlet. As expected, the simulation data fit the experimental data very well because of the moderate rise of the surface reactor temperature at low flowrate (20 mL/min). Indeed, the experimental and simulated surface temperatures of the reactor at 20 mL/min were respectively 130 °C and 128.5 °C. The temperature distribution of the reactor is shown in Figure 3-6. From this figure, it can be observed that the temperature in the catalyst-bed is relatively homogeneous and close to the temperature at the external surface of the reactor.

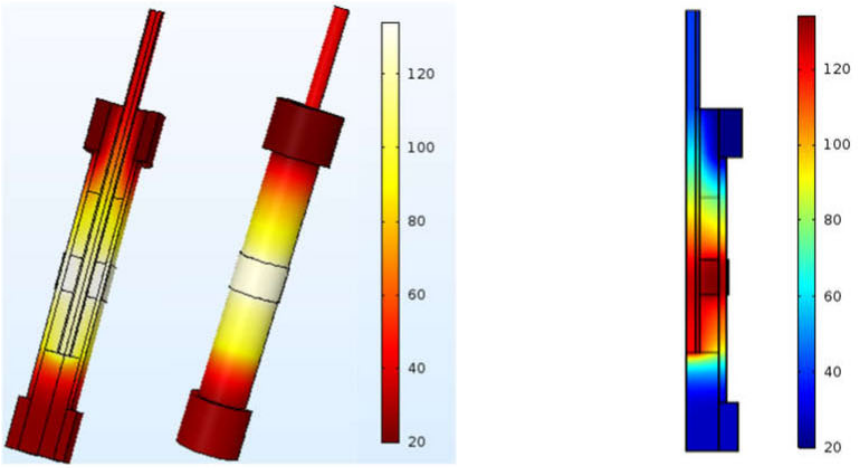

(a) (b)

Figure 3-6. Temperature distribution of the reactor with a flowrate at 20mL/min at 19kV: (a) 3D temperature distribution; (b) 2D temperature distribution

In order to have precisely the temperature inside the catalyst bed zone, a cut line EF was created in the model, as can be seen in Figure 3-7a. From E to F, it is copper (act as high voltage electrode), alumina tube, catalyst bed, quartz tube, and grounded electrode. Figure 3-7b is the temperature profile in the reactor on the cut line EF, and point E is the beginning point (125.5 °C).

It can be noted from Figure 3-7b that the highest temperature is attained in the catalytic bed. The width of the catalytic bed is 2.5mm, and there is a temperature gradient of 6°C (from around 127.5 °C to 133.5 °C) in the catalytic bed. The average temperature of the catalyst bed calculated by COMSOL Multiphysics® using the function "line average" is 130 °C. Finally, at 20 mL/min, the difference between the average temperature of the catalyst and the temperature of the external surface is only 2 °C. Considering the precision of the measurement of the temperature in the plasma process, the difference of 2 °C could be neglected. Therefore, we consider that the temperature of the catalyst-bed is equal to the temperature of the external reactor surface.

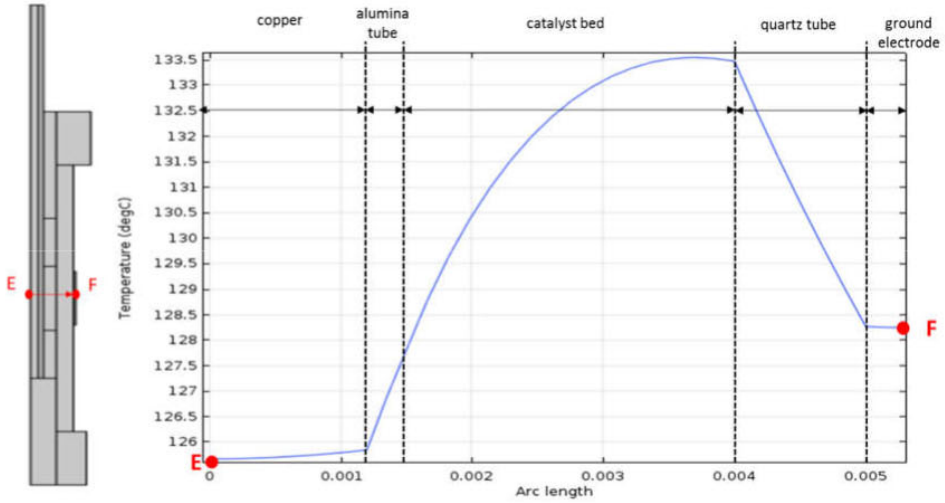

(a) (b)

Figure 3-7. Temperature profile of the reactor (from E to F) with a power of 21.1W: (a) schematic diagram cut line EF in the reactor; (b) temperature profile on the cut line EF

From part 3.2, it was estimated that under plasma exposure, the Sabatier reaction could take place quantitatively even if the temperature at the reactor surface is as low as 116 °C. According to the simulation results presented in Figure 3-7, the difference between the catalyst bed temperature and the reactor surface temperature is only 2 °C at low flowrate (20 mL/min), which is almost negligible. Therefore, in the plasma catalysis process, the plasma threshold temperature for the Sabatier reaction can be finally evaluated at 116°C.

In conclusion, the objective of this part was to determine the "plasma threshold temperature" of the Sabatier reaction, defined as the minimum temperature at which the Sabatier reaction takes place under plasma conditions. When the CO_2 methanation is studied in traditional lab-scale plasma catalytic reactors, the heat of the reaction is mainly evacuated through radiation and natural convection from the external surface of the reactor. Because these processes are not very efficient, a sudden and significant rise of the reactor temperature is generally observed as soon as the Sabatier reaction is initiated, making a precise measurement of the threshold temperature difficult. To allow a precise measurement of the plasma threshold temperature, experiments with lower inlet mixture flowrates were performed in order to reduce the

influence of the power released by the reaction. It was then estimated that under plasma exposure, the Sabatier reaction could take place quantitatively even if the temperature at the reactor surface is as low as 116 °C. To determine the true plasma threshold temperature, which is the temperature inside the catalytic bed in the same conditions, a simulation model was created in COMSOL Multiphysics® software to determine the temperature distribution of the reactor in the plasma catalytic hybrid process. As the simulation indicated that the temperature difference between the reactor surface and the catalyst bed was almost negligible, the plasma threshold temperature for the Sabatier reaction was finally evaluated at 116°C.

3.4 Study of the respective role of temperature and plasma power

As mentioned before, the plasma reactor is placed in the ambient air, and most of the heat produced by the plasma discharge is lost by convection from the reactor surface. Thus, the temperature is mainly controlled by the peak to peak voltage (plasma power) applied on the reactor. To study the respective roles of temperature and plasma power, new reactors were designed for the control of the temperature independently of the applied plasma power. However, due to technical constraints, different experimental set-ups were used for the studies at low temperatures and high temperatures.

3.4.1 What are the key parameters to trigger CO_2 methanation: Voltage? Plasma power? Temperature?

Before the study of respectively role of temperature and power in the plasma-catalytic process, there is one question has to be answered: What is the key parameter to trigger CO_2 methanation: Voltage? Plasma power? Temperature? Unlike the thermal condition, in which the only parameter has to be considered is temperature, there are three parameters has to be considered in the plasma-catalytic process: voltage, plasma power, and temperature. But these parameters are not independent, the temperature and power mainly depend on the voltage applied on the reactor. Moreover, the temperature is also infected by the air convection.

In this work, it was observed that for the same configuration of the plasma reactor, the voltage

used to trigger the reaction can be different, thus the plasma power will be different. There is an example for the different voltage and power in Table 3-3. As can be seen from the table, the voltage used to trigger the reaction can decrease from 19 kV to 16 kV, and the corresponding plasma power decreased from 14.1 W to 6.5 W. However, in this two conditions, the reaction temperature are the same, which was 220°C, and the CO_2 conversion did not change. The decrease of trigger voltage and plasma power could be explained by the threshold temperature theory in part 3.3.

Table 3-3. Different trigger voltage for CO_2 methanation in plasma-catalytic process

	Voltage (kV)	**Power (W)**	**Temperature (°C)**	**CO_2 conversion (%)**
Experiment 1	19	14.1	220	80
Experiment 2	16	6.5	220	80

In the plasma-catalytic process of CO_2 methanation at 200mL/min, there is a threshold temperature, which is 116°C, the reaction could take place as the temperature is higher than this temperature. And the temperature is mainly depended on the applied voltage and air convection. If the air convection keeps the same, the temperature is only determined by the applied voltage, thus the trigger voltage will be the same. However, if the air convection changes, the temperature will be influenced by both voltage and air convection, then the voltage applied to achieve the threshold temperature will change.

The influence of air convection on the plasma-catalytic process was investigated in COMSOL Multiphysics® software, as mentioned in part 3.3. The air convection coefficient was chosen as 40 and 5 $W \cdot m^{-2} \cdot K^{-1}$ to study the difference, as shown in Table 3-4. The process studied here was a typical plasma-catalytic process, as mentioned in part 3.3.1. The plasma power was measured at each voltage in the range of 15 to 19 kV. And the plasma power value was put in the simulation model to obtain the reactor temperature at different air convection coefficient. T_1 and T_2 represent the reactor temperature when the air convection coefficient was 40 and 5 $W \cdot m^{-2} \cdot K^{-1}$ respectively.

It can be state clearly that the air convection has an important effect on the process. For a given plasma power, there was a huge difference of reactor temperature as the air convection coefficient changes from 40 to 5 $W \cdot m^{-2} \cdot K^{-1}$. And the temperature difference increased from 29 to 59℃ when voltage was applied from 15 to 19 kV.

Table 3-4. The influence of air convection on the plasma-catalytic process

Voltage(kV)	Power(W)	T_1(℃)	T_2(℃)
15	4.8	66	95
16	6.5	74	118
17	7.6	93	135
18	9.2	108	154
19	15.1	163	222

The reactor temperature profile that changes with voltage under different air convection coefficient was shown in Figure 3-8. As can be seen, under a certain voltage, the reactor temperature was higher when air convection coefficient was lower. That is to say, when air convection coefficient was lower, the voltage to create the same temperature was lower. In this case, the temperature was threshold temperature, which is 116℃, and the CO_2 methanation could take place when the temperature was higher than this value.

As shown in Figure 3-8, when the air convection coefficient h was 40 $W \cdot m^{-2} \cdot K^{-1}$, this temperature was achieved when the voltage was applied to 19 kV, then the reaction occurred, and the reaction could not take place when the voltage was lower than 19 kV. This is the typical plasma-catalytic process studied in part 3.3.1.

However, when h was chosen lower as 5 $W \cdot m^{-2} \cdot K^{-1}$, the temperature of 119℃ could be achieved at the voltage of 16 kV, and this temperature was higher than threshold temperature, and then thus the reaction will take place at 16 kV. This is why the reaction could take place at a lower voltage and power even the equipment and plasma reactor are the same.

The air convection has a then an important influence on the applied voltage and power needed for the activation of CO_2 methanation

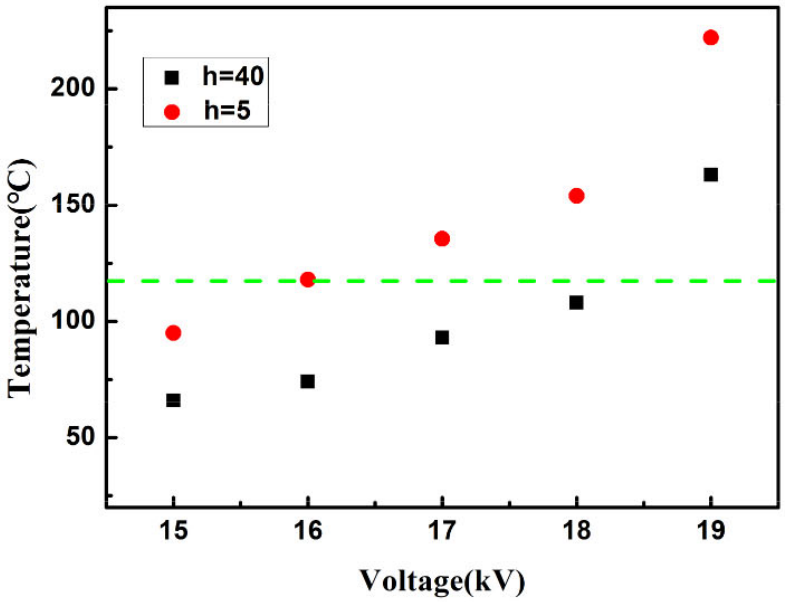

Figure 3-8. The reactor temperature profile that changes with voltage under different air convection coefficient

In this work, the plasma-catalytic process was performed in the fume hood, however, the air convection in the fume hood cannot be controlled, and it changes during the research, and this is why the applied voltage and power that used for the activation of the reaction can change.

3.4.2 CO_2 methanation at low temperature (28 to 150 °C) in the plasma state

To control the temperature the reactor independently of plasma power, a device was designed, and the scheme of the set-up is shown in Figure 3-9. It is worth to mention that, due to the decrease of air convection in the fume hood, the voltage needed for the reaction when the reactor was placed in the ambient air has changed, therefore, the plasma power needed was also different, as mentioned before. In section 3.3, the air convection was 40 $W \cdot m^{-2} \cdot K^{-1}$ (according to the COMSOL simulation model), the reaction toke place at the voltage of 19 kV when the

reaction was placed in the ambient air, and the temperature was 220 °C with a plasma power of 15.1W. However, in this section, the air convection was decreased to around 5 $W \cdot m^{-2} \cdot K^{-1}$ (according to the COMSOL simulation model), the voltage needed for the reaction decreased to 16 kV, and the temperature was the same as 220 °C, but the power was much lower as 7.0 W with a CO_2 conversion of 81%.

A jacket tube was fixed around the plasma reactor for the circulation of the silicon oil. The silicon oil was heated using a hotplate and a magneton was used to make a good transfer of the heat. And then the oil was then circulated into the jacket tube by a peristaltic pump. A K-type thermocouple was placed on the surface of the reactor to measure the surface temperature of the reactor as before, and then the thermocouple was connected to the system through an existence in the middle of the jacket tube. And the grounded electrode was connected to the ground through the same existence as the thermocouple. The reactor was covered by glass wool to minimize heat loss. In this reactor, the temperature of oil was set from room temperature to 150 °C. It was not possible to exceed 150°C because the peristaltic pump could not work properly when the oil temperature was higher than this temperature.

Based on the simulation before, the surface temperature was assumed as the temperature of the catalyst-bed. During the experiments, the procedure was as follows: the surface temperature was first kept stable at 28, 70, 115 or 150°C respectively, then the desired peak to peak voltage (from 16 kV to 20 kV) was applied on the high voltage electrode to study the CO_2 methanation in the plasma-catalytic process.

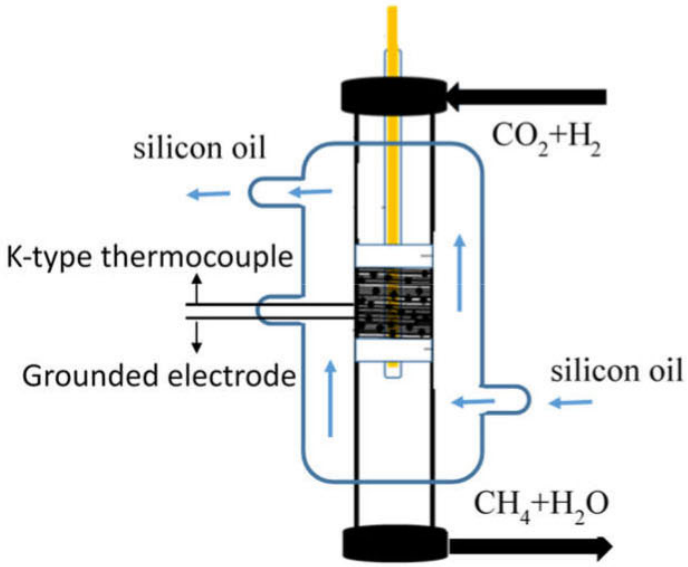

Figure 3-9. Scheme of set-up for the controlling the reactor temperature

(low temperature)

In the system shown the Figure 3-9, the reactor temperature was kept stable at different temperature independently of the applied high voltages. The plasma power created with different voltages under different reactor temperatures are presented in Figure 3-10. As can be seen from the figure, there was some difference between powers created at the same applied voltage. However, these difference could be ignored considering the precision of measurement the plasma power. Therefore, it could be concluded that, in the temperature range of 28 to 150°C, the plasma power created at the same applied voltage was the same regardless of the reactor temperature and the plasma power was increased around from 7 W to 15 W while the voltage was increased from 16 kV to 20 kV. It is worth to mention that, when the reactor was placed in the ambient air, at 220 °C, the plasma power at 16 kV was the same as 7.0 W, but CO_2 conversion was 81%. However, at the same power and voltage, the CO_2 conversion at 150°C was only 20%, while the reaction did not take place at a lower temperature. With the decrease of the temperature from 150 to 70°C, the minimum voltage necessary to trigger the CO_2 methanation increases from 16 to 19 kV. This means more plasma power was needed to trigger

the reaction at lower temperature. Moreover, at 28 °C, the CO_2 methanation could not take place no matter what voltage was applied on the reactor.

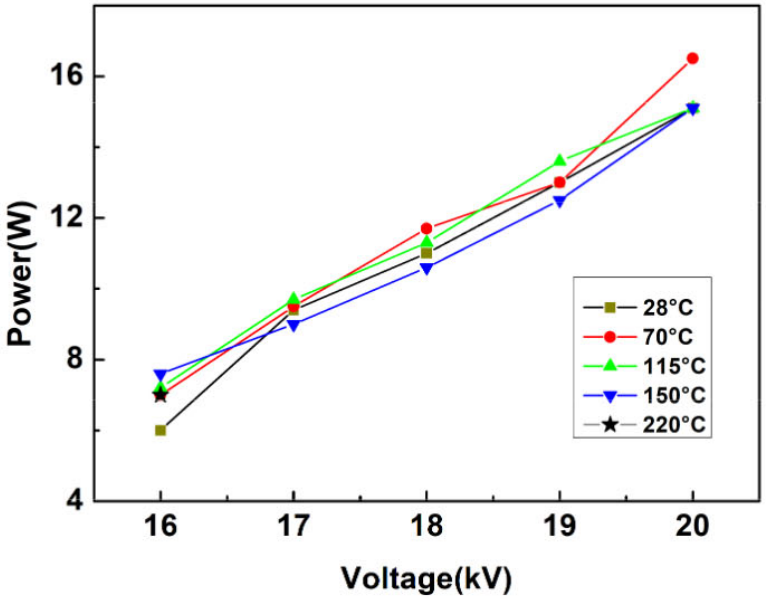

Figure 3-10. The plasma power created with different voltages under different reactor temperatures

Under different temperatures, the catalyst had different CO_2 conversion at the same voltage, as shown in Figure 3-11. First of all, there is no CH_4 detected at the exit of the rector at all the voltages when the reactor temperature is 28°C. At 70°C, the reaction take place 19 kV with a CO_2 conversion of 23%. And the CO_2 conversion increased to 52% when the applied voltage was increased to 20 kV. This trend that CO_2 conversion increased with applied voltage was also observed and was much clear when the reactor temperature was 115°C and 150°C respectively. When reactor temperature was heated to 150°C, the CO_2 methanation took place at 16 kV with the CO_2 conversion of 20%, and the CO_2 conversion increased with the applied voltage, until reached the maximum value of 74% at 20 kV. The reason why CO_2 conversion increased with voltage is that the plasma power increased with voltage, a higher plasma power means more reactive species, which helps to achieve a high CO_2 conversion at the same temperature.

The effect temperature on the reaction at the same power could be also seen from Figure 3-11. For example, at 19 kV, the CO_2 conversion was 0% at 28°C, when the temperature was

increased to 70°C, the CO_2 conversion was also increased to 23%. And then the CO_2 conversion continually increased with temperature, until reached 72% at 150°C. As studied before, the plasma created at the same voltage was identical. Thus it could be concluded that at a certain plasma power, the CO_2 conversion increased with reactor temperature. Moreover, the difference in CO_2 conversion between different temperatures decrease with the increase of the voltage. For example, when compared the CO_2 conversion at 70°C and 150°C, the difference of CO_2 conversion is 68% at 18 kV, and then decrease to 49% and 22% respectively at 19 kV and 20 kV.

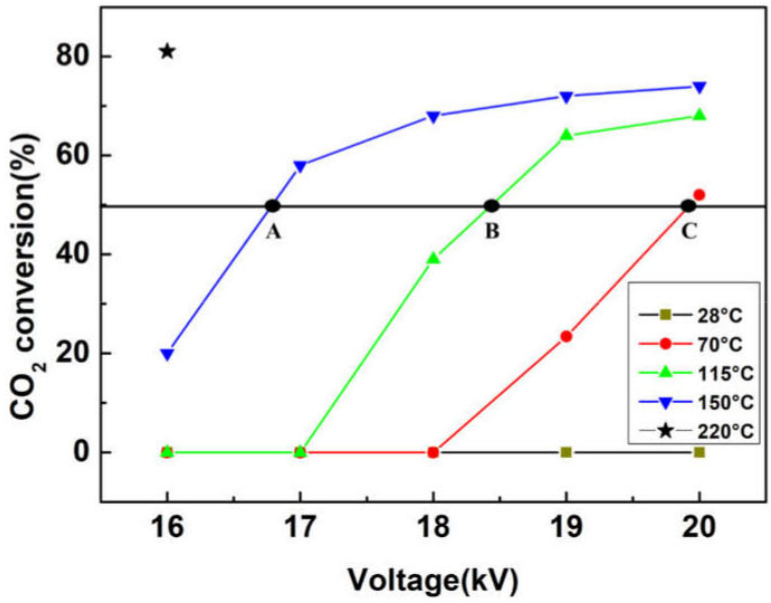

Figure 3-11. CO_2 conversion with different voltages under different reactor temperatures

To compare the influence of temperature on the CO_2 conversion, the voltage to achieve 50% of CO_2 conversion was extracted from the figure: point A, B and C. Point A, B, and C respectively represent the voltage to achieve 50% of CO_2 conversion at temperature of 150, 115 and 70°C, which are 16.8, 18.4, and 19.9 kV. This means that to obtain the same CO_2 conversion at lower temperature (70°C), a higher voltage was needed, that is to say, higher power is needed.

The maximum CO_2 conversion obtained in this experiment is 74% at 150°C under the voltage of 20 kV. And this CO_2 conversion is lower than 81%, which is achieved at 220°C at 16 kV.

This means that the CO_2 conversion obtained at 150°C and 20 kV still have the potential to increase at optimal condition, maybe by increasing the temperature or increasing the voltage.

The CH_4 selectivity at different temperatures and voltages is presented in Figure 3-12. Compared with CO_2 conversion, the CH_4 selectivity had the similar trend as temperature and voltage vary. The difference is that CH_4 selectivity reached the maximum value at a lower temperature and voltage. The maximum CH4 selectivity was 92% at 150°C, which is slight lower than the value at 220°C (94%).

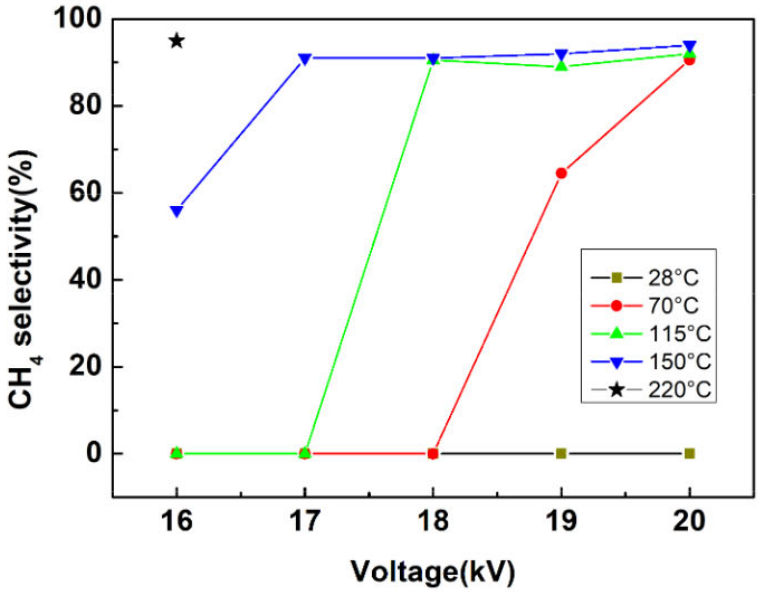

Figure 3-12. CH_4 selectivity with different voltages under different reactor temperatures

As a conclusion, the CO_2 methanation could take place at low temperature (lower than 220°C), but a higher voltage and power was needed, and the CO_2 conversion was lower. The CO_2 methanation could not occur at 28°C no matter which voltage was applied on the reactor. In the temperature of 70 to 150°C, at a certain temperature, the CO_2 conversion increased with the applied voltage (plasma power), and the CO_2 conversion increased with temperature at the same voltage (plasma power).

3.4.3 CO_2 methanation at high temperature (300 to 400 °C) in the plasma state

The respective role of high temperature and power in the reaction was studied in this section. The experiment set-up is shown in Figure 3-13. In this experiment, the plasma was placed in an electrical furnace. The electrical furnace was used to keep the temperature at stable state. And its temperature was adjusted by a regulated system. Due to the low convention from the reactor surface in the furnace, stable state of the temperature was 300 °C as the reaction took place, and the temperature could only be increased in the electric furnace. Therefore the temperature range studied in this section is from 300 °C to 400 °C.

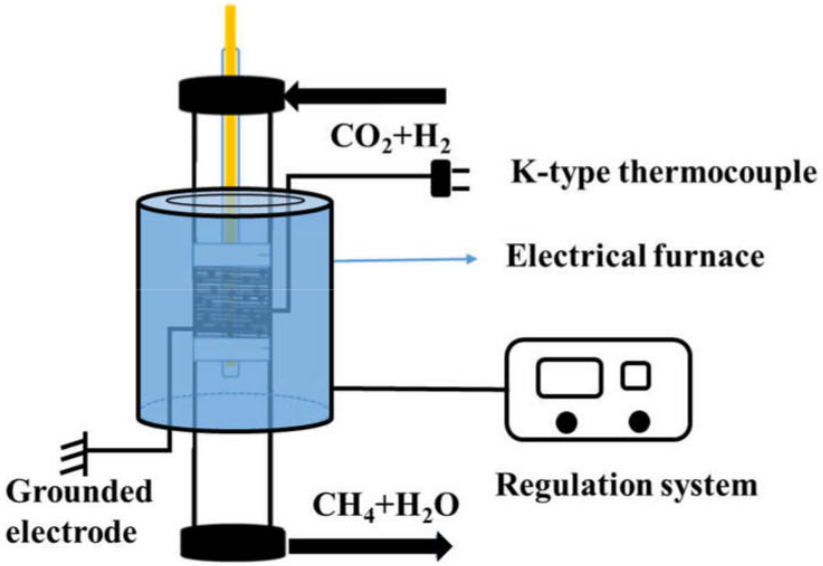

Figure 3-13. Scheme of set-up for the controlling the reactor temperature (high temperature)

Applied voltage was fixed at 11 kV, 13 kV and 15kV respectively to study the effect of the plasma power on the CO_2 conversion. As shown in Figure 3-14, at a fixed applied voltage, the CO_2 conversion decrease with the increase of temperature. For example, at 11 kV, the CO_2 conversion decrease from 85% to 80% when the temperature increase from 300 °C to 400 °C, and this could be explained by the reverse water-gas shift reaction (RWGS reaction) that

produces CO from CO_2 and H_2. Besides, at a certain temperature, a higher CO_2 conversion is obtained at a lower applied voltage, which means a lower applied plasma power. This phenomenon is more obvious at higher temperature (400 °C). At 400 °C, the CO_2 conversion is 80% at the applied voltage of 11 kV, and the CO_2 conversion decrease to 76% while the applied voltage increase to 15 kV. This maybe because that the plasma power is 7.3 W at 15 kV, which is way more than 2.7W at 11 kV, excess plasma energy leads to more active species, that helps to the reverse water-gas reaction at high temperature, thus the CO_2 conversion decrease.

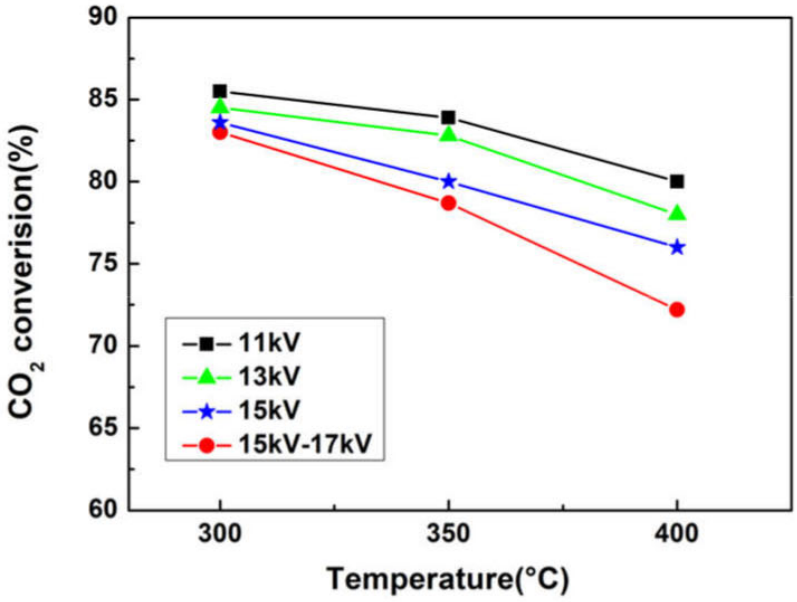

Figure 3-14. The CO_2 conversion varies with temperature under different applied voltage (peak to peak)

Compared to the experiment that the applied voltage is fixed at 15 kV, instead of using the heating system, the applied voltage is increased to 16 kV and 17 kV to keep the stable temperature at 350 °C and 400 °C respectively. And the CO_2 conversion decrease to 79% and 72% at 16 kV and 17 kV respectively from 83% at 15 kV. At 400 °C, when the temperature is kept stable at 17 kV, the CO_2 conversion is 4% lower than that at 15 kV. Besides, the plasma

power at 17 kV is 16.1W, which is a lot higher than 7.3W at 15 kV. This also prove that when the temperature is the same, the CO_2 conversion is lower when the applied power is higher.

Worth to mention, the applied plasma power at a fixed voltage increase a little with the increase of temperature, for example, at 11 kV, the applied plasma power increased from 2.7 W to 3.2 W when the temperature increase from 300 °C to 400 °C, as shown in Table 3-5. However, compared to different power applied to the reactor, this increase of power is ignorable.

Table 3-5. The increase of plasma power under different temperature

Voltage(kV)	Power(W)		
	300 °C	**350 °C**	**400 °C**
11	2.7	3.0	3.2
13	4.1	4.2	4.4
15	7.3	7.5	8.0
15-17	7.3	10.1	16.1

In conclusion, in the plasma-catalytic hybrid system, the CO_2 conversion decrease with the increase of temperature under a constant plasma power due to the reverse water-gas shift reaction. This is no need to perform the Sabatier reaction at higher temperature. And when the temperature is higher than 300 °C, the CO_2 conversion is lower when the applied plasma power is higher.

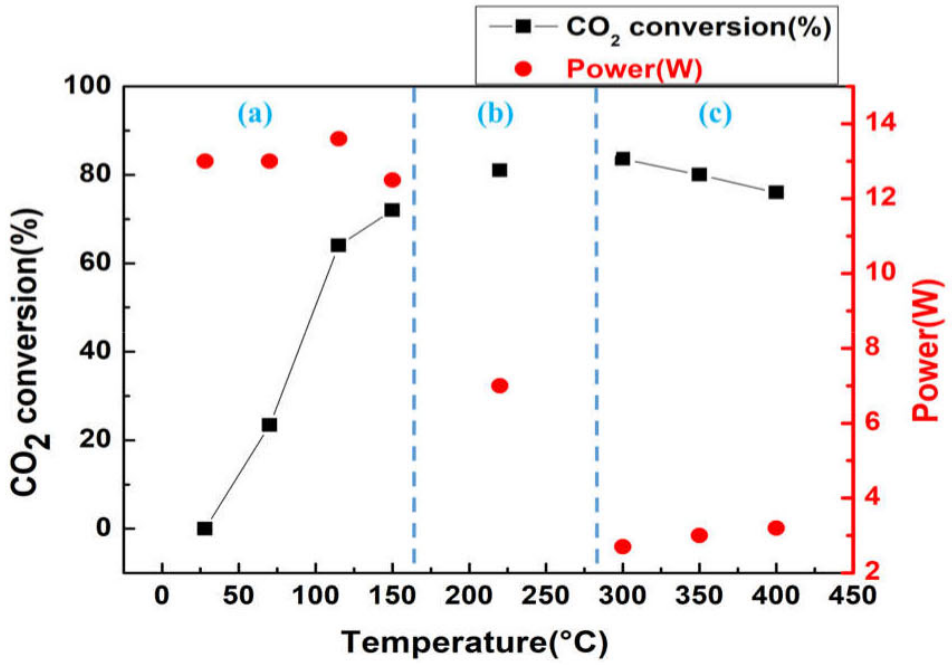

Figure 3-15. The CO_2 conversion at different temperatures in plasma-catalytic process: (a) low temperature system; (b) in the ambient air; (c) high temperature system

As a result, the CO_2 conversion at different temperatures is presented in Figure 3-15. It is worth to mention that the plasma power at different temperatures is different, which is also shown in the figure. Regardless of the plasma power, it can be seen that in the plasma-catalytic process, the CO_2 conversion increased with temperature before 220°C, and then CO_2 conversion decreased slightly with the increase of the temperature after 300°C. Besides, the temperature to obtain the maximum CO_2 conversion was between 220 and 300°C. However, it can be also stated from the figure that to make the reaction take place at low temperature (lower than 220°C), higher power was needed compared with the plasma power needed at higher temperature. For example, to have 23% of CO_2 conversion at 70°C, the plasma power needed was 13W, while with the consume of 7W of plasma power at 220°C, a CO_2 conversion of 81% can be achieved. Moreover, the plasma power needed at higher temperature was even lower as 3W. It is worthy to mention that due to the technical limitations, two temperature periods of 150 to 220°C and

220 to 300°C were not investigated in this research, which was also very important for the process.

As for the effect of plasma power on the CO_2 conversion independent of the temperature, it could be concluded that at low temperature (lower than 220°C), CO_2 conversion increased with plasma power, however, at high temperature (higher than 300°C) CO_2 conversion is lower at a higher plasma power.

As show in Figure 3-15, It is clear that the for the CO_2 methanation in plasma-catalytic process, high power was needed for the activation of the reaction at low temperature, and this power decreased with the increase of the reaction temperature. The reason maybe that in the plasma-catalytic process for the methanation of CO_2, the provided activation energy for this reaction is combination of plasma power and temperature. To achieve the minimum barrier energy that the reaction could take place, high plasma power energy is needed because the thermal activation energy is small at low temperature. However, the thermal activation energy increase with the temperature, so that the energy provided by plasma decrease. Moreover, the plasma power needed when the temperature is higher than 350°C could be lower as zero to have a high CO_2 performance.

In a conclusion, in the plasma catalytic process, the CO_2 conversion was influenced by temperature and plasma power. The influence of temperature on CO_2 conversion cannot be discussed without the consideration of plasma power. Moreover, it was difficult to determine the temperature to obtain the highest CO_2 conversion due to the lack of research in the temperature period between 220 °C and 300 °C and complex influence of plasma power on the CO_2 methanation process.

Moreover, the capacitance of the reactor was measured by Q-U Lissajous method under different temperature in plasma process. It was found that no remarkable difference of capacitance of the reactor was observed in the range of temperature studied, and the capacitance of the cylinder plasma reactor was around 2.4 pf. Thus the relative permittivity of the catalyst-bed was also a constant, which is 8 according to the simulation model.

3.5 CO_2 methanation in the adiabatic plasma reactor

One of the most interesting parameter in the industrial process is the power consumption. In the plasma-catalytic process for CO_2 methanation, the activation energy was only plasma power. Plenty of effort has been made to decrease the plasma power in the process, such as the optimization of configuration plasma reactor, the choice of the material, and the optimization of the catalyst particle size and the pressure in the reactor etc. As show previously, working at elevated temperature (above 200°C) allows to decrease the electrical power consumed by the plasma discharge.

In this plasma catalytic process, the CO_2 methanation could be activated by only plasma at 15 kV with a power consumption of 7.3 W. Besides, the CO_2 methanation could also be activated by the synergy of plasma and thermal heating, for example, the reaction could take place under voltage of 11 kV with thermal heating, the plasma power used in this condition is 2.7 W. But extra heating system is needed to help to activate the reaction in this process, it is not economic and not recommended. Therefore, only the case that the reaction is activated by plasma will be discussed in this part.

It is well known that the CO_2 methanation is a highly exothermic reaction, therefore plenty of reaction heat will be released as the reaction take place. However, in the former research of plasma-catalytic of CO_2 methanation, this energy (reaction heat) was released into the air as a waste. As a result, part of the plasma power injected in the reactor was used only to heat the reactor, therefore the plasma power was maybe higher than necessary.

In this part therefore, the objective is to decrease the plasma power by taking advantage of the exothermicity of the CO_2 methanation.

As discussed before in section 3.4.1, the voltage applied to activate the CO_2 methanation decrease if the air convection of the reactor surface decrease, thus the applied plasma power decrease. Besides, the reaction could take place under low applied voltage with the help of heating system. Therefore, an adiabatic plasma reactor and activation method that could make Sabatier reaction take place under low voltage and low power was designed, by which the power

consumption could be decreased during the whole process. The thermal isolation of the plasma reactor is achieved by the glass wool covered around the reactor. The scheme of set-up of the adiabatic plasma reactor is shown in Figure 3-16.

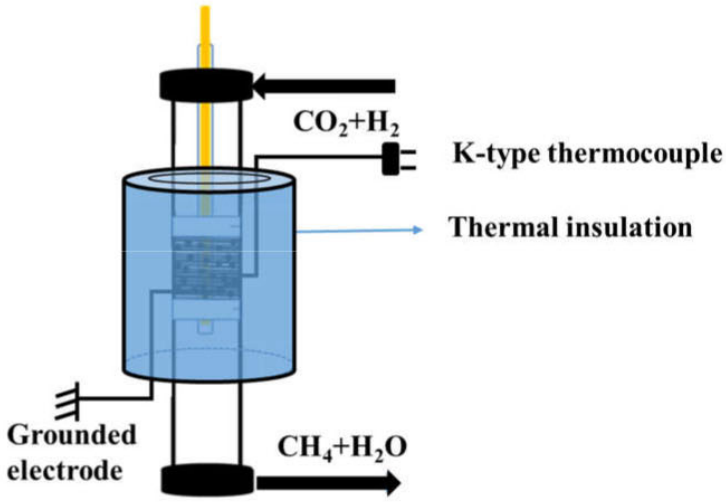

Figure 3-16. Scheme of set-up of the adiabatic plasma reactor

The procedure to activate the CO_2 methanation in the adiabatic plasma reactor is shown in Figure 3-17. The experiment started at the applied voltage of 13 kV, and the temperature was 128 °C with a power consumption of 3.6W, while no CH_4 was detected at this voltage. The applied voltage was increased with a step of 1 kV, and at each state, the voltage was kept stable for 30 mins to achieve a stable state. The CO_2 methanation did not take place until the voltage of 15 kV was applied to the reactor, and the temperature was 300 °C with a power consumption of 7.3 W, and the CO_2 conversion was 84% at this voltage. After keeping stable at 15 kV for 30 mins, the voltage was decreased step by step to study the CO_2 conversion at lower voltage. With the decrease of voltage, the minimum voltage that CO_2 methanation could take place was at 11 kV, and the CO_2 conversion is 80% with a power consumption of 2.7 W. When the voltage was lower than the voltage, the reaction stopped.

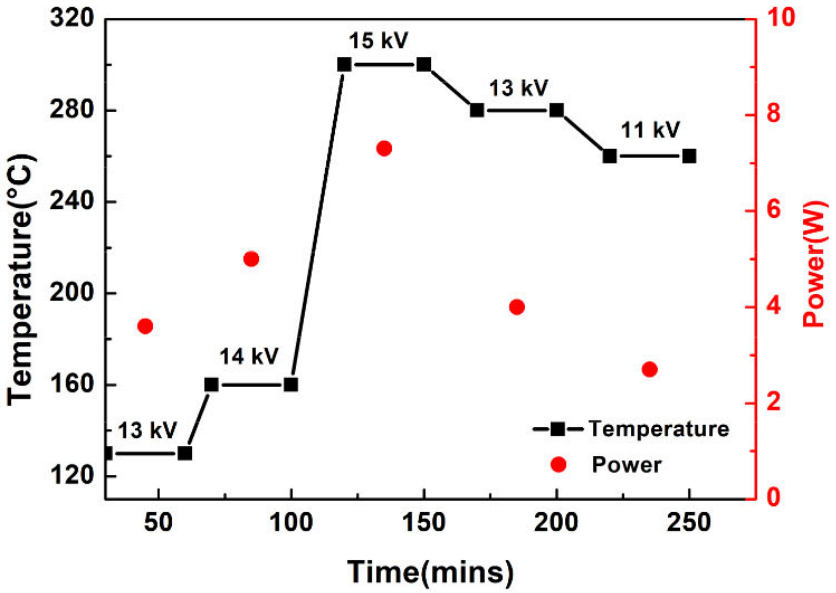

Figure 3-17. The procedure to activate the CO_2 methanation in adiabatic plasma reactor

In this process, the reaction took place at 15 kV, but there was extra energy for the activation of the CO_2 methanation at this state. Therefore, decreasing the voltage to optimal voltage could help make the most of the energy, which meets the economic needs of the industry. Although the CO_2 conversion decreased with voltage, the plasma power also decreased. As shown in Figure 3-18, compared to the c.a. 4% decrease of the CO_2 conversion from 84% to 80% when the voltage decreased from 15 kV to 11 kV, the plasma power decrease from 7.3 W to 2.7 W, which was a decrease of 63% the power.

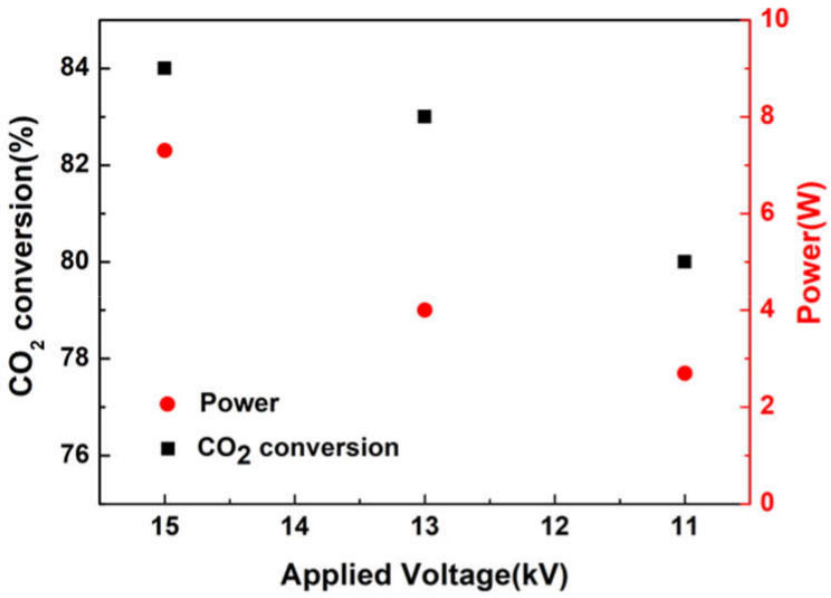

Figure 3-18. The CO_2 conversion in the adiabatic plasma reactor

The principle of this process is thus to take advantage of the exothermicity of the CO_2 methanation. As we know, there is plenty of heat released from the reaction as it take places, and this research demonstrates that this energy could be used to maintain the reaction together with plasma, thus the plasma power could be decreased. There is two steps in this process, the first step is to activate the reaction only with plasma power at the voltage of 15 kV with 7.3W.

The second step is to maintain the reaction at a lower voltage with the help the released heat from the reaction owing to the thermal isolation of the reactor. In this second step, the voltage applied is 11 kV with a plasma power of 2.7 W, which is a large decrease of power compared to 7.3 W at 15 kV. And in this process, there is no extra heating system, thus the process is easy to scale-up and it is economic.

3.6 Summary

This chapter is concentrated on the influence of temperature on the plasma-catalytic process for the methanation of CO_2 using a catalyst of $Ni/Ce_{0.58}Zr_{0.42}O_2$.

First, CO2 methanation was respectively performed in thermal catalysis process and plasma-catalytic process. Under the same GHSV of 46300 h^{-1}, to have a CO_2 conversion around 80%,

the temperature in plasma catalytic process was 220°C, which is around 130°C lower than the temperature in thermal process. Besides, in the plasma catalytic process, the CO_2 conversion decreased with the increase of applied voltage due to the increase of temperature and plasma power.

To determine the threshold temperature of the CO_2 methanation in plasma-catalytic process, a set of experiments with different flowrates of inlet gas mixture was performed. It was found that the temperature decreased with flowrate of inlet gas mixture. The threshold temperature was deduced when the flowrate is 0 mL/min, which is 116°C. Besides, COMSOL Multiphysics® software was used to simulate the temperature distribution of the reactor. The simulation indicated that the temperature difference between the reactor surface and the catalyst bed was almost negligible. As a result, the plasma threshold temperature for the Sabatier reaction was finally evaluated at 116°C based on experiment results and COMSOL Multiphysics® simulation.

Moreover, it was observed that the trigger voltage and power for the activation of CO_2 methanation could decrease due to the decrease of air convection in plasma process. Two systems that could control the temperature independent of plasma power were designed to study the respective roles of temperature and plasma power. It can be concluded that the influence of temperature and plasma power on CO_2 methanation were different in different temperature range. And it was also observed that the CO_2 methanation could be activated at various conditions: such as high power at low temperature or low power at high temperature. And this provide various potential for different aims in the industrial process in the future. However, it was difficult to determine the temperature, at which the best CO_2 conversion could be obtained, due to the technical limitation and the complex influence of plasma power on the process.

Finally, the CO_2 conversion was performed in the adiabatic plasma reactor. It was demonstrated that the exothermic heat released from the reaction could be used for the activation of the reaction, therefore, to decrease the consumed plasma power for the reaction. As a result, to achieve a CO_2 conversion of 80%, the plasma power used was 2.7 W, which is only 37% of the plasma power consumed in the normal condition.

Chapter IV Effect of physical parameters on CO_2 methanation in thermal and plasma catalytic processes

4.1 Introduction

Plasma-catalytic methanation of CO_2 was assayed in the presence of a CeZrOx-supported Ni catalyst, proving that high CO_2 conversions and high methane yields can be obtained under dielectric barrier discharge (DBD) plasma conditions and that they are maintained with time-on-stream over 100 h operating time.[143] In the previous chapter, temperature distribution of the reactor was studied with COMSOL Multiphysics® software, and it was found that the temperature measured on the reactor surface is almost equal to the temperature inside the catalytic bed, and that the threshold temperature of CO_2 methanation is around 116°C. To the best of our knowledge, there is a lack in the literature about studying the influence of physical parameters related to the catalysts such as the particle size or the influence of physical parameters related to the process (pressure...) on the activity and plasma discharge behavior.
Therefore, herein, ceria-zirconia nickel based catalysts were prepared within three different particle sizes, and were characterized by SEM, BET, TPD, TPR, and XRD. The catalyst activity was then tested in conventional thermal heating system and plasma-catalytic system to investigate the effect of particle size on the CO_2 methanation. The effect of Gas hourly space velocity (GHSV) on the CO_2 methanation in both processes (thermal and DBD plasma) was also investigated. Furthermore, the influence of pressure on CO_2 methanation in in both processes (thermal and DBD plasma) was studied.

4.2 Characterization of catalysts in different particle sizes

Three catalysts in different particle sizes were made in following procedure (Figure 4-1): first, the catalyst was prepared in the same way as before, and original catalyst powders were pressed into a tablet with a mold. Afterwards the tablet was crushed into small pieces with different particle sizes, finally catalyst particles were separated into different sizes with several meshes

(250μm, 325μm, 500μm), finally, three types of catalytic particles were obtained: C1 with particle size below 30 μm (original size), C2 with particle size between 250 μm and 325 μm, and C3 with particle size above 500 μm.

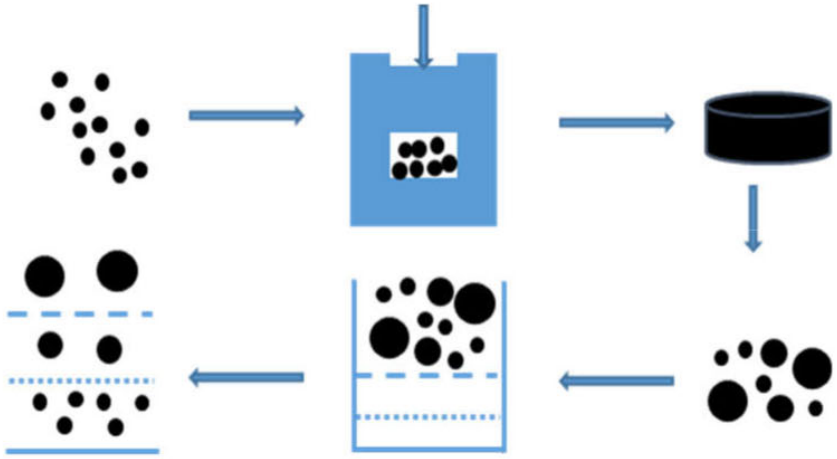

Figure 4-1. The protocolto prepare catalysts with different particle sizes

Before the activity tests, catalysts have been characterized by various methods to determine the physical and chemical properties of different catalysts.

SEM pictures of the three types of catalysts with different particle size are presented in **Figure *4-2***. Fig. 2-(a), Fig. 2-(c), and Fig. 2-(e) show the macroscopic shape of these particles, while the surface of the catalyst could be seen in Fig. 2-(b), Fig. 2-(d) and Fig. 2-(f). It is obvious that the catalyst surface remained similar while the particle size increase.

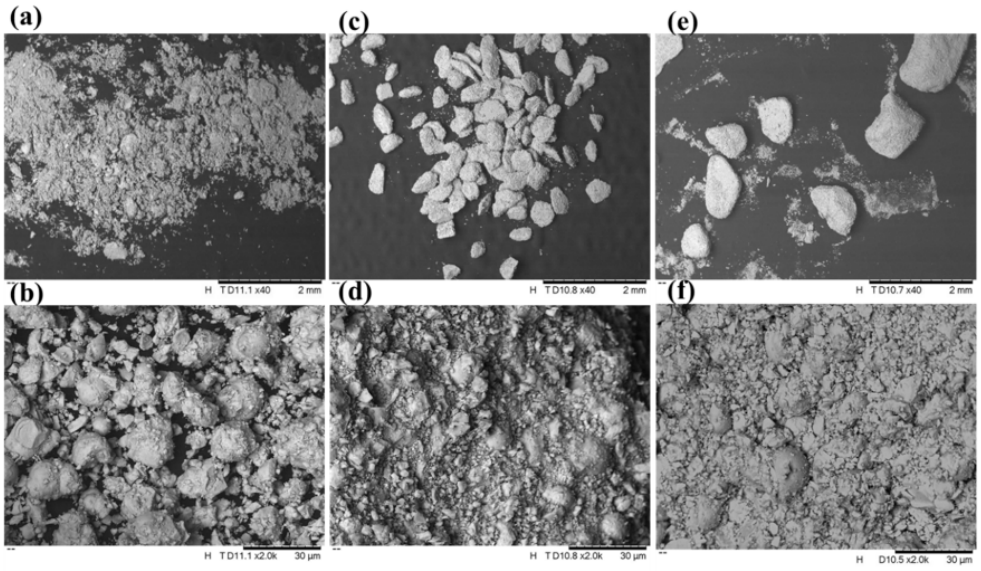

Figure 4-2. SEM pictures of three catalysts with different particle sizes: Fig.2-(a) and Fig.2-(b) catalyst with a particle size below 30 μm, C1; Fig.2-(c) and Fig.2-(d) catalyst with a particle size between 250 - 325 μm, C2; Fig.2-(e) and Fig.2-(f) catalyst with a particle size higher than 500 μm, C3

The specific surface area (S_{BET}), pore volume and radius of pore of catalyst with different particle sizes measured by N_2 adsorption-desorption method are shown in Table 4-1. There is no difference between these properties: the three catalysts present similar specific surface area (56.00 m^2/g), pore volume (0.139 cm^3/g) and radius of the pore (4.61 nm) despite of the great difference of particle sizes. This means that the preparation of the catalyst with bigger particle size does not affect the micro-structure of the catalyst.

Table 4-1. Physical property of catalyst with different particle sizes

	Surface area [m^2/g]	**Pore volume (p/p_0=0.981) [cm^3/g]**	**$r_{p,peak}$(Area) [nm]**	**H_2 consumption [mmol H_2/g]**
C1	56.00	0.139	4.61	1.2
C2	55.67	0.158	4.61	1.2
C3	56.40	0.155	4.61	1.1

Figure 4-3 presents the hydrogen consumption profiles of the three catalysts investigated in the study. Two reduction peaks at about 400 °C and 470 °C, denominated α and β, respectively, can be observed for all the tested catalysts. The first peak (α, 400 °C) corresponded to the reduction of the NiO species of weak interaction with CZ oxide. The second peak (β, 470 °C) is ascribed to the reduction of incorporated Ni cations (Ni^{2+}) into the CZ oxide, thus in strong interaction with the support.[60] For this latter peak, there was no shift in temperature with the increase of catalyst particle size. Finally, for C1, C2 and C3, the H_2 consumption remained the same with 1.2 mmol of H_2 consumed per gram of catalyst. This means there are same amount oxide of NiO have been reduced to metallic nickel.

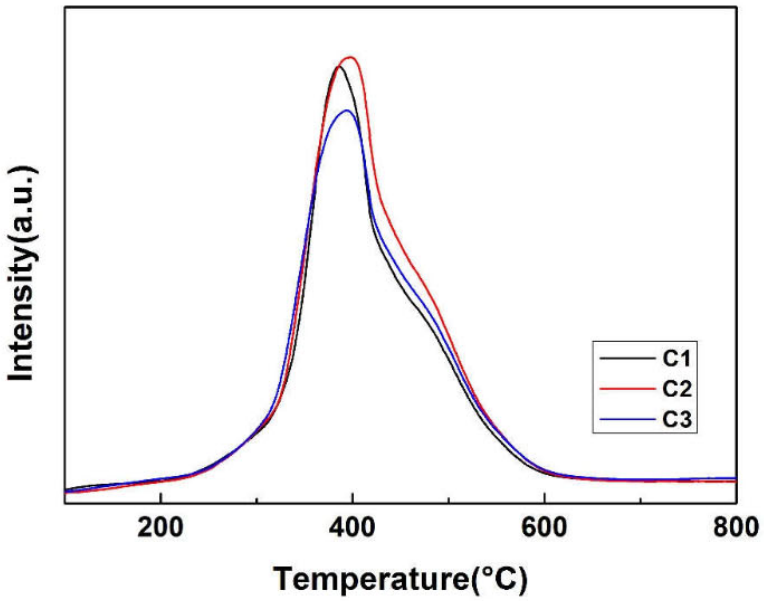

Figure 4-3. H_2-TPR of catalysts with different particle sizes

A CO_2 temperature-programmed desorption (CO_2 TPD) experiment was conducted to determine the basicity of catalysts, as shown in Figure 4-4. As expected, three peaks can be identified for each catalyst. The total number of basic sites increased from 185 to 214 μmolCO_2/g and 207 μmolCO_2/g with the particle size increasing from around 30 μm to 300 μm and 500 μm respectively (Table 4-2). As already described elsewhere[144, 145], there are three types of basic sites (weak, medium-strength and strong). The second peak (medium basic sites) and the third peak (strong basic sites) shifted to low temperature with the increase of the catalyst particle size. Furthermore, the basicity of the strong peak (third peak) increased from 47 to 64

μmol CO_2/g and 66 μmol CO_2/g when the particle size increasing from 30 μm to 300 μm and 500 μm respectively. This explained the increase the total basicity with the increase of the catalyst particle size.

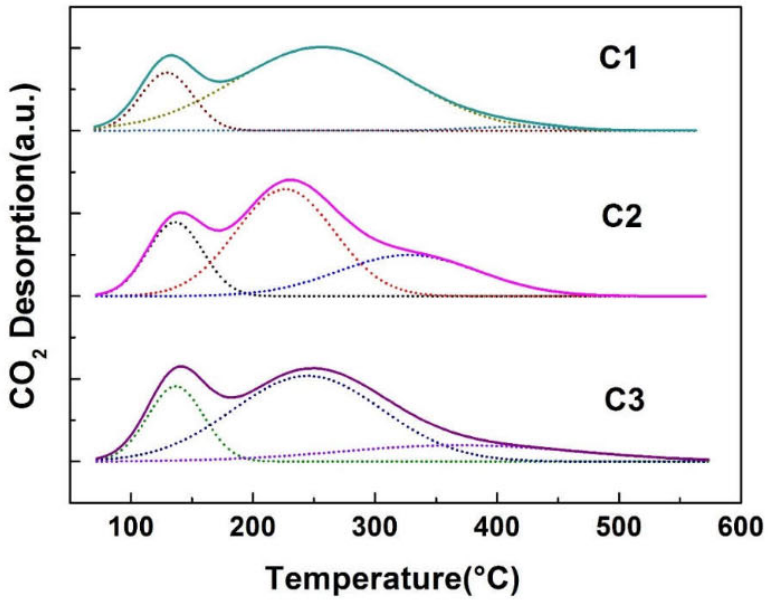

Figure 4-4. CO_2-TPD profiles for catalysts with different particle sizes: C1(30μm); C2(250 -325μm); C3(>500μm)

Table 4-2. Peak position and deconvolution of the CO_2-TPD profiles obtained for catalysts with different particle size

	Temperature[°C]			**Basicity [μmolCO_2/g]**			**Total basicity [μmolCO_2/g]**
	1st peak	2nd peak	3rd peak	1st peak	2nd peak	3rd peak	
C1	130	257	420	18	120	47	185
C2	135	226	332	15	135	64	214
C3	136	243	385	21	120	66	207

The XRD patterns of the different catalysts prior thermo-catalytic and plasma-catalytic tests

and after tests in thermal and plasma-catalytic processes are given in Figure 4-5a and Figure 4-5b respectively. Prior thermal process, catalysts were reduced in the presence of 50 vol%. H_2/Ar mixture at 470 °C for 2 h, while the catalysts were reduced by H_2 plasma under the applied voltage of 19 kV for 30 mins with the temperature around 200 °C prior the plasma-catalytic process.[146] As shown in Figure 4-5, in the XRD patterns, the reflection at 44.5° is the metallic Ni, while catalysts exhibit very small reflections at 37°, 43°, 63° that can be attributed to the presence of NiO. Prior run, the XRD patterns evidence that only Ni crystalline phases is present after thermal reduction except for C3, maybe because of insufficient reduction. After plasma reduction (a-C1, c-C2, e-C3), there are several marked diffraction peaks corresponding to the presence of both NiO and Ni° crystalline phases for catalyst C1, while XRD patterns only evidence the presence of the Ni crystalline phases for catalysts C2 and C3, thus indicating a complete reduction of NiO to Ni°. After methantion experiments, the presence of NiO (around 43°) was observed in both processes, due to the oxidation of Ni.However the peak of NiO in plasma process was less obvious compared to thermal process, maybe because the plasma continuously reduced NiO the during the process.

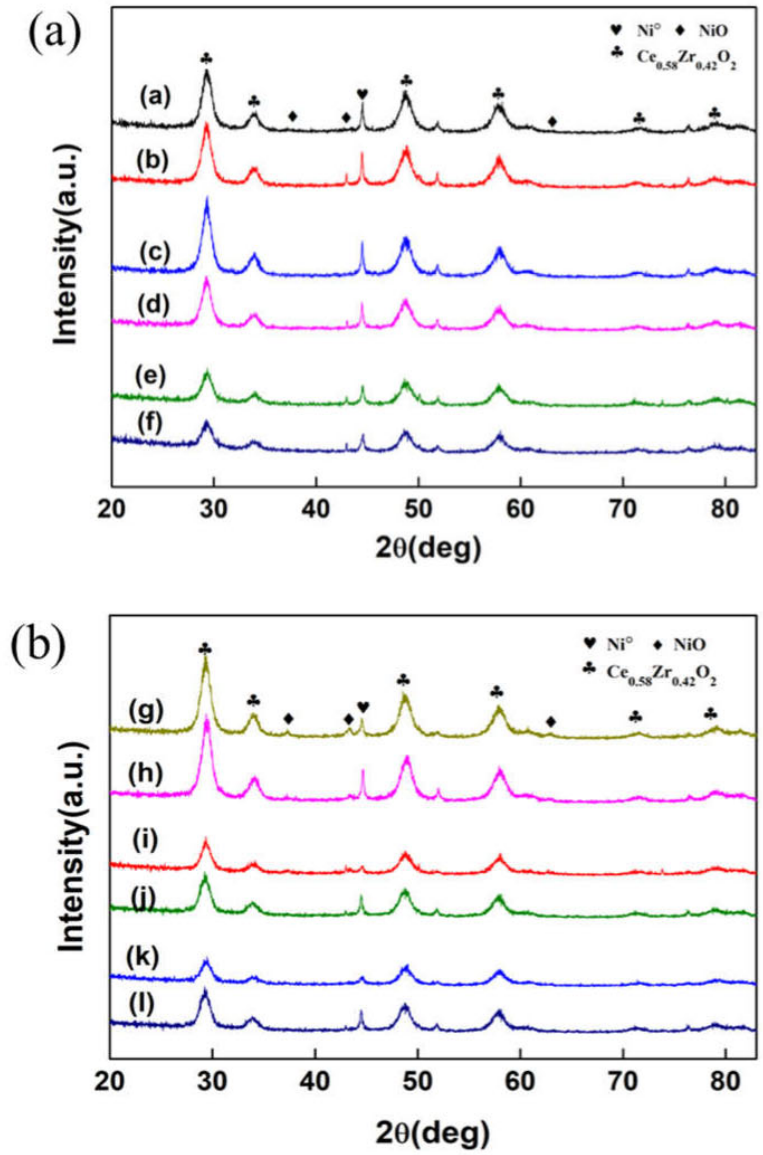

Figure 4-5. XRD patterns acquired for catalysts with different particle sizes: (a) thermal process: a-C1 after reduction, b-C1 after test, c-C2 after reduction,d-C2 after test, e-C3 after reduction, f-C3 after test; (b) plasma-catalytic process: g-C1 after reduction, h-C1 after test, i-C2 after reduction, j-C2 after test, k-C3 after reduction, l-C3 after test.

Table 4-3 presents the metallic Ni crystallite sizes, calculated from XRD file using Scherrer equation based on the reflection peak of Ni crystallite at 44.5°, after reduction and methanation

tests. In this equation, K is a dimensionless shape factor, with a value close to unity, and in this calculation, the typical value used was 0.89. λ is the X-ray wavelength, 0.15418 nm. β is the line broadening at half the maximum intensity (FWHM), which can be read from the XRD file. Finally θ is the Bragg angle, which is around 22.25° in this case).

$$\mathbf{D} = \frac{K \cdot \lambda}{\beta \cdot cos\theta}$$ Scherrer equation

In thermal process, after reduction, the metallic Ni crystallite sizes were smaller when the catalyst particle size was bigger, thus indicating a higher dispersion of the active metal phase on the support during the reduction. After test the Ni crystallite sizes increase because of the well-known metal sintering effect. In the plasma-catalytic process, the evolution of Ni crystallite size shows similar tendency. It is noteworthy mentioning that the Ni crystallite sizes in the plasma-catalytic process are smaller than those in thermal process, proving a better dispersion of the active metal phase on the support. This maybe due to the different reduction temperature used in two process. Indeed, in thermal reduction process, the temperature used was 470 °C, while the temperature used in the plasma-catalytic reduction process was only around 200 °C. The Ni crystallite size was larger in the thermal conduction process because of the sinter effect at high temperature.

Table 4-3. Ni crystallite size calculated for XRD patterns using Scherrer equation (nm)

catalyst	Thermal process		Plasma-catalytic process	
	After reduction	After reaction	After reduction	After reaction
C1	32±1.6	34±1.7	25±1.3	32±1.6
C2	27±1.4	29±1.5	23±1.2	24±1.2
C3	27±1.4	28±1.4	20±1.0	26±1.3

4.3 Effect of catalyst particle size on the CO_2 methanation

The effect of catalyst particle size on the CO_2 methanation was then studied in thermal and plasma-catalytic process respectively. In thermal process, catalyst activity was tested in the U

reactor placed in the oven, while in plasma-catalytic process, it was tested in the cylinder plasma reactor.

4.3.1 Catalyst activity tests in thermal process

The catalytic activity for CO_2 methanation in thermal process is presented in Figure 4-6.

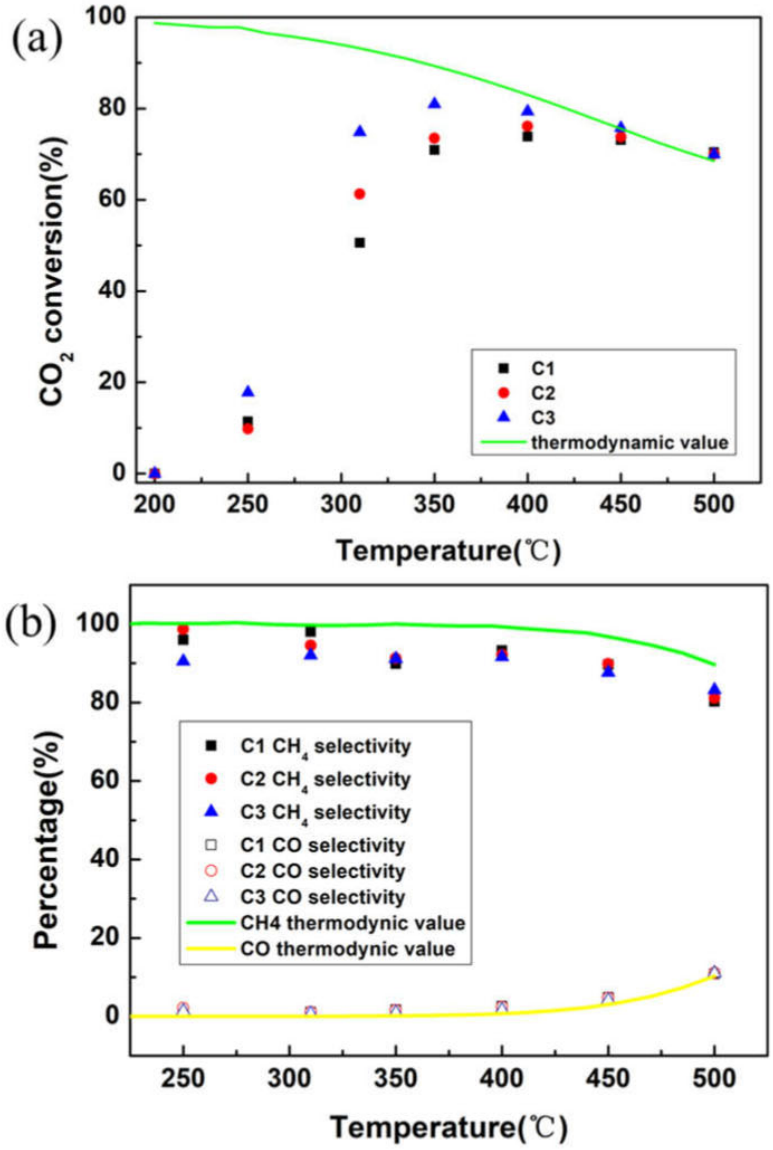

Figure 4-6. Activity of catalysts with different particle sizes for CO_2 methanation in thermal process: (a) CO_2 conversion; (b) CH_4 selectivity and CO selectivity *(GHSV=46300 h^{-1})*

From the temperature range of 200 °C to 500 °C, the CO_2 conversion is higher when the catalyst particle size is larger, as shown in Figure 4-6a. Especially at 310 °C, the CO_2 conversions of catalyst C1, C2 and C3 were respectively 51 %, 61 %, and 75 %. Besides, the highest CO_2 conversion of catalyst C3 was 81 % at 350 °C, while the highest CO_2 conversion of catalyst C1 was 74 % at 400 °C. Therefore, the increase of particle size from 30μm to 500μm contributed not only to an increase of CO_2 conversion of 8%, but also to a shift of the temperature for the best catalyst activity from 400 °C to 350 °C. In addition, there was no significant difference in the CH_4 and CO selectivities, as is shown in Figure 4-6b.

The reason why the temperature for having the best conversion shifted to lower temperature maybe can be linked with strong basicity properties. Indeed, it was found that the third peak in TPD, corresponding to the strong basic sites, shifted to lower temperature with the increase of particle size. It is worthy to mention that the increase of the total basicity from 185 to 207 μmolCO_2/g may not be the reason for the increase of the CO_2 conversion. Because the increase of basicity was mainly from the strong basic site, while the CO_2 methanation mainly takes place on weak and medium basic site.[144, 147] The explanation for the increase of the CO_2 conversion could be that the smaller metallic Ni crystallite size (27 nm) of catalyst C3 and C2 after reduction compared with catalyst C1 (32 nm), thus confirming a better dispersion of Ni on the support, which contribute to a better CO_2 conversion. Indeed, according to the literature, the methanation reaction is strongly structure sensitive,[148] the catalyst with smaller metallic Ni crystallite size can exhibit better catalyst activity.[149] Besides, the Ni crystallite sizes increased after test because of the metal sintering effect.

Moreover, gas flow maldistribution in the catalyst bed maybe also have an influence on the catalyst activity. Due to the gas flow maldistribution, the gas velocity inside the porous catalytic bed is not uniform. In some areas the gas velocity is more rapid due to a “channeling effect”, thus results in the insufficient contact of the mixture and catalyst surface. The maldistribution could be maybe be more important when the particles are small. Besides, the shape of catalyst with bigger particle size was not uniform, namely bringing in the sharp geometrical variations along the gas path. The gas path in the catalyst bed maybe longer due to the collision of the gas

and catalyst, which may results in a higher residence time of gas mixture in the catalyst-bed, and contributes to a better CO_2 conversion.

4.3.2 Catalyst activity tests in plasma catalytic process

CO_2 methanation at the flow rate of 200 mL/min

To compare the effect of particle size on the CO_2 methantaion in plasma-catalytic process, 300 mg of each catalyst was loaded in the plasma cylinder reactor. The catalyst activity tests at plasma conditions was first performed at the flow rate of gas mixture of H_2 and CO_2 at 200 mL/min with a stoichiometric ratio of 4:1. The experiment started at the voltage of 17 kV, where no CH_4 was ovserved. The voltage was increased by 1 kV at each step. The CO_2 methanation did not takes place until the voltage of 19 kV was applied on the reactor, and the voltage needed to trigger the reaction was the same whatever the size of the catalyst. The catalyst performances for CO_2 methanation at 19 kVand 20 kV are presented in Table 4-4.

Table 4-4. Performance of catalyst with different particle sizes in plasma-catalytic process (GHSV=46300 h^{-1})

	19 kV			**20 kV**		
	X_{CO_2} (%)	**Power (W)**	**T (°C)**	**X_{CO_2} (%)**	**Power (W)**	**T (°C)**
C1	68 ± 2	14.9 ± 1	215 ± 5	66 ± 2	19.0 ± 1	235 ± 5
C2	79 ± 2	15.2 ± 1	225 ± 5	76 ± 2	20.2 ± 1	240 ± 5
C3	79 ± 2	15.9 ± 1	220 ± 5	78 ± 2	20.0 ± 1	240 ± 5

X_{CO_2} is the conversion of the CO_2; T is the temperature of the reactor

As already said in chapter 3, to obtain a similar CO_2 conversion at the same GHSV, the temperature needed in plasma condition was only 220 °C, which is much lower than the temperature (350 °C) in thermal condition.

From Table 4-4, one can see that catalyst particle size affects the CO_2 conversion in a plasma-catalytic hybrid process. At 19 kV, catalyst C1 (30 μm) presented a CO_2 conversion of 67.6%, while the larger particle catalysts C2 (250μm - 300 μm) and C3 **(> 500 μm)** had a CO_2 conversion of around 79 %, which increased by 16.9% compared with the CO_2 conversion of

catalyst C1. The same phenomenon that catalyst with bigger particle size had higher CO_2 conversion was also observed at 20 kV. With the increase of voltage to 20 kV, there was a slight decrease of CO_2 conversion for all three catalysts due to the increase of the temperature and plasma power, which does not favor the reaction equilibrium. As for selectivity, three catalysts with different particles size had the same CO and CH_4 selectivities for 19 kV and 20 kV. Moreover, the reactor temperatures for three catalysts are the same at a certain voltage, which was around 220°C at 19kV, and the temperature increased to 240°C with the increase of voltage to 20 kV, and they are not influenced by the particle size of catalysts. Therefore, it is clear that increasing the catalyst particle size had a positive influence on the CO_2 conversion in a plasma-catalysis hybrid process as in the thermal process, but its influence on the selectivity, temperature and power could be ignored.

The reason could be again that the metallic Ni crystallite size was smaller with C3 (catalyst of larger particle size), thus confirming a higher dispersion of the active metal phase on the support during the reduction. And this helps to achieve a better CO_2 conversion as described in former part. Moreover, when the particle size of catalyst was bigger, the porosity of the catalyst-bed was bigger, and this results in a better homogeneity of the plasma inside the porous bed, which could also explain why CO_2 conversion was higher of the catalyst with bigger particle size. This phenomenon of better homogeneity of plasma with bigger particle size could be seen in chapter 5.

CO_2 methanation at different flowrates

The influence of flowrate on the CO_2 methanation was also studied in plasma catalytic process with the three catalysts of different particle sizes, as shown in Figure 4-7. In this experiment, the flowrate of inlet reactant mixture increase from 100 mL/min to 350mL/min with a stoichiometric ratio of H_2 and CO_2 of 4:1. As studied before, the voltage applied on the reactor was 19 kV to performe CO_2 methanation.

The CO_2 conversion of different catalysts at different flowrates is presented in Figure 4-7. It can be seen that for all three catalysts, the CO_2 conversion decreased with the increase of flowrate due to the increase of GHSV, which means a decreased residence time of the gas mixture in the catalyst-bed, which has also been observed elsewhere. Besides, the decreased of

CO2 conversion could be also due to the increase of temperature and plasma power with the increase of flowrate, which has been discussed in chapter 3. Moreover, it is clear that the CO_2 conversion of catalyst with bigger particle sizes (catalyst C2 and catalyst C3) was higher than the CO_2 conversion of catalyst C1 at different flowrates. This therefore confirms that increasing the particle size has a positive effect on the conversion of CO_2.

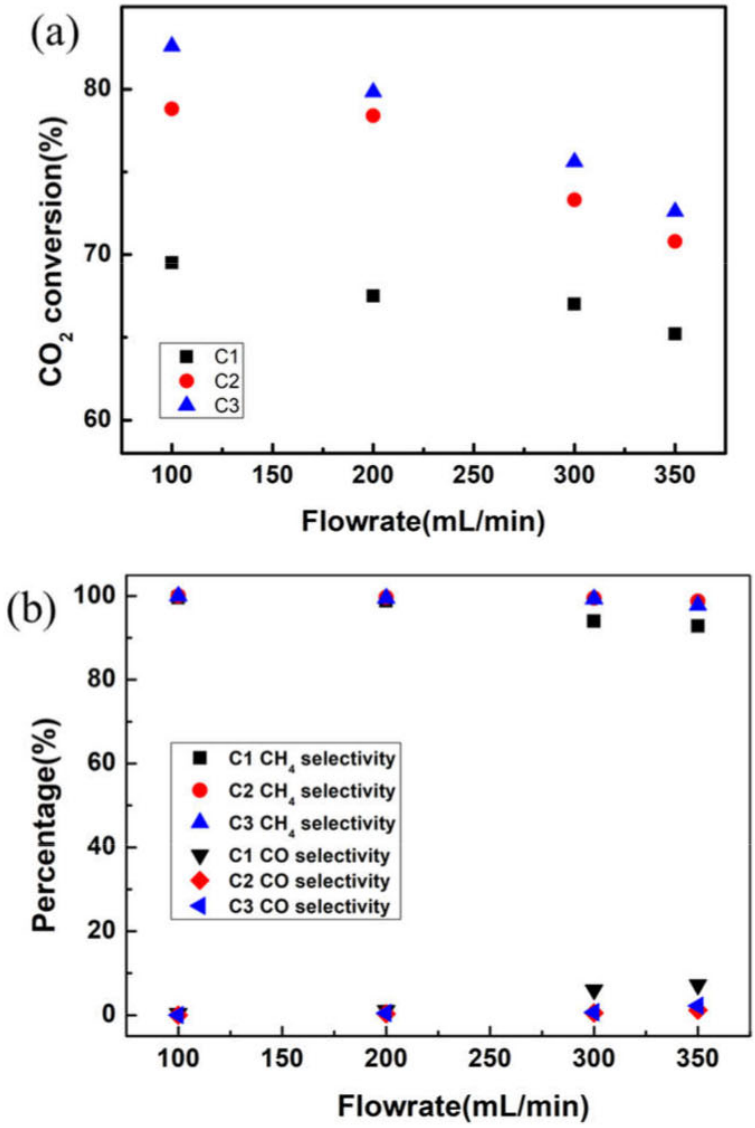

Figure 4-7. CO_2 methanation of catalysts with different particle sizes under different flowrates in plasma catalytic process: (a) CO_2 conversion; (b) CH_4 selectivity and CO selectivity

It can be also observed that this effect is less pronounced with the increase of flowrate, the difference of CO_2 conversion between three catalysts decreased from around 10% to 5% when the flowrate increased from 100 to 350 mL/min. This may be explained by the change of the temperature and plasma power. As can be seen from Figure 4-8, the temperature and power increased with flowrate, which is not favorable for the CO_2 methanation. At low flowrate, the difference of CO_2 conversion was mainly due to the different Ni crystallite size at low temperature. However, with the increase of flowrate, the temperature and plasma power also increased. At high flowrate, the temperature and plasma power maybe the main parameter predominate the performance of the catalyst, and the temperature and plasma power for three catalysts were the same at the same flowrate, so the difference of the CO_2 conversion decreased.

The Figure 4-8 present the temperature and the plasma power for each flowrate. As studied before, in the plasma-catalytic process, the temperature increased with flowrate of gas mixture due to the fact that (i) the reaction is exothermic and (ii) the reactor is not thermostated. In this set of experiments, the temperature increased from 180 °C to 270 °C when the flowrate increased from 100 to 350 mL/min, as shown in Figure 4-8a. Moreover, plasma power was also systematically measured (Figure 4-8b). It can be seen that plasma power increased with flowrate, which was also observed in chapter 3 and can be explained by the temperature increase. Finally, there was not an obvious difference of power and temperature between different particle sizes.

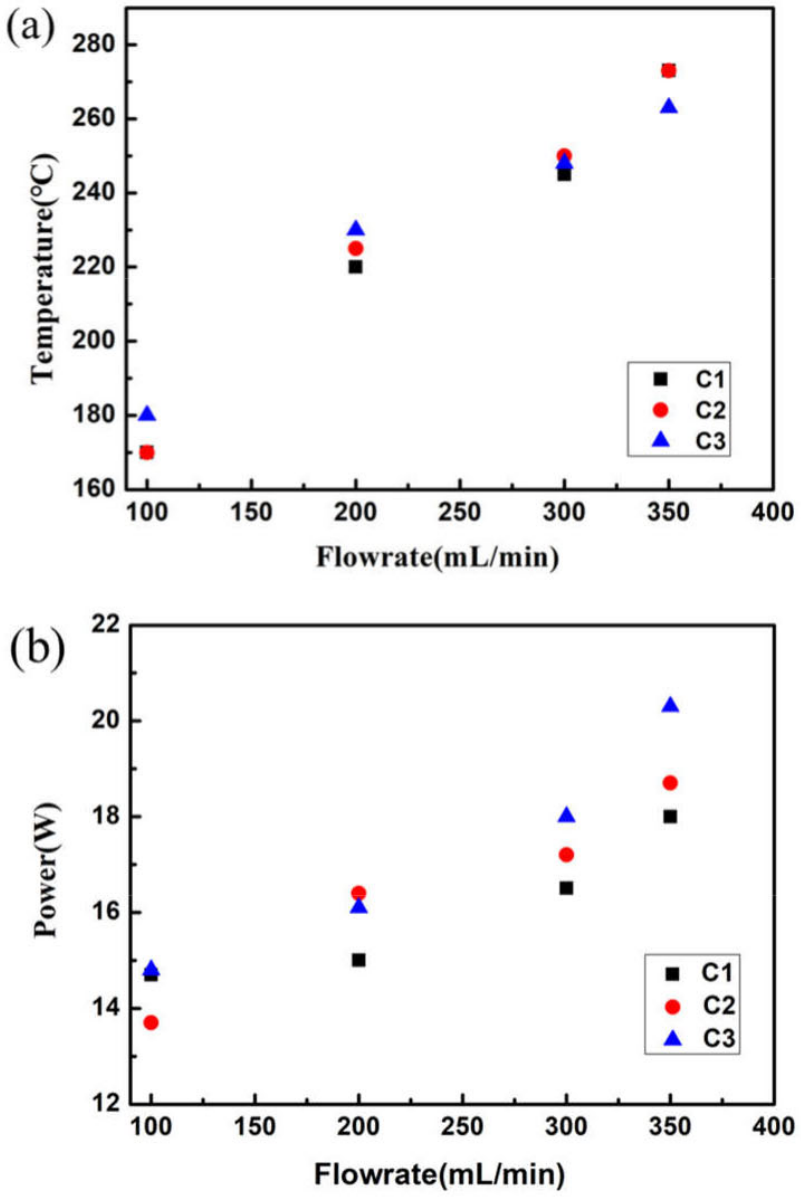

Figure 4-8. Power and temperature of catalysts with different particle sizes under different flowrates in plasma catalytic process: (a) Power; (b) Temperature

4.4 Effect of gas hourly space velocity (GHSV) on the CO_2 methanation

Effect of GHSV on the CO_2 methanation using catalytic particles of 500 micrometers size (catalyst C3) was investigated in plasma catalytic process and thermal process, respectively. Figure 4-9 presents CO_2 conversion and temperature in plasma catalytic process with a catalyst mass of 300 and 600 mg respectively in the reactor under different flowrates of inlet reactant mixture, corresponding GHSV are presented in Figure 4-10.

Due to the different catalysts loaded in the reactor, the catalyst-bed length was different for the catalyst mass of 300 and 600 mg, which was 6 and 12mm respectively. Therefore, lengths of electrode and plasma zone were also different, 6 and 12mm respectively, the same as the length of catalyst-bed. In these experiments, the applied high voltage was 18 kV, and the reactor was exposed to the ambient atmosphere as previously. The experiment parameters were summarized in Table 4-5.

Table 4-5. Experiment parameters for different mass of catalyst

Mass of catalyst (mg)	Catalyst-bed length (mm)	Electrode length (mm)	Plasma zone length (mm)	Applied voltage (kV)
300	6	6	6	18
600	12	12	12	18

Plasma power measured from experiment and power released from the reaction were represented in Figure 4-9. The plasma power measured by Q-U Lissajous method increased slightly with flowrate at a given mass of catalyst, which was also observed in chapter 3. Moreover, it was observed that when the mass of catalyst was increased to 600 mg from 300 mg, the plasma power was the same the same at a given flowrate even though the catalyst-bed length and grounded electrode length were extended from 6 mm to 12 mm. This means the plasma power mainly depended on the applied voltage and temperature, and not the electrode area. This result is surprising and may be explained by the plasma power consumption in this process mainly based on the voltage applied on the reactor. While the plasma zone length was different for two configurations, the applied voltage was the same as 18 kV. Because in the Q-

U Lissajous method, the power was calculated based on the voltage applied on the reactor and capacitor. Besides, it was also observed in chapter 3 that, as the applied voltage on the reactor decreased from 19 kV to 16 kV due to the decrease of air convection, the measured power decreased from 15 W to 7 W. Therefore, while higher CO_2 conversion was obtained with a bigger mass of catalyst loaded in the reactor, the power consumption was the same due to the same applied voltage.

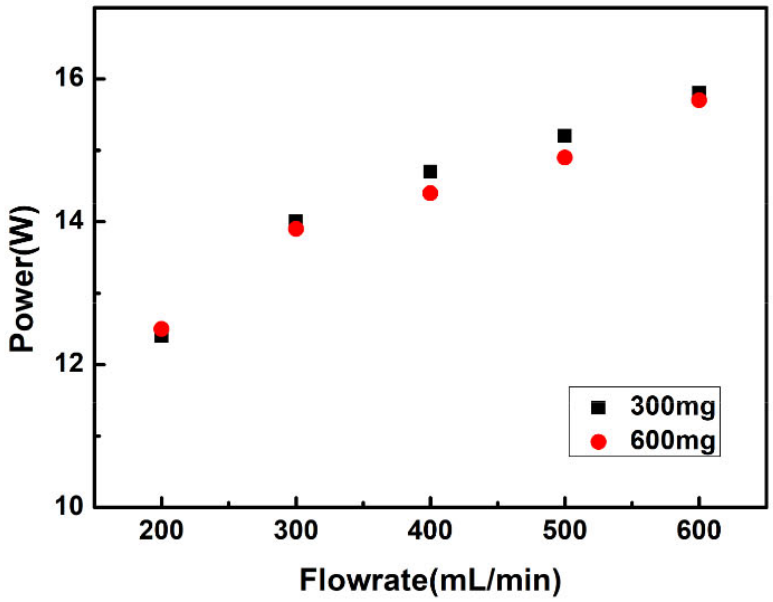

Figure 4-9. Plasma power with different mass of catalyst under different flowrates of inlet reactant mixture in plasma catalytic process at 18 kV

Moreover, the power released from the reaction due to its exothermicity was calculated from its flowrate, CO_2 conversion and enthalpy. The released power increase d from around 4 to 11W mainly due to the increase of flowrate from 200 to 600 mL/min. Besides, the released power was slightly higher when catalyst mass was 600 mg because of its higher CO_2 conversion.

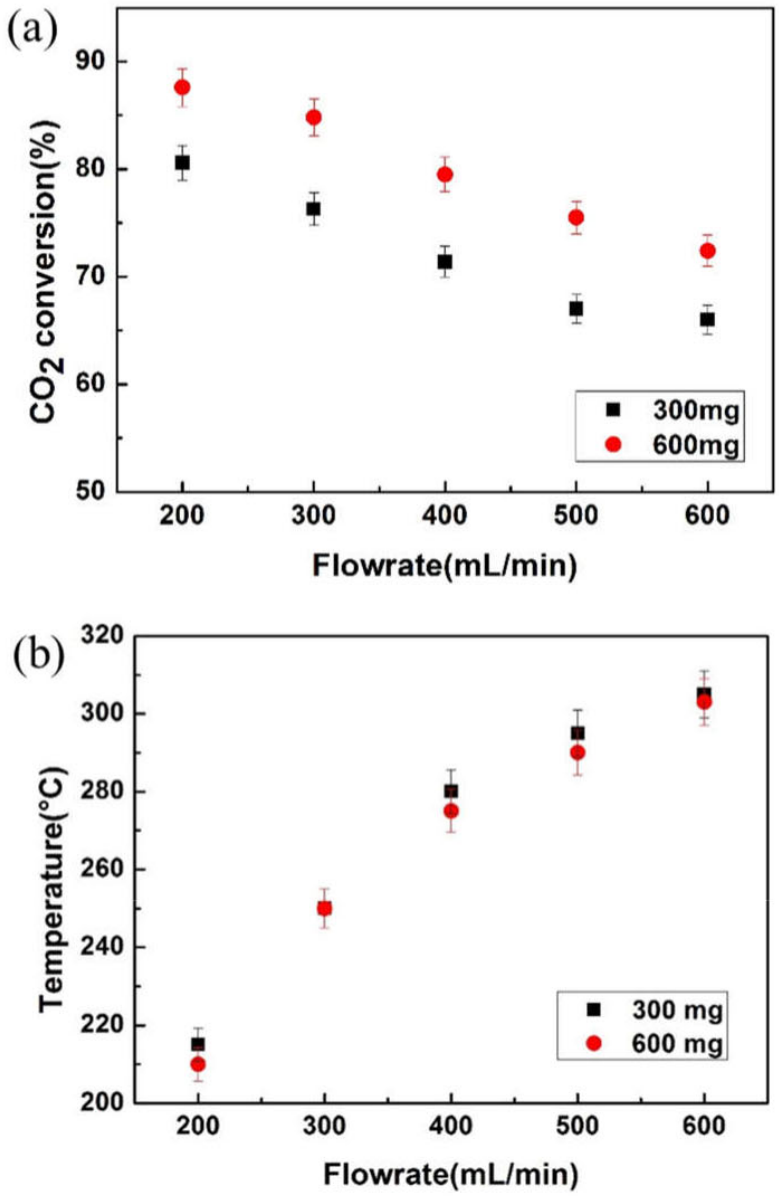

Figure 4-10. Catalytic performance and reaction temperature with different mass of catalyst under different flowrates of inlet reactant mixture in plasma catalytic process at 18 kV: (a) CO_2 conversion; (b) reaction temperature

As reported in Figure 4-10a, the CO_2 conversion decreased with the increase of the flowrate of the inlet reactant mixture at a certain mass of catalyst due to the increase of GHSV, temperature

and plasma power, as already studied before. Besides, it was clear that when the reactor was loaded of 600 mg of catalyst, the CO_2 conversion was around 8% higher than when the catalyst mass was 300mg, this was due to the decrease of GHSV. And corresponding GHSV with different mass of catalyst was presented in Figure 4-11.

Moreover, it is worth to mention that in plasma catalytic process, the temperature only increased with the flowrate of inlet reactant mixture due to the increasing released heat from the reaction, and it did not depend either on the GHSV or on the mass of catalyst loaded in the reactor. As presented in Figure 4-10b, even though the mass of catalyst loaded in the reactor is different, the temperature is the same at a given flowrate of the inlet gas mixture, and temperature increased from around 210 to 310°C when the flowrate increased from 200 to 600 mL/min.

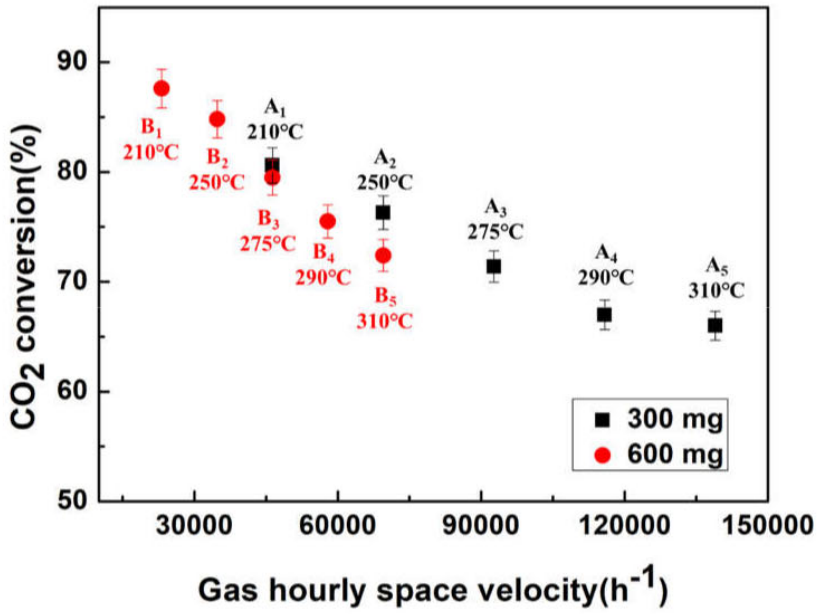

Figure 4-11. Effect of GHSV on CO_2 conversion in the plasma-catalytic process

Effect of GHSV on CO_2 conversion in plasma-catalytic process is presented in Figure 4-11. Logically the CO_2 conversion decreased with the increase of GHSV. For example the CO_2 conversion decreased by 25 % (from 88% to 66%) while the GHSV increased by 500% (from 23200 h^{-1} to 139000 h^{-1}). However, there could be an influence of the catalyst mass on the CO_2 conversion at the same GHSV. For example, at the GHSV of 70 000 h^{-1}, the CO_2 conversion

was smaller in the reactor loaded with 600 mg of catalyst compared to the one loaded with 300 mg. This can be explained by the fact that the temperatures and plasma power for these two conditions are different, even though the GHSV are the same. As mentioned before, different GHSV are achieved by varying the flowrate, and the temperature increase with flowrate. So point A_2 represents the CO_2 at 300 mL/min with 300mg of catalyst, the temperature is 250 ℃, while the temperature of point B_5 is 310 ℃ at 600 mL/min with a catalyst loaded of 600mg. The difference of temperature was due to the different released power from the reaction, which was respectively 5.9 and 11.4 W for point A_2 and point B_5. High temperature is not favorable for the methanation of CO_2, therefore, the CO_2 of point B_5 was lower than the CO_2 conversion of point A_2. Besides, the plasma power at A_2 and B_5 was respectively 14 W and 16 W. As studied in Chapter 3, the increase of plasma power is not favorable for the reaction after the reaction occurred. Moreover, the CO_2 conversion with different GHSV at the same temperature in plasma process could also be seen from the figure. At a certain temperature, the CO_2 conversion was lower when the GHSV was higher. For example, at 275℃, the CO_2 conversion at GHSV OF 46300 was 79.5%, while at a higher GHSV of 92600, the CO_2 conversion was 71.4%. And this was mainly due to the decrease of residence time with the increase of GHSV.

The effect of GHSV on CO_2 methanation in thermal process was studied with the different flowrates at a fixed temperature of 350 °C. The geometry of the reactor used in the thermal process was identical as the plasma reactor. The comparison of the influence of GHSV on CO_2 conversion between thermal process and plasma-catalytic process is presented in Figure 4-12. One can state that the decrease of CO_2 conversion with increase of GHSV is remarkably similar in the thermal process and in the plasma catalytic process. CO_2 conversion was roughly the same in both process when the GHSV was smaller than 100 000 h^{-1}. When the GHSV was bigger than 100 000 h^{-1}, the CO_2 conversion in plasma catalytic process was slightly lower compared to the thermal process, maybe because in plasma-catalytic process, the increase of temperature, plasma power and GHSV all result in the decrease of CO_2 conversion, while in the thermal process, the CO_2 conversion was only decreased due to the increase of GHSV.

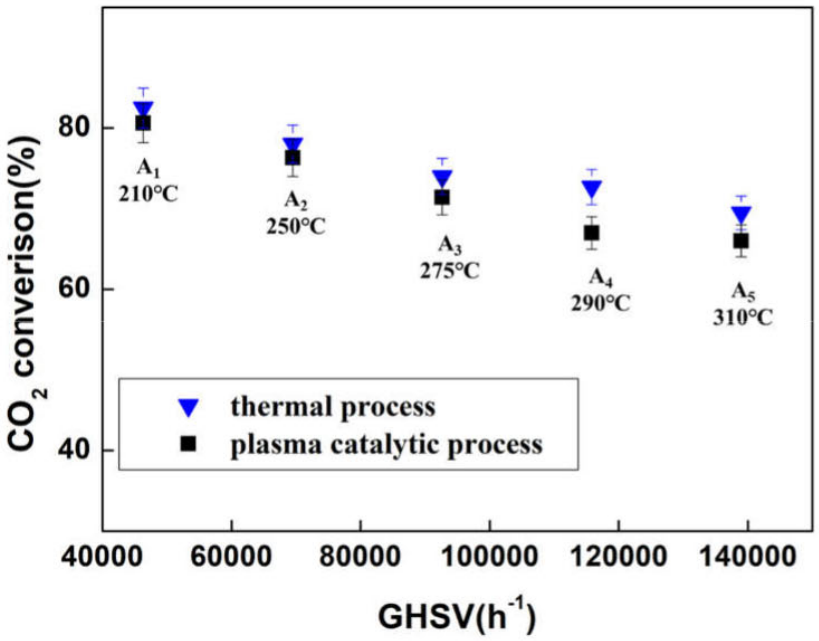

Figure 4- 12. Comparison of the effect of GHSV on CO_2 conversion between thermal process (350°C) and plasma-catalytic process

4.5 Effect of pressure on the CO_2 methanation

As the CO_2 methanation was a reaction of mixture gas, thus the pressure has an important effect on the reaction. In this part, the influence of pressure on thermal process and plasma-catalytic process was studied respectively.

In the plasma-catalytic hybrid process

In the plasma reactor, different pressure was first created, then the voltage was applied from 17 kV to 21 kV to study its influence on the CO_2 methanation. Figure 4-13a shows the plasma power measured by Q-V Lissajous method at different voltages under the three different pressures.

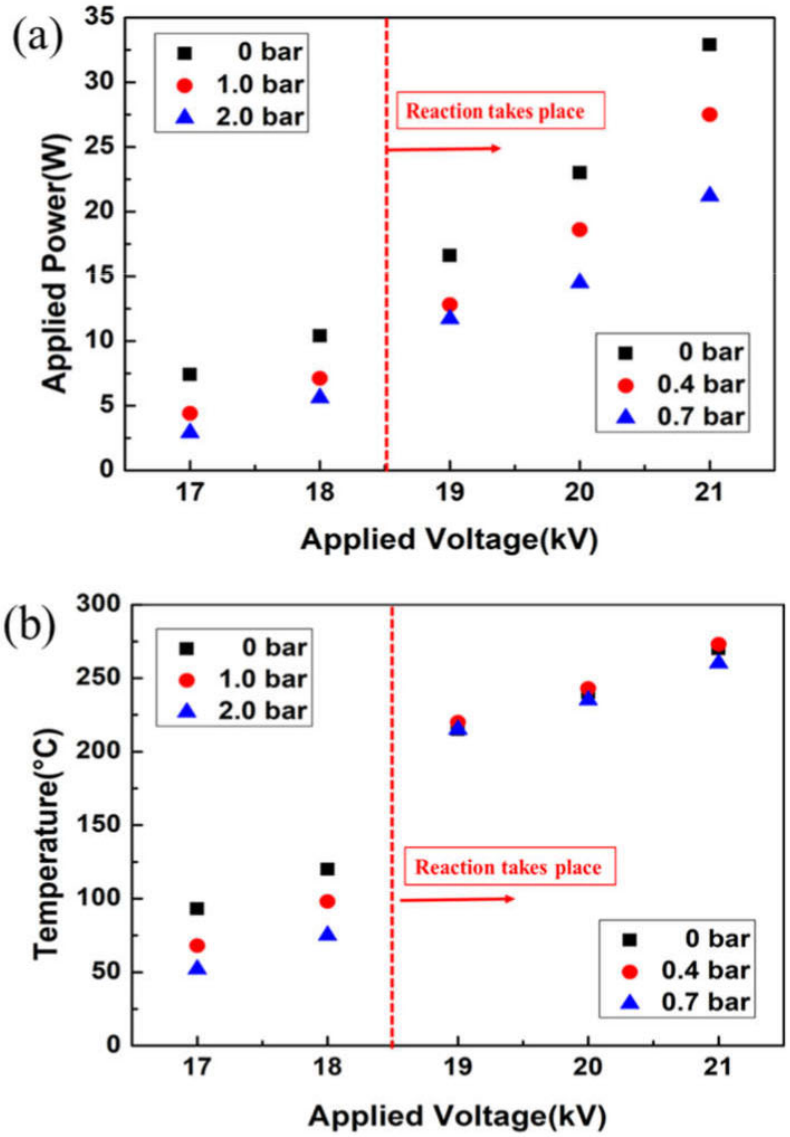

Figure 4-13. Plasma powers and temperatures measured at different voltages under different pressures during the plasma catalytic process (GHSV=46300 h^{-1}): Initial pressure of 2.0 bar and 1.0 bar decreased to 0.7 bar 0.4 bar respectively as the reaction took place at 19 kV

It is clear that at the same voltage, the plasma power created inside the reactor was lower when the pressure inside of reactor was higher. This is because DBD plasma is more difficult to create under high pressure reference. The consequence is that at 17 and 18 kV the highest the pressure is, the lowest the temperature is. As previously, CO_2 methanation did not take place until the

high voltage reached 19 kV. It is worth to mention that, in the presence of the reaction, the reactor pressures of 2.0 bar and 1.0 bar decreased to 0.7 bar and 0.4 bar respectively. This is because that CO_2 methanation is a reaction involving a decrease in the number of gas molecules from 5 to 1, as the reaction happened, the molecule in the reactor decreased, so that the pressure decreased. One the other hand, from 19 to 21 kV there is only a slight difference of temperature for the three different pressures as shown in Figure 4-13b even if the plasma power is significantly different (e.g. 14 and 22 W at 20 kV for 2 and 0 bar respectively).This was due to the change of relationship between temperature and plasma, as shown in Figure 4-14.

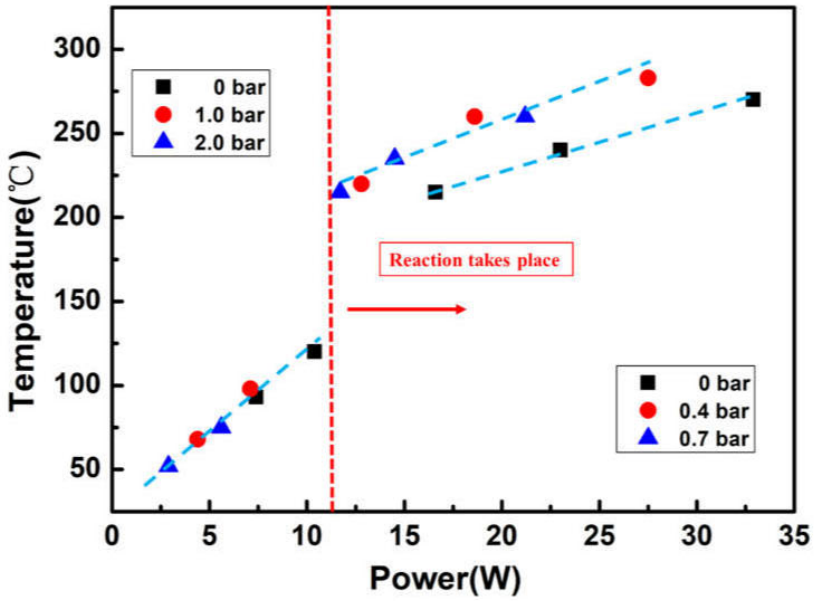

Figure 4-14. The relationship between power and temperature under different pressures during the plasma catalytic process (GHSV=46300 h^{-1}): Initial pressure of 2.0 bar and 1.0 bar decreased to 0.7 bar 0.4 bar respectively as the reaction took place at 19 kV

Figure 4-14 presents the relationship between plasma and temperature during the experiment. As can be seen from the figure, before reaction happened, the relationship between plasma and temperature was identical when the power was lower than 12 W, thus when the pressure was higher, the temperature was lower at the same applied voltage due to the lower created power inside the reactor. However, after the reaction toke place at 19 kV, the relationship between

temperature and plasma changed. Its relationship was almost the same under the pressure of 0.4 bar and 0.7 bar, while at atmospheric pressure, it was different. In this condition, higher plasma power was needed to create the same temperature.

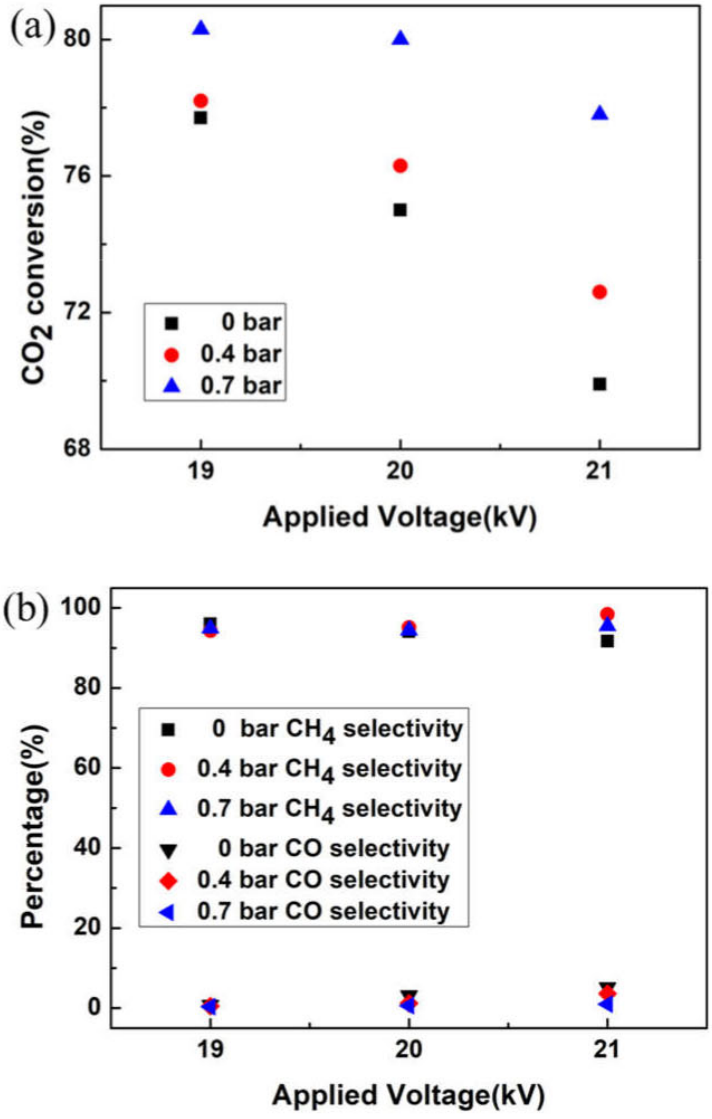

Figure 4-15. Catalytic performance of catalyst C3 under different pressures in plasma-catalytic process (GHSV=46300 h^{-1}): a) CO_2 conversion; b) CO selectivity and CH_4 selectivity

The influence of pressure on the catalytic performance for CO_2 methanation in a plasma-catalytic hybrid process is presented in Figure 4-15. As shown in Figure 4-15a, the increase of

the pressure inside of the reactor lead to a slight increase of the CO_2 conversion, while no difference of CO and CH_4 selectivity was observed in Figure 4-15b. At 19 kV, the CO_2 conversion from 78 % to 80 % (increased by 2.6%) as the pressure increased from 0 to 0.7 bar, and the difference of CO_2 conversion under different pressures was more obvious with the increase of voltage. In the range of 19 kV to 21 kV, the CO_2 conversion decreased with the increase of the voltage under a certain pressure because of the increase of the temperature from 220 to 270℃, as shown in Figure 4-13b.

In addition, under a pressure of 0.7 bar, the CO_2 conversion decreased slower than that at atmosphere pressure with the increase of the voltage: the CO_2 conversion decrease from 80% to 78% (decreased by 2.5%) with the voltage increasing from 19 kV to 21 kV under 0.7 bar, while the CO_2 conversion decreased from 78% to 70% (decreased by 10.3%) when the pressure inside of the reactor was atmosphere pressure. This may be explained by the faster increase of power under atmosphere pressure, as shown in Figure 4-13. Under atmosphere pressure, the plasma power increased 16.3 W (from 16.6 to 32.9 W) with increase of voltage from 19 kV to 21 kV, while the plasma power increased 10.4 W (from 11.7 to 21.1 W) under the pressure of 0.7 bar. Compared with the power increased under 0.7 bar, there existed an excess increased power of 5.9 W at atmosphere pressure. As studied in chapter 3, when the reaction happened at the temperature higher than 220 °C, the CO_2 conversion was lower when the plasma power was higher. In the atmospheric pressure, the plasma power increased faster with voltage, thus the CO_2 conversion decreased faster than in the pressure of 0.4 bar and 0.7 bar.

Finally, in our experimental conditions, increasing the pressure from atmospheric pressure to 0.7 bar leads only to a slight increase of the CO_2 conversion of 2.6%. However, it was possible working at higher pressure to decrease drastically the plasma power of around 30% (from 16.6 W to 11.7 W) at 19 kV. According to the calculation, the decrease of plasma power was mainly due to the decrease of electron number, which decreased by 24% (from $1.44e^{10}$ to $1.10e^{10}$) as the pressure increase to 0.7 bar from atmosphere pressure. This means that the mean electron energy was almost the same under different pressure condition, this is why it is possible to

activate the reaction at a lower power.

In the thermal process

For comparison, the effect of pressure on the CO_2 methanation in thermal process was also studied. Pressures of 0.7 bar and 2.0 bar were respectively fixed in the reactor to compare with the condition when no pressure was created in the reactor. The temperature was set at 350°C because the catalyst have best performance at this temperature, and the results are presented in Table 4-6.

It can be stated that in the thermal process, increasing the pressure also has a positive effect on the CO_2 conversion. This is because CO_2 methanation is a molecule reducing reaction, increasing the pressure could help shift the reaction towards product side. Compared with CO_2 conversion of 74% at atmosphere pressure, the CO_2 conversion increased respectively to 76% and 79% when the pressure increased to 0.7 bar and 2.0 bar. There is also no difference of CH_4 selectivity as pressure changes.

Table 4-6. CO_2 methanation under different pressures in thermal process (350°C)

Pressure (bar)	**CO_2 conversion (%)**	**CH_4 selectivity (%)**
0	74	98.5
0.7	76	99.0
2.0	79	99.0

In a conclusion, the pressure has a positive effect on the CO_2 methanation. Increasing the pressure contributes to a higher CO_2 conversion in both processes. Moreover, in the plasma-catalytic process, under a higher pressure, the power consumption was smaller while the CO2 conversion was slightly higher.

4.6 Conclusion

In this study, catalysts of different particle sizes were fabricated and the influence of catalyst

particle size on CO_2 methanation was studied. Catalyst particle size and pressure had positive influence on the CO_2 methanation in both thermal and plasma process. Increasing the catalyst particle size could improve the CO_2 conversion due to the smaller metallic Ni particle size after reduction. The CO_2 conversion decreased with the increase of GHSV in in thermal and plasma catalytic process, and had similar value at the same GHSV. Besides, in plasma process, the temperature increased with the flowrate because of the increased released power from the reaction, and it did not depend either on GHSV or on the mass of catalyst loaded in the reactor. Concerning the effect of pressure, increasing the pressure inside of the reactor could slightly increase the CO_2 conversion, and it can also help to decrease around 30% the plasma power needed for the reaction in plasma process. The same trend that a slightly higher CO_2 conversion could be obtained under a higher pressure was also observed in thermal CO_2 methanation.

Chapter V Prospective study of CO_2 methanation in milli-reactor

In this chapter, a prospective study of CO_2 methanation in the milli-reactor was performed. The aim is to use transparent electrode ITO, so that the plasma in catalyst-bed could be seen, and thus the optical emission spectrometry (OES) could be used for the detection of the active species in the plasma zone to study the mechanism of the reaction. The configuration of milli-reactor was designed and optimized, and then CO_2 methanation by plasma assisted catalysis was performed in this reactor under plasma condition.

5.1 Configuration of the plasma milli-reactor

Figure 5-1 is the optimization of the configuration of the milli-reactor. During the design process of the milli-reactor, various parameters were tested: the material of the electrode, the dielectric material, and the gap distance between the two electrodes.

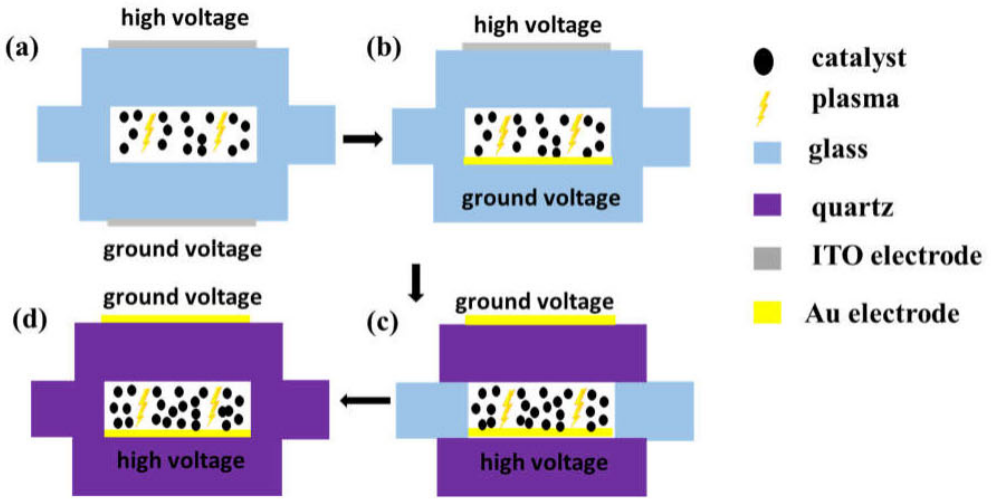

Figure 5-1. Optimization of the configuration of milli-reactor

At the beginning, ITO was used as high voltage electrode and grounded electrode because of its transparency, allowing a visual observation of the plasma inside the reactor, as shown in Figure 5-2, which is argon plasma created inside the reactor. From this figure, it is clear that the plasma is rather homogeneous. However, maybe due to the low conductivity of the ITO

electrode, the voltage needed to create plasma under the gas mixture of CO_2 and H_2 was high when the configuration of Figure 5-1a was used. To decrease the breakdown voltage of the reactor, electrode mater such as silver paint and gold deposition (Figure 5-1b) were tried. Gold deposition was chosen as the final electrode material for high voltage electrode and grounded electrode to decrease the applied voltage.

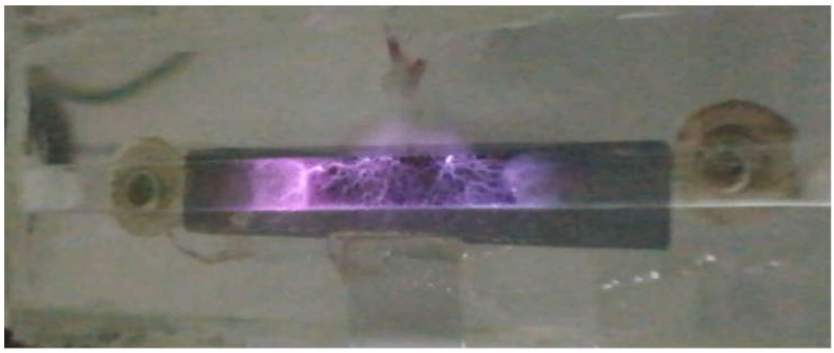

Figure 5-2. DBD plasma created in milli-reactor with ITO as electrode (Argon, applied voltage = 8.0 kV, f = 42 kHz, reactor configuration (Figure 5-1a))

Glass slides have been used as the dielectric material to create DBD plasma at the begining. However, it turns out that the glass could not work at high voltages and high temperatures. When glass was used as dielectric material, the reactor was always broken at voltages higher than 13 kV. One can distinguish a hole on the glass due to plasma arcing in Figure 5-3. This problem was solved when the glass slide was replaced by a quartz slide, which has better dielectric strength at high voltage and temperatures.

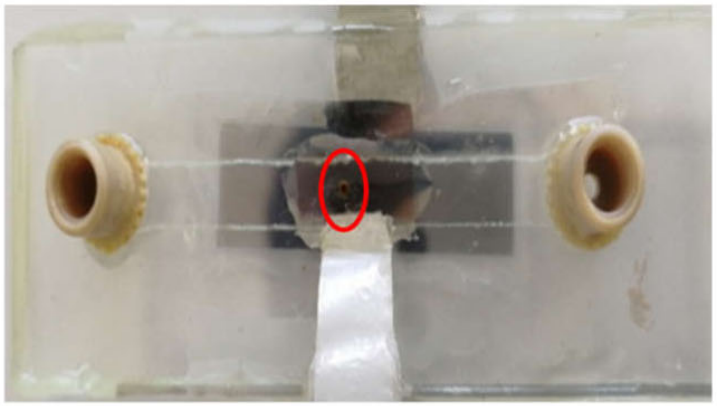

Figure 5-3. The broken reactor used glass as the dielectric material

According to Paschen's law, a lower breakdown voltage can be achieved by decreasing the gap

distance between two electrodes. In the configuration Figure 5-1b, the gap distance was also decreased from 3mm to 2mm by placing the high voltage electrode inside the reactor to decrease the breakdown voltage. In this configuration, the electrode was moved from the outside of the reactor to the inside of the reactor. Table 5-1 indicates breakdown voltage of the milli-reactor in different configuration. As shown in the table, the breakdown voltage decreased from 12 kV to 8 kV from configuration Figure5-1a to 5-1b, mainly due to the decrease of the gap distance from 3 mm to 2 mm. And by replacing the one ITO electrode by gold deposition on the quartz slide, the breakdown also decreased by 1 kV. It has to be mentioned that the gas was the mixture of H_2 and CO_2 while measuring the breakdown voltage. Therefore, the electrode was directly contacted with the catalyst bed and plasma. Besides, glass slides that were used to make the channel were also replaced by quartz slide because the glass will break at high voltage and high temperature.

Table 5-1. Table 5-1. Breakdown voltages of the milli-reactor in different configuration (H_2/CO_2, 20 ml/min, f = 42 kHz, catalyst C3)

Configuration	**Figure 5-1a**	**Figure 5-1b**	**Figure 5-1c**	**Figure 5-1d**
Breakdown voltage (kV)	12	8	7	7

Moreover, another problem that we pointed out was the presence of surface discharge. In general, the electrode was covered by a transparent glue to avoid the surface discharge. However, the transparent glue cannot work well when the temperature was higher than 100°C. Finally, a black and opaque glue that could work at high temperature (250°C) was used to cover the external upper electrode to prevent external surface discharge. Indeed, such surface plasma discharge was not only a waste of power, but also could remove the electrode (gold deposition) deposited on the quartz slide.

Figure 5-4 is the final configuration of the plasma milli-reactor used for methanation tests. This reactor is a mono DBD rectangular reactor. The quartz slide was chosen as the dielectric material and gold deposition on the slide acted as high voltage electrode and grounded electrode.

The thickness of the quartz slide used was 1 mm. As can be seen from the figure, the gap distance between the two electrodes was 2 mm, and the length of the electrode was 25 mm with a width of electrode of 4 mm. The catalyst was loaded inside the reactor and glass wool was used to fix the catalyst on both sides. The mass of catalyst used in the milli-reactor was 100 mg of catalyst C3 (500 μm), and the length of catalyst-bed was 25 mm, giving an apparent volumic mass of the porous bed of 1 g/cm3. The inlet gas mixture was pure mixture of H_2 and CO_2 with a ratio of 4:1. The temperature was measure by a K-type thermocouple placed on the surface of the reactor.

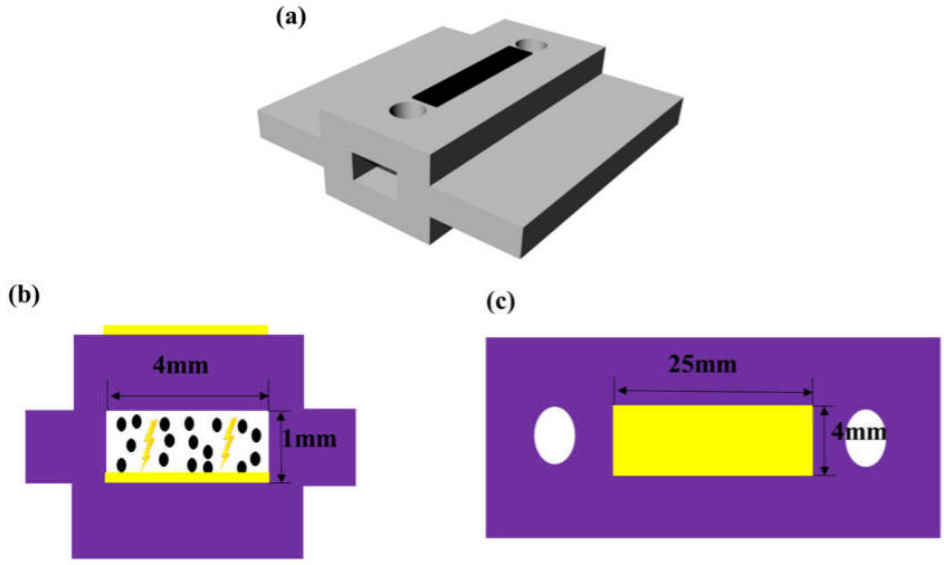

Figure 5-4. Configuration of the plasma milli-reactor: (a) 3D model; (b) front view; (c) vertical view

5.2 Comparison of plasma homogeneity in the catalyst-bed with different sizes of catalyst

The plasma with different particle size and plasma intensity was studied in the milli-reactor of configuration 5-1a, so that plasma created inside the reactor could be visualised. The type of plasma used in this part is argon plasma.

The pressure drop in the catalyst bed under different flowrate is presented in Figure 5-5. As can

be seen from the figure, the pressure drop of the catalyst-bed increased with flowrate, and when the catalyst particle was smaller (catalyst C1), the pressure drop of the catalyst-bed was much higher. For example, at 20 mL/min, the pressure drop of catalyst bed with smaller particle size (catalyst C1) was 6.4 kPa, which was almost 12 times higher than the pressure drop of 0.54 kPa in the catalyst-bed with larger particle size (catalyst C3). Moreover, it is clear that the pressure drop in catalyst C1 increased much faster with flowrate than catalyst C3, thus the difference of pressure drop between two catalyst-bed also increased with flowrate. Besides, during the measurement of the pressure-drop of catalyst bed while loaded with catalysts with different particle sizes, the mass of catalyst (0.035 g) and the length of catalyst-bed (6mm) were the same for two catalyst beds. Thus, it could be concluded that the porosity of catalyst bed C3 was bigger than catalyst bed C1.

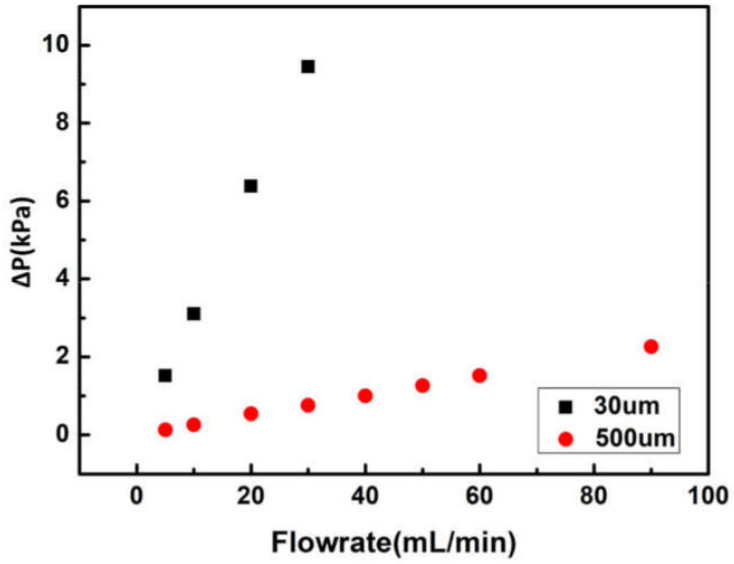

Figure 5-5. Pressure drop in the catalyst beds under different flowrate

Catalysts with different particle size were loaded inside the milli-reactor to observe the plasma homogeneity. As shown in Figure 5-6, the plasma homogeneity depends on the particle size of the catalyst. When the reactor was loaded of catalyst C3 (mean size: 500 micrometers), the plasma in the catalytic bed was much more homogenous compared with the case where the catalyst C1 (mean size: 30 micrometer) is used. This can be explained by bigger particles with

a narrow size distribution for C3, involving a higher porosity of the catalyst-bed, and then creating more space for the existence of the plasma inside the catalyst-bed. In this condition, it can be supposed that the interaction between plasma and catalyst is better when catalyst C3 is used. Finally, these visual observations of the plasma homogeneity could also explain the results described in chapter 4. Indeed, in the cylindrical reactor, catalyst C3 had a higher CO_2 conversion compared with catalyst C1. This confirms that this difference could be also due to a better plasma homogeneity when large catalytic particles are used.

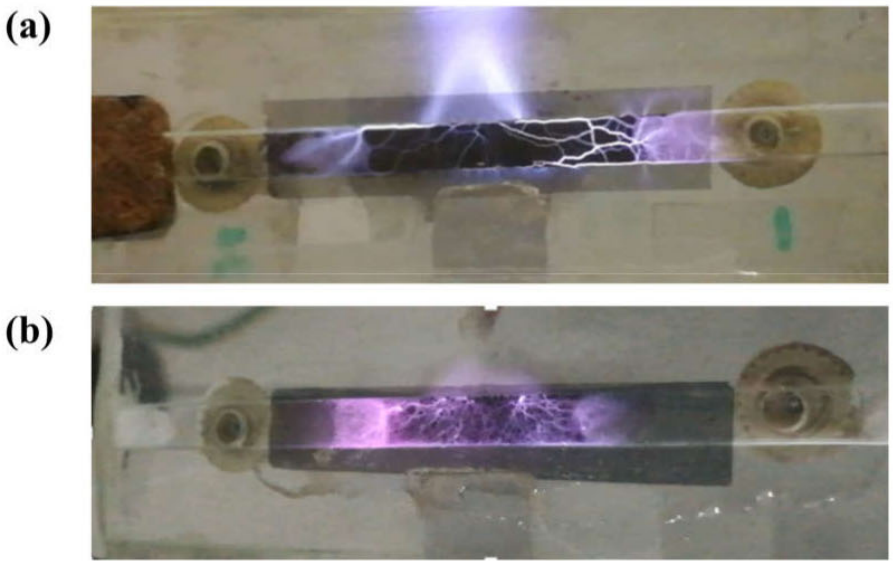

Figure 5-6. Argon plasma created inside the milli-reactor with catalyst of different particle size (Voltage= 4 kV, frequency: 42 kHz, argon plasma): (a) catalyst C1(30 μm); (b) catalyst C3(500 μm)

5.3 CO_2 methanation in milli-reactor in plasma-catalysis process

The CO_2 methanation was performed in the milli-reactor of configuration 5-1d, and the results are presented in Table 5-2. The flowrate used in the milli-reactor is 20 mL/min under the control of Bronkhorst massic flowmeter, and the mass of catalyst C3 loaded in the reactor was 100 mg with a length of 25 mm. The experiment was started at the voltage (peak to peak) of 12 kV, and the voltage was increased up to 18 kV with steps of 1 kV. This experiment started at 12 kV because the power and temperature were too low at a lower voltage, where the reaction could not occur. The flowrate of the outlet product gas was measured by a bubble flowmeter, and the

gas composition of the mixture was analyzed by the microGC-490 with a TCD detector. Plasma power and temperature were recorded during the experiment. Table 5-2 presents the power, temperature, CO_2 conversion and CH_4 selectivity.

Table 5-2. The performance of catalyst for CO_2 methanation in plasma milli-reactor

Voltage (kV)	**Power (W)**	**T (℃)**	**X_{CO2} （%）**	**S_{CH4} （%）**	**Released power from the reaction**
12	4.4	83			
13	4.9	110			
14	6.8	148			
15	12.0	188	17	56	0.19
16	13.3	210	28	100	0.28
17	16.0	230	58	100	0.30
18	17.6	242	72	98	0.36

Figure 5-7 presents powers and temperatures at different voltages in the experiment. The experiment began at the voltage of 12 kV, with a plasma power of 4.4 W and a temperature of 83 ℃. Then the plasma power and temperature increased with applied voltage. The CH4 was not detected until the voltage of 15 kV was applied. The maximum voltage applied in this experiment is 18 kV. The plasma power increased from 4.4 W to 17.6 W when the applied voltage was increased from 12 kV to 18 kV. And there was a sharp increase of plasma power at 15 kV as the reaction take place, which was also observed in the experiment performed in cylinder reactor (section 3.3). This is because that as the reaction took place, the gas composition has changed, thus the plasma power generated has also changed. However, in cylinder reactor there was also a sharp increase of the temperature with the occurrence of the reaction and the sharp increase of power which was not observed in the milli-reactor. This is maybe because in the milli-reactor, the heat released from the reaction is small compared with the plasma power. For example, at the voltage of 15kV, the plasma power is 12 W whereas the

heat released from the reaction is only 0.19 W. Even with the increase of voltage to 18 kV, corresponding to a plasma power of 17.6W and a CO2 conversion of 72%, the released heat from the reaction was only 0.36 W. The reaction heat is then always negligible. On the contrary, in the cylindrical reactor the power released by the reaction was not negligible compared to the plasma power (4 W against 15.1 W for plasma power). As mentioned before, CH_4 was detected at the voltage of15 kV. In this condition the CO_2 conversion was 17% and the temperature was 188°C. Then, the reactor temperature increased from 188 °C to 242 °C with the increase of voltage from 15 kV to 18 kV.

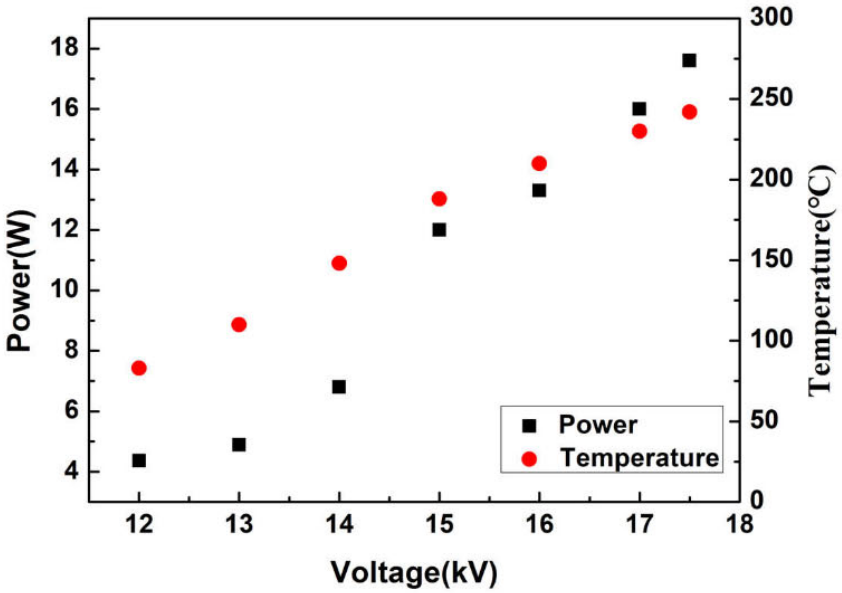

Figure 5-7. Power and temperature vary at different voltages in the milli-reactor

The CO_2 conversion at different voltages is shown in Figure 5-8. The reaction did not occurred until the voltage of 15 kV was applied to the reactor, and the CO_2 conversion was 17% at the temperature of 188°C. The CO_2 conversion then increased from 17% to 72% with applied voltage in the range of 15 kV to 18 kV. This is due to the increased temperature and power with the increase of applied voltage. The maximum CO_2 conversion of 72% was obtained at 18 kV with a CH_4 selectivity of 98%, a temperature of 242°C and a power consumption of 17.6W. However, this may be not the best performance of the reactor because the maximum tested voltage was only 18kV. However, the CO_2 conversion may continue to increase with voltage.

In this study, the experiment was stopped at 18 kV due to the concern that the reactor may break under a higher temperature and voltage.

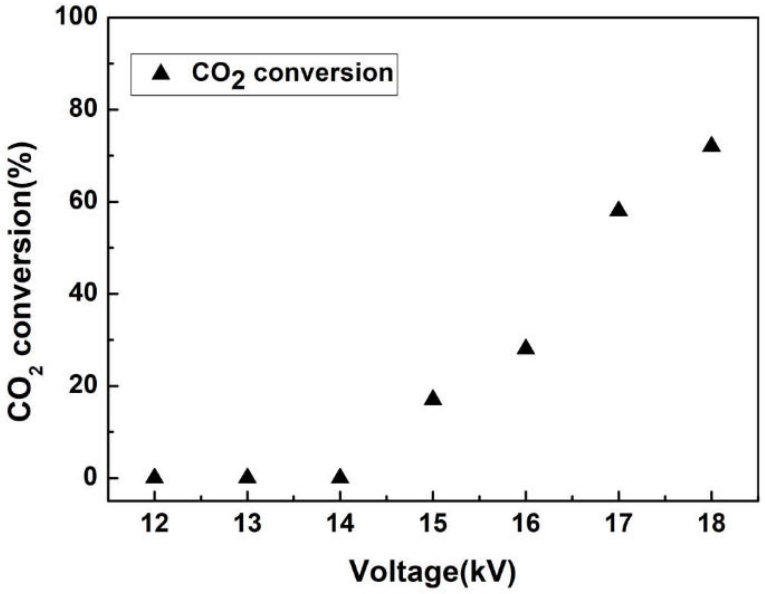

Figure 5-8. CO_2 conversion vary at different voltages in the milli-reactor

In this research, high CO_2 conversion could be obtained in the milli-reactor. However, in the configuration of this milli-reactor, the high voltage electrode was placed inside the reactor, thus it was directly exposed to DBD plasma. As a result, the high voltage electrode (Au deposition) was slowly destroyed by the DBD plasma, and will disappear after a long-time operation of CO_2 methanation. The reactor, therefore, has to be changed. Besides, because gold deposit was not transparent, the optical emission spectrometry (OES) could not be carried out with the milli-reactor to study the active species during the plasma methanation.

5.4 Comparison of the performance of CO_2 methanation in milli-reactor and cylinder reactor

The CO_2 methanation was respectively performed in cylinder reactor and milli-reactor. There were some similar phenomenon in two reactors, however, there were also several major differences.

Table 5-3 summarizes the differences in terms of geometry and materials of the two reactors.

Table 5-3. The parameters and material used for two reactors

	Gap distance (mm)	**Gaseous gap (mm)**	**Breakdown voltage in H_2/CO_2 (kV)**	**High voltage electrode**	**Grounded electrode**	**Dielectric material**
Cylinder reactor	4.1	2.5	9.0	copper	Iron wire	Quartz /Alumina tube
Milli-reactor	2.0	1.0	7.0	Gold deposition	Gold deposition	Quartz slide

The main difference of these two reactors were the material of electrodes and the gap distance between the two electrodes. Due to these differences, the breakdown voltages in the mixture of H_2 and CO_2 were 9.0 kV and 7.0 kV for the cylinder reactor and milli-reactor respectively.

Two electrostatic 2D models were created in COMSOLMultiphysics® software to study the electric field distribution in the reactors. The geomtries of cylinder reactor and milli-reactor were respectively created in the model and the material parameters were chosen for the cylinder reactor and milli-reactor. In the models, the relative permittivities (ε_r) of alumina, quartz and catalyst bed used were 10.0, 4.5 and 3.0 respectively. The relative permittivities of alumina and quartz were chosen from the data on website The Engineering ToolBox,[150] while the relative permittivity of catalyst bed was calculated form the COMSOL model of cylinder reactor. First, the total capacitance of the cylinder reactor filled with catalyst C3 was measured by Q-U Lissajous method as mentioned in chapter 2. A value of 2.4 pf was obtained for the capacitance of the cylinder reactor. Then a value of relative permittivity of catalyst bed was put into the model to simulate the capacitance of the reactor. The simulated value of the total capacitance was not the same as the experiment value of 2.4 pf until in the model, the value of 3 was put for the relative permittivity of catalyst bed. Therefore, the relative permittivity of catalyst bed was determined as 3.

Then the same value of 19 kV for the applied high voltage was put in these two models to see the distribution of electric field in the two reactors, as shown in Figure 5-9. It can be seen that

the electric field was different for two reactors for the same applied voltage of 19 kV. In cylinder reactor, the electric filed was lower than that in the milli-reactor, but it was not clear in the 2D figure due to the color range. Therefore, to study the electric field in the catalyst-bed, a cutline was created in the model to show its value, as shown in Figure 5-10.

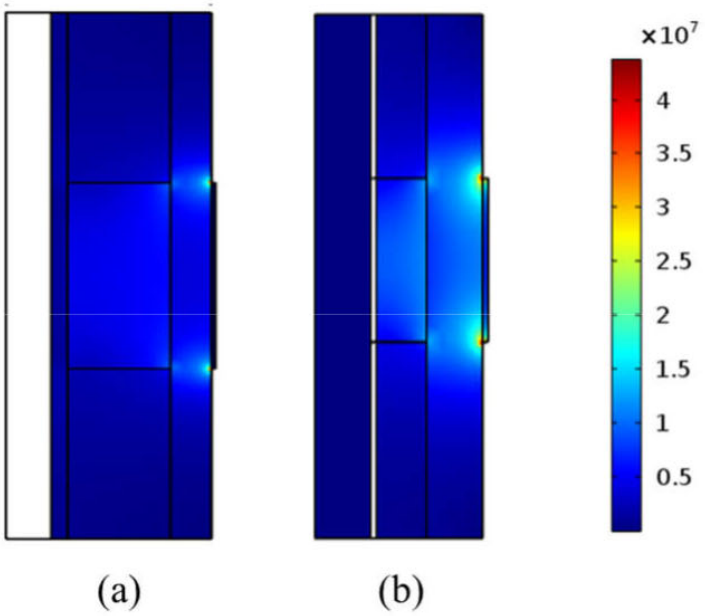

Figure 5-9. Electric filed (V/m) distribution of reactors: (a) cylinder reactor; (b) milli-reactor

Figure 5-10 presents the electric field in the catalyst bed. As shown in the figure, a cut line was created in the middle of the catalyst bed, and the electric field on this line was presented. The average of electric field was calculated as the average value of the maximum and minimum value. It can be seen that under the same applied voltage, the electric field is around $9.9*e^{10}$ V/m in the milli-reactor, while it is only $6.0*e^{10}$ V/m in the cylinder reactor. This explains why the reaction can take place at a lower voltage in the milli-reactor and why the breakdown voltage is also lower in the millireactor.

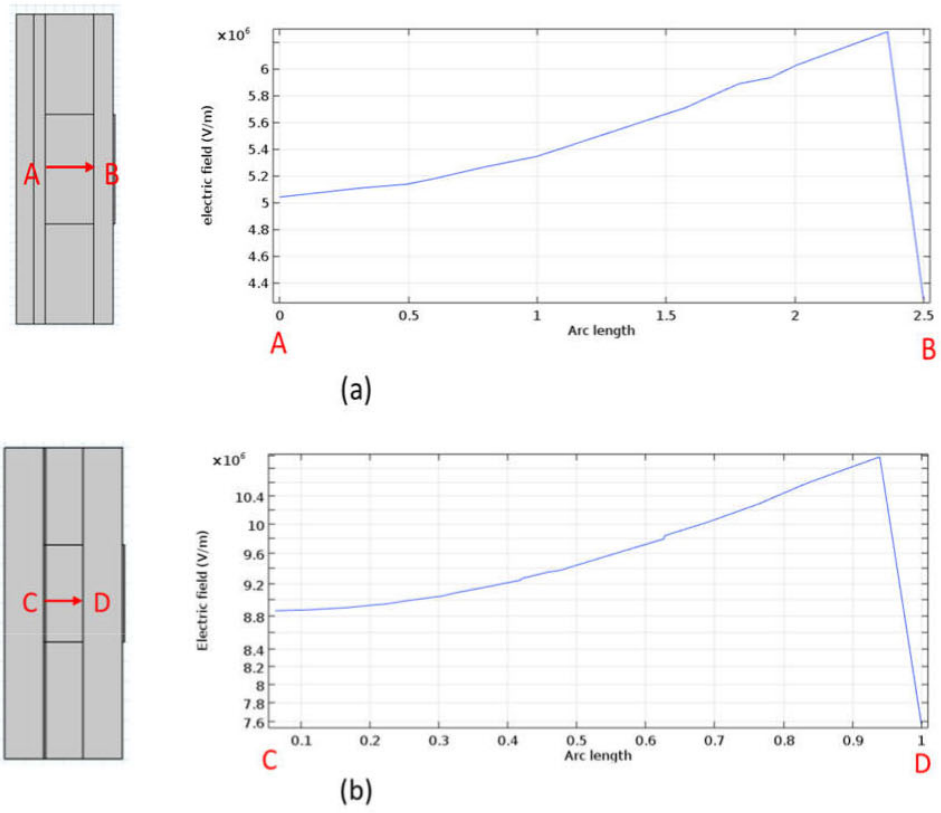

Figure 5-10. Electric filed (V/m) in the catalyst bed: (a) cylinder reactor; (b) milli-reactor (applied voltage: 19 kV)

Table 5-4 summarizes the conditions in terms of GHSV, SIE and temperatures used to carry out CO_2 methanation in cylinder and milli-reactor. It has to be mentioned that in cylinder reactor, different flowrates were used while in milli-reactor, the tests were performed at a fixed flowrate of 20 mL/min due to the lack of time at the end of this work. In the cylinder reactor, the voltage was fixed at 19 kV, while in the milli-reactor, the voltage was varied from 16 kV to 18 kV.

Table 5-4. Comparison of SIE of CO_2 methanation in cylinder and milli-reactor

Cylinder reactor					Milli-reactor				
Flowrate (mL/min)	**T (°C)**	**GHSV (h^{-1})**	**SIE (J·L)**	**X_{co_2} (%)**	**Flowrate (mL/min)**	**T (°C)**	**GHSV (h^{-1})**	**SIE (J/L)**	**X_{co_2} (%)**
20	130	4630	32700	57	20	210	12000	39300	28
50	150	11575	14280	67.8	20	230	12000	48000	58
100	180	23150	7740	78.5	20	240	12000	52800	72
200	220	46300	4530	77.5					
300	245	69450	3080	74.7					
350	255	81025	2777	72.4					

In the millireactor, the GHSV was 12000 h^{-1} and the maximum of the CO_2 conversion obtained was 72% at a SIE of 52 800 J/L. Using a similar GHSV of 11575 h^{-1} in the cylinder reactor, the CO_2 conversion was only slightly lower (68%) whereas the SIE was almost four times lower (14 280 J/L). It can be noted that the temperature in the milli-reactor (230 °C) was higher than the temperature of 150°C in the cylinder reactor what is logical considering the higher SIE in the millireactor.

It can be seen from the table that in cylinder reactor with a fixed voltage of 19 kV, the SIE decreased from 32700 to 2777 J/L with the increase of flowrate from 20 to 350 mL/min, but in the same time the decrease of CO_2 conversion from 200 mL/min was small. This means that the CO_2 methanation would be more efficient at high flowrate or at low SIE.

Figure 5-11 is the comparison of SIE of CO_2 methanation in cylinder and milli-reactor. It can be seen that the SIE in cylinder reactor was much lower than the SIE in milli-reactor. This is mainly because in cylinder reactor, the flowrate was different as mentioned before, and the SIE decrease with the increase of flowrate. Comparing the result at 20 mL/min in both reactors, it was observed that to have almost the same CO_2 conversion of 58%, the SIE in cylinder reactor was 32 700 J/L, which was smaller than the value of 48 000 J/L in milli-reactor.

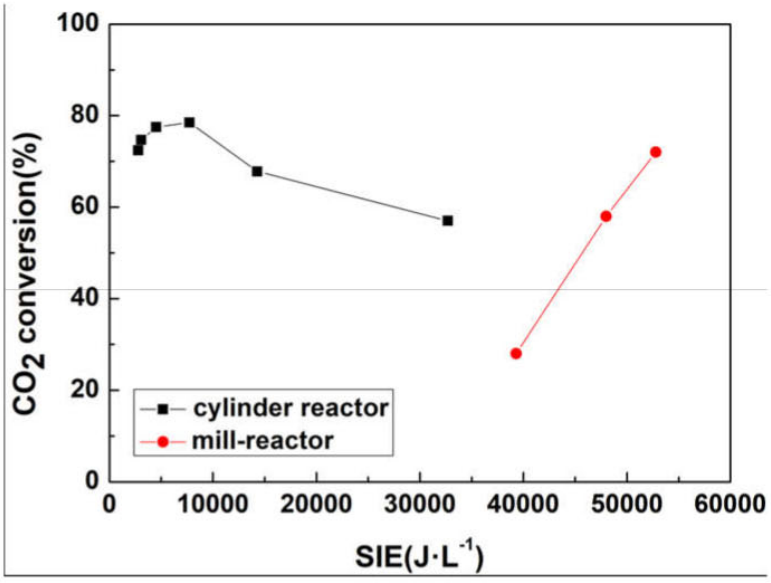

Figure 5-11. Comparison of SIE of the CO_2 conversion in cylinder reactor (20-350 mL/min) and milli-reactor (20 mL/min) (catalyst C3)

As a conclusion, the performance of the CO_2 methanation in cylinder reactor was better than that in milli-reactor. The reaction could take place at lower SIE in cylinder reactor. However, the performance of CO_2 methanation was not the best possible, and optimization still could be made to increase the performance. For example, by decreasing the gap distance to eventually trigger the reaction at lower voltage and decrease the plasma power.

Moreover, due to the configuration of the cylinder and the choice of the electrode material, the cylinder reactor could work for a long time, until the reactor was broken due to the wrong operation or accident. On the contrary the milli-reactor has to be replaced after a relatively short period of the experiment (around 3 hours), because the gold deposition would be slowly removed by the plasma created inside the reactor.

Due to the limited time for the research of CO_2 methanation in milli-reactor, there are still lots of improvement could be made to improve the catalytic performance in milli-reactor.

5.5 Summary

In this chapter, prospective study of CO_2 methanation is milli-reactor was performed. First, a

milli-reactor with ITO as electrodes was designed to create DBD plasma. However, due to the low conductivity of the ITO, the voltage needed to trigger the reaction was very high, and the reactor broke before the reaction took place. Thus, an optimization of the milli-reactor was performed: gold deposition on the slide was chose as the electrode to decrease the voltage need for the reaction, and dielectric material was replaced by quartz slide, which could work at high voltage and temperature.

Catalysts with different particle sizes were loaded in the reactor, and it turns out that the plasma was more homogenous in the catalyst-bed when catalyst C3 (500 μm) was loaded in the reactor. CO_2 methanation was performed in the milli-reactor. The maximum CO_2 conversion of 72% was achieved at 18 kV, and the temperature was 242°C.Compared with the energy efficiency in the cylinder, the energy efficiency in milli-reactor was much lower.

However, this is only perspective research of CO_2 methanation in milli-reactor, there are still lot of improvement needed to be made. For example, how to make the reaction took place in the milli-reactor while using the transparent electrode ITO. And how to avoid the loss of the electrode during the experiment.

Chapter VI Conclusions and perspectives of this work

6.1 Conclusions

This work focused on the plasma-catalytic process for the methanation of CO_2 using a catalyst of $Ni/Ce_{0.58}Zr_{0.42}O_2$. In the same time, the CO_2 methanation under thermal activation was also performed for comparison. The plasma-catalytic process was performed in the quartz cylinder reactor, and a prospective study was also made in a rectangular milli-reactor.

In the first part, the role of temperature in the plasma-catalytic process for CO2 methanation was investigated. CO_2 methanation was respectively performed in thermal catalysis process and plasma-catalytic process. In this part, there was no external heating device for plasma reactor and the reactor surface was directly exposed at ambient air. Under the same GHSV of 46300 h^{-1}, to get a CO_2 conversion around 80%, the temperature needed in thermal process was 350°C, while in the plasma-catalytic process, the same CO_2 conversion could be obtained at the temperature of 220°C, which is around 130°C lower than the temperature in thermal process.

A set of experiments with different flowrates of inlet gas mixture was then performed, and it was found that the temperature measured at the reactor surface could be tuned by the decrease of the flowrate of inlet gas mixture due to the decrease of the power released by the methanation reaction. A binomial relationship between the surface temperature of the reactor and the flowrate of the inlet reactant mixture was found. A threshold temperature of 116°C was deduced when the flowrate is extrapolated to 0 mL/min. However, this is the temperature on the surface of the reactor. To study the temperature gradient in the reactor, COMSOL Multiphysics® software was used to simulate the heat transfer inside the reactor. The simulation indicated that the temperature difference between the reactor surface and the catalyst bed was almost negligible, the plasma threshold temperature for the Sabatier reaction was then finally evaluated at 116°C.

Moreover, it was observed that the voltage and power needed to trigger CO_2 methanation could decrease due to the decrease of air convection around plasma reactor. Two thermostat systems that could control the temperature independently of plasma power and feed flowrate were

designed to study the respective roles of temperature and plasma power. It was concluded that the influence of temperature and plasma power on CO_2 methanation were different in different temperature range. Regardless of the plasma power, it can be seen that in the plasma-catalytic process, the CO_2 conversion increased with temperature before 220°C, and then CO_2 conversion decreased with the increase of the temperature after 300°C. As for the effect of plasma power on the CO_2 conversion, it could be concluded that at low temperature (lower than 220°C), CO_2 conversion increased with plasma power, however, at high temperature (higher than 300°C) CO_2 conversion is lower at a higher plasma power. Finally, it could be concluded that the plasma/catalysis CO_2 methanation could be performed at various conditions: high power and low temperature or low power and high temperature. This provide various possible operating conditions for different aims in the industrial process in the future.

The CO_2 conversion was also performed in a thermally insulated plasma reactor to optimize the power consumption. It was demonstrated that the exothermic heat released from the reaction could be used for the activation of the reaction, and therefore helped to decrease the consumed plasma power for the reaction. As a result, to achieve a CO_2 conversion of 80%, the plasma power used could be decreased to 2.7 W, which is only 37% of the plasma power consumed when the plasma reactor is directly exposed to ambient air.

In the second part, different particle sizes of catalyst were made and its influence on CO_2 methanation was studied. Increasing catalyst particle size and pressure had positive influence on the CO_2 methanation in both thermal and plasma process. Increasing the catalyst particle size from around 30 μm to 500 μm could improve by 10% the CO_2 conversion, maybe due to the smaller metallic Ni particle size after reduction and/or better flow uniformity. The CO_2 conversion decreased from around 80 to 70 % when the GHSV increased from around 45 000 h^{-1} to 140 000 h^{-1} in both thermal and plasma catalytic process. Besides, in plasma-catalytic process, because the temperature depended on the released power from the reaction, it increased from 220 °C to 310 °C when the flowrate increased from 200 mL/min to 600 mL/min. Concerning the effect of pressure, increasing the pressure inside the reactor from atmospheric pressure to 0.7 bar could slightly increase the CO_2 conversion, and it could also help to decrease

around 30% the plasma power needed for the reaction in plasma process.

Finally, prospective study of CO_2 methanation is milli-reactor was performed. First, a milli-reactor with ITO as electrodes was designed. However, due to the low conductivity of the ITO, the voltage needed to trigger the reaction was very high, and the reactor broke before the reaction took place. Thus, the electrodes were fabricated by gold deposition to decrease the voltage need for the reaction, and glass slides were replaced by quartz slides, which could work at high voltage and temperature.

Catalysts with different particle sizes were loaded in the reactor, and it turns out that the plasma was more homogenous when catalyst C3 (500 μm) was loaded in the reactor.

CO_2 methanation was performed in the milli-reactor. The maximum CO_2 conversion of 72% was achieved at 18 kV, and the temperature was 242°C. Compared with the energy efficiency in the cylinder, the energy efficiency in milli-reactor was much lower, and there are still improvements needs to be made for this process.

6.2 Perspectives

Plasma-catalytic process for the methanation of CO_2 is a promising technology for the mitigation of CO_2 in the atmosphere, and easy to couple with the current industry infrastructure. In this work, the respective role of plasma and temperature in the process have been investigated, and various parameters have been optimized to obtain a better performance in the plasma-catalytic process for CO_2 methanation. However, there are some improvements that could still be made in the process of industrialization. As a result, several promising perspectives are listed as follows:

- Development of catalysts that could have a better performance in the plasma-catalytic process, for example, higher CO_2 conversion, lower reaction temperature. Moreover, the plasma power consumed in the process maybe related the type of catalyst, which also should be paid attention.
- In the plasma-catalytic process, it was demonstrated that the CO_2 methantion could take place at low temperature and high plasma power or at high temperature and low

plasma power. However, there is not an agreement for the optimal operation condition. Therefore, long-term stability test for these conditions could be performed to further choose the optimal operation parameters for different aims.

- The influence of impurities of the gas mixture on the CO_2 methanation in plasma-catalytic process. In general, the inlet gas mixture in the industrialization process is not a pure mixture of H_2 and CO_2 and there is always some gaseous impurities, such as CO, H_2S, or CH_4. Their influence on the process could be further studied.
- Application of optical emission spectroscopy (OES) on the process to study the mechanism of the reaction. To do this, a transparent electrode should be further developed for the process.

References:

[1] R. F Keeling CDK, (2017). . Atmospheric Monthly In Situ CO_2 Data - Mauna Loa Observatory, Hawaii. In Scripps CO_2 Program Data. UC San Diego Library Digital Collections. https://doi.org/10.6075/J08W3BHW Accessed on 2019, 5.

[2] Unde RB. Kinetics and reaction engineering aspects of syngas production by the heterogeneously catalysed reverse water gas shift reaction: Universitaet Bayreuth (Germany); 2012.

[3] Wang J, Huang L, Yang R, Zhang Z, Wu J, Gao Y, et al. Recent advances in solid sorbents for CO_2 capture and new development trends. Energy & Environmental Science. 2014;7:3478-518.

[4] Perry RJ, Grocela-Rocha TA, O'Brien MJ, Genovese S, Wood BR, Lewis LN, et al. Aminosilicone solvents for CO_2 capture. ChemSusChem. 2010;3:919-30.

[5] Song C. Global challenges and strategies for control, conversion and utilization of CO_2 for sustainable development involving energy, catalysis, adsorption and chemical processing. Catalysis today. 2006;115:2-32.

[6] Aresta M, Tommasi I. Carbon dioxide utilisation in the chemical industry. Energy conversion and management. 1997;38:S373-S8.

[7] Jurković DL, Pohar A, Dasireddy VD, Likozar B. Effect of Copper-based Catalyst Support on Reverse Water-Gas Shift Reaction (RWGS) Activity for CO_2 Reduction. Chemical Engineering & Technology. 2017;40:973-80.

[8] Aramouni NAK, Touma JG, Tarboush BA, Zeaiter J, Ahmad MN. Catalyst design for dry reforming of methane: Analysis review. Renewable and Sustainable Energy Reviews. 2018;82:2570-85.

[9] Huš M, Kopač D, Štefančič NS, Jurković DL, Dasireddy VD, Likozar B. Unravelling the mechanisms of CO_2 hydrogenation to methanol on Cu-based catalysts using first-principles multiscale modelling and experiments. Catalysis Science & Technology. 2017;7:5900-13.

[10] Leonzio G. State of art and perspectives about the production of methanol, dimethyl ether and syngas by carbon dioxide hydrogenation. Journal of CO_2 Utilization. 2018;27:326-54.

[11] Mukherjee D, Park S-E, Reddy BM. CO_2 as a soft oxidant for oxidative dehydrogenation reaction: An eco benign process for industry. Journal of CO_2 Utilization. 2016;16:301-12.

[12] Chakrabarti D, de Klerk A, Prasad V, Gnanamani MK, Shafer WD, Jacobs G, et al. Conversion of CO_2 over a co-based Fischer–Tropsch catalyst. Industrial & Engineering Chemistry Research. 2015;54:1189-96.

[13] Weatherbee GD, Bartholomew CH. Hydrogenation of CO_2 on group VIII metals: IV. Specific activities and selectivities of silica-supported Co, Fe, and Ru. Journal of Catalysis. 1984;87:352-62.

[14] Fisher IA, Bell AT. A comparative study of CO and CO_2 Hydrogenation over Rh/SiO_2. Journal of catalysis. 1996;162:54-65.

[15] Dębek R, Azzolina-Jury F, Travert A, Maugé F. A review on plasma-catalytic methanation of carbon dioxide–Looking for an efficient catalyst. Renewable and Sustainable Energy Reviews. 2019;116:109427.

[16] Nizio M, Benrabbah R, Krzak M, Debek R, Motak M, Cavadias S, et al. Low temperature hybrid plasma-catalytic methanation over Ni-Ce-Zr hydrotalcite-derived catalysts. Catalysis Communications. 2016;83:14-7.

[17] Chen H, Mu Y, Shao Y, Chansai S, Xu S, Stere CE, et al. Coupling non-thermal plasma with Ni catalysts supported on BETA zeolite for catalytic CO_2 methanation. Catalysis Science & Technology. 2019;9:4135-45.

[18] Zeng Y, Tu X. Plasma-catalytic CO_2 hydrogenation at low temperatures. IEEE Transactions on Plasma Science. 2015;44:405-11.

[19]https://www.epa.gov/ghgemissions/global-greenhouse-gas-emissions-data#Reference%201.

[20] https://www.joboneforhumanity.org/global_warming.

[21] Wang W, Wang S, Ma X, Gong J. Recent advances in catalytic hydrogenation of carbon dioxide. Chemical Society Reviews. 2011;40:3703-27.

[22] Olivier JG, Peters JA, Janssens-Maenhout G. Trends in global CO_2 emissions 2012 report. 2012.

[23] Boden TA, G. Marland, and R.J. Andres. Global, Regional, and National Fossil-Fuel CO_2

Emissions.Carbon Dioxide Information Analysis Center, Oak Ridge National Laboratory, U.S. Department of Energy, Oak Ridge, Tenn., U.S.A. doi 10.3334/CDIAC/00001_V2017. 2017.

[24] Song C. CO_2 conversion and utilization: an overview. ACS Publications; 2002.

[25] Aresta M, Dibenedetto A, Angelini A. The changing paradigm in CO_2 utilization. Journal of CO_2 Utilization. 2013;3:65-73.

[26] Beckman EJ. Supercritical and near-critical CO_2 in green chemical synthesis and processing. The Journal of Supercritical Fluids. 2004;28:121-91.

[27] Safi R, Agarwal RK, Banerjee S. Numerical simulation and optimization of CO_2 utilization for enhanced oil recovery from depleted reservoirs. Chemical Engineering Science. 2016;144:30-8.

[28] Luu MT, Milani D, Abbas A. Analysis of CO_2 utilization for methanol synthesis integrated with enhanced gas recovery. Journal of Cleaner Production. 2016;112:3540-54.

[29] Zhang F-Z, Xu R-N, Jiang P-X. Thermodynamic analysis of enhanced geothermal systems using impure CO_2 as the geofluid. Applied Thermal Engineering. 2016;99:1277-85.

[30] Rafiee A, Khalilpour KR, Milani D, Panahi M. Trends in CO_2 conversion and utilization: A review from process systems perspective. Journal of environmental chemical engineering. 2018;6:5771-94.

[31] Jacquemin M, Beuls A, Ruiz P. Catalytic production of methane from CO_2 and H_2 at low temperature: Insight on the reaction mechanism. Catalysis Today. 2010;157:462-6.

[32] Henry CR. Surface studies of supported model catalysts. Surface science reports. 1998;31:231-325.

[33] Xiaoding X, Moulijn J. Mitigation of CO_2 by chemical conversion: plausible chemical reactions and promising products. Energy & Fuels. 1996;10:305-25.

[34] Lin Q, Liu XY, Jiang Y, Wang Y, Huang Y, Zhang T. Crystal phase effects on the structure and performance of ruthenium nanoparticles for CO_2 hydrogenation. Catalysis Science & Technology. 2014;4:2058-63.

[35] Gao J, Wang Y, Ping Y, Hu D, Xu G, Gu F, et al. A thermodynamic analysis of methanation reactions of carbon oxides for the production of synthetic natural gas. RSC advances. 2012;2:2358-68.

[36] Swapnesh A, Srivastava VC, Mall ID. Comparative study on thermodynamic analysis of CO_2 utilization reactions. Chemical Engineering & Technology. 2014;37:1765-77.

[37] Sahebdelfar S, Ravanchi MT. Carbon dioxide utilization for methane production: a thermodynamic analysis. Journal of Petroleum Science and Engineering. 2015;134:14-22.

[38] Du G, Lim S, Yang Y, Wang C, Pfefferle L, Haller GL. Methanation of carbon dioxide on Ni-incorporated MCM-41 catalysts: The influence of catalyst pretreatment and study of steady-state reaction. Journal of catalysis. 2007;249:370-9.

[39] Beuls A, Swalus C, Jacquemin M, Heyen G, Karelovic A, Ruiz P. Methanation of CO_2: Further insight into the mechanism over $Rh/\gamma\text{-}Al_2O_3$ catalyst. Applied Catalysis B: Environmental. 2012;113:2-10.

[40] Müller K, Fleige M, Rachow F, Schmeißer D. Sabatier based CO_2-methanation of flue gas emitted by conventional power plants. Energy Procedia. 2013;40:240-8.

[41] Lunde PJ, Kester FL. Carbon dioxide methanation on a ruthenium catalyst. Industrial & Engineering Chemistry Process Design and Development. 1974;13:27-33.

[42] Du G, Lim S, Yang Y, Wang C, Pfefferle L, Haller GL. Methanation of carbon dioxide on Ni-incorporated MCM-41 catalysts: The influence of catalyst pretreatment and study of steady-state reaction. Journal of catalysis. 2007;249:370-9.

[43] Park J-N, McFarland EW. A highly dispersed $Pd–Mg/SiO_2$ catalyst active for methanation of CO_2. Journal of Catalysis. 2009;266:92-7.

[44] Abe T, Tanizawa M, Watanabe K, Taguchi A. CO_2 methanation property of Ru nanoparticle-loaded TiO_2 prepared by a polygonal barrel-sputtering method. Energy & Environmental Science. 2009;2:315-21.

[45] Kowalczyk Z, Stołecki K, Rarog-Pilecka W, Miśkiewicz E, Wilczkowska E, Karpiński Z. Supported ruthenium catalysts for selective methanation of carbon oxides at very low CO_x/H_2 ratios. Applied Catalysis A: General. 2008;342:35-9.

[46] Agnelli M, Kolb M, Mirodatos C. CO hydrogenation on a nickel catalyst.: 1. kinetics and modeling of a low-temperature sintering process. Journal of Catalysis. 1994;148:9-21.

[47] Graça I, González L, Bacariza M, Fernandes A, Henriques C, Lopes J, et al. 105.CO_2 hydrogenation into CH_4 on NiHNaUSY zeolites. Applied Catalysis B: Environmental.

2014;147:101-10.

[48] Rahmani S, Rezaei M, Meshkani F. Preparation of highly active nickel catalysts supported on mesoporous nanocrystalline γ-Al_2O_3 for CO_2 methanation. Journal of Industrial and Engineering Chemistry. 2014;20:1346-52.

[49] Chihaia V, Sohlberg K, Gabrovska M, Edreva-Kardjieva R, Crişan D, Tzvetkov P, et al. Ni–Al layered double hydroxides as catalyst precursors for CO_2 removal by methanation. Reaction Kinetics, Mechanisms and Catalysis. 2012;105:79-99.

[50] Liu J, Li C, Wang F, He S, Chen H, Zhao Y, et al. Enhanced low-temperature activity of CO_2 methanation over highly-dispersed Ni/TiO_2 catalyst. Catalysis Science & Technology. 2013;3:2627-33.

[51] Chang F-W, Kuo M-S, Tsay M-T, Hsieh M-C. Hydrogenation of CO_2 over nickel catalysts on rice husk ash-alumina prepared by incipient wetness impregnation. Applied Catalysis A: General. 2003;247:309-20.

[52] Chang F-W, Hsiao T-J, Chung S-W, Lo J-J. Nickel supported on rice husk ash—activity and selectivity in CO_2 methanation. Applied Catalysis A: General. 1997;164:225-36.

[53] Chang F-W, Tsay M-T, Liang S-P. Hydrogenation of CO_2 over nickel catalysts supported on rice husk ash prepared by ion exchange. Applied Catalysis A: General. 2001;209:217-27.

[54] Chang F-W, Tsay M-T, Kuo M-S. Effect of thermal treatments on catalyst reducibility and activity in nickel supported on RHA–Al_2O_3 systems. Thermochimica acta. 2002;386:161-72.

[55] Borgschulte A, Gallandat N, Probst B, Suter R, Callini E, Ferri D, et al. Sorption enhanced CO_2 methanation. Physical Chemistry Chemical Physics. 2013;15:9620-5.

[56] Liu J, Li C, Wang F, He S, Chen H, Zhao Y, et al. Enhanced low-temperature activity of CO_2 methanation over highly-dispersed Ni/TiO_2 catalyst. Catalysis Science & Technology. 2013;3:2627-33.

[57] Tada S, Shimizu T, Kameyama H, Haneda T, Kikuchi R. Ni/CeO_2 catalysts with high CO_2 methanation activity and high CH_4 selectivity at low temperatures. International Journal of Hydrogen Energy. 2012;37:5527-31.

[58] Aldana PU, Ocampo F, Kobl K, Louis B, Thibault-Starzyk F, Daturi M, et al. Catalytic CO_2 valorization into CH_4 on Ni-based ceria-zirconia. Reaction mechanism by operando IR

spectroscopy. Catalysis Today. 2013;215:201-7.

[59] Ocampo F, Louis B, Kiwi-Minsker L, Roger A-C. Effect of Ce/Zr composition and noble metal promotion on nickel based $Ce_xZr_{1-x}O_2$ catalysts for carbon dioxide methanation. Applied Catalysis A: General. 2011;392:36-44.

[60] Ocampo F, Louis B, Roger A-C. Methanation of carbon dioxide over nickel-based $Ce_{0.72}Zr_{0.28}O_2$ mixed oxide catalysts prepared by sol–gel method. Applied Catalysis A: General. 2009;369:90-6.

[61] Razzaq R, Zhu H, Jiang L, Muhammad U, Li C, Zhang S. Catalytic methanation of CO and CO_2 in coke oven gas over Ni–Co/ZrO_2–CeO_2. Industrial & Engineering Chemistry Research. 2013;52:2247-56.

[62] Zhi G, Guo X, Wang Y, Jin G, Guo X. Effect of La_2O_3 modification on the catalytic performance of Ni/SiC for methanation of carbon dioxide. Catalysis Communications. 2011;16:56-9.

[63] Guo M, Lu G. The effect of impregnation strategy on structural characters and CO_2 methanation properties over MgO modified Ni/SiO_2 catalysts. Catalysis Communications. 2014;54:55-60.

[64] Guo M, Lu G. The difference of roles of alkaline-earth metal oxides on silica-supported nickel catalysts for CO_2 methanation. RSC Advances. 2014;4:58171-7.

[65] Zhu H, Razzaq R, Li C, Muhmmad Y, Zhang S. Catalytic Methanation of Carbon Dioxide by Active Oxygen Material $Ce_xZr_{1-x}O_2$ Supported Ni Co Bimetallic Nanocatalysts. AIChE Journal. 2013;59:2567-76.

[66] Hwang S, Hong UG, Lee J, Baik JH, Koh DJ, Lim H, et al. Methanation of carbon dioxide over mesoporous nickel–M–alumina (M= Fe, Zr, Ni, Y, and Mg) xerogel catalysts: Effect of second metal. Catalysis letters. 2012;142:860-8.

[67] Lu B, Kawamoto K. Preparation of the highly loaded and well-dispersed NiO/SBA-15 for methanation of producer gas. Fuel. 2013;103:699-704.

[68] Zhang X, Sun W-j, Wei C. Effect of glow discharge plasma treatment on the performance of Ni/SiO2 catalyst in CO_2 methanation. Journal of Fuel Chemistry and Technology. 2013;41:96-101.

[69] Cai W, Zhong Q, Zhao Y. Fractional-hydrolysis-driven formation of non-uniform dopant concentration catalyst nanoparticles of $Ni/Ce_xZr_{1-x}O_2$ and its catalysis in methanation of CO_2. Catalysis Communications. 2013;39:30-4.

[70] Liu H, Zou X, Wang X, Lu X, Ding W. Effect of CeO_2 addition on Ni/Al_2O_3 catalysts for methanation of carbon dioxide with hydrogen. Journal of Natural Gas Chemistry. 2012;21:703-7.

[71] Cai M, Wen J, Chu W, Cheng X, Li Z. Methanation of carbon dioxide on Ni/ZrO_2-Al_2O_3 catalysts: Effects of ZrO_2 promoter and preparation method of novel ZrO_2-$Al2O_3$ carrier. Journal of natural gas chemistry. 2011;20:318-24.

[72] Jwa E, Lee S, Lee H, Mok Y. Plasma-assisted catalytic methanation of CO and CO_2 over Ni–zeolite catalysts. Fuel processing technology. 2013;108:89-93.

[73] He S, Li C, Chen H, Su D, Zhang B, Cao X, et al. A surface defect-promoted Ni nanocatalyst with simultaneously enhanced activity and stability. Chemistry of Materials. 2013;25:1040-6.

[74] Rahmani S, Rezaei M, Meshkani F. Preparation of highly active nickel catalysts supported on mesoporous nanocrystalline γ-Al_2O_3 for CO_2 methanation. Journal of Industrial and Engineering Chemistry. 2014;20:1346-52.

[75] Graça I, González L, Bacariza M, Fernandes A, Henriques C, Lopes J, et al. CO_2 hydrogenation into CH_4 on NiHNaUSY zeolites. Applied Catalysis B: Environmental. 2014;147:101-10.

[76] Beuls A, Swalus C, Jacquemin M, Heyen G, Karelovic A, Ruiz P. Methanation of CO_2: Further insight into the mechanism over Rh/γ-Al_2O_3 catalyst. Applied Catalysis B: Environmental. 2012;113:2-10.

[77] Karelovic A, Ruiz P. CO_2 hydrogenation at low temperature over Rh/γ-Al_2O_3 catalysts: Effect of the metal particle size on catalytic performances and reaction mechanism. Applied Catalysis B: Environmental. 2012;113:237-49.

[78] Lapidus A, Gaidai N, Nekrasov N, Tishkova L, Agafonov YA, Myshenkova T. The mechanism of carbon dioxide hydrogenation on copper and nickel catalysts. Petroleum Chemistry. 2007;47:75-82.

[79] Sehested J, Dahl S, Jacobsen J, Rostrup-Nielsen JR. Methanation of CO over nickel: mechanism and kinetics at high H_2/CO ratios. The Journal of Physical Chemistry B. 2005;109:2432-8.

[80] Fechete I, Vedrine JC. Nanoporous materials as new engineered catalysts for the synthesis of green fuels. Molecules. 2015;20:5638-66.

[81] Marwood M, Doepper R, Renken A. In-situ surface and gas phase analysis for kinetic studies under transient conditions. The catalytic hydrogenation of CO . Applied Catalysis A: General. 1997;151:223-46.

[82] Peebles D, Goodman D, White J. Methanation of carbon dioxide on nickel (100) and the effects of surface modifiers. The Journal of Physical Chemistry. 1983;87:4378-87.

[83] Choe S-J, Kang H-J, Kim S-J, Park S-B, Park D-H, Huh D-S. Adsorbed carbon formation and carbon hydrogenation for CO_2 methanation on the Ni (111) surface: ASED-MO study. Bulletin of the Korean Chemical Society. 2005;26:1682-8.

[84] Mikhail M, Da Costa P, Amouroux J, Cavadias S, Tatoulian M, Ognier S, et al. Electrocatalytic behaviour of CeZrOx-supported Ni catalysts in plasma assisted CO_2 methanation. Catalysis Science & Technology. 2020.

[85] Morozov AI. Introduction to plasma dynamics: CRC Press; 2012.

[86] Fridman A. Plasma chemistry: Cambridge university press; 2008.

[87] Tendero C, Tixier C, Tristant P, Desmaison J, Leprince P. Atmospheric pressure plasmas: A review. Spectrochimica Acta Part B: Atomic Spectroscopy. 2006;61:2-30.

[88] Odeyemi OO. Generation of Hydrogen-Rich Gas Using Non Equilibrium Plasma Discharges: Drexel University; 2012.

[89] Whitehead JC. Plasma–catalysis: the known knowns, the known unknowns and the unknown unknowns. Journal of Physics D: Applied Physics. 2016;49:243001.

[90] Gallon HJ, Whitehead C. Dry reforming of methane using non-thermal plasma-catalysis: University of Manchester; 2011.

[91] Fridman A, Kennedy LA. Plasma physics and engineering: CRC press; 2004.

[92] Bogaerts A, Kozák T, Van Laer K, Snoeckx R. Plasma-based conversion of CO_2: current status and future challenges. Faraday discussions. 2015;183:217-32.

[93] El-Aragi G. Gliding arc discharge (GAD) experiment. Plasma Physics and Nuclear Fusion Dept, Nuclear Research Center, AEA, PO. 2009;13759.

[94] Zhang J-Q, Yang Y-J, Zhang J-S, Liu Q. Study on the Conversion of CH_4 and CO_2 Using a Pulsed Microwave Plasma under Atmospheric Pressure. ACTA CHIMICA SINICA-CHINESE EDITION-. 2002;60:1973-80.

[95] Paulussen S, Verheyde B, Tu X, De Bie C, Martens T, Petrovic D, et al. Conversion of carbon dioxide to value-added chemicals in atmospheric pressure dielectric barrier discharges. Plasma Sources Science and Technology. 2010;19:034015.

[96] Snoeckx R, Bogaerts A. Plasma technology–a novel solution for CO_2 conversion? Chemical Society Reviews. 2017;46:5805-63.

[97] Nunnally T, Gutsol K, Rabinovich A, Fridman A, Gutsol A, Kemoun A. Dissociation of CO_2 in a low current gliding arc plasmatron. Journal of Physics D: Applied Physics. 2011;44:274009.

[98] Indarto A, Yang DR, Choi J-W, Lee H, Song HK. Gliding arc plasma processing of CO_2 conversion. Journal of hazardous materials. 2007;146:309-15.

[99] Indarto A, Choi J-W, Lee H, Song HK. Conversion of CO_2 by gliding arc plasma. Environmental engineering science. 2006;23:1033-43.

[100] Wang W, Mei D, Tu X, Bogaerts A. Gliding arc plasma for CO_2 conversion: better insights by a combined experimental and modelling approach. Chemical Engineering Journal. 2017;330:11-25.

[101] Liu J-B, Li X-S, Liu J-L, Zhu A-M. Insight into gliding arc (GA) plasma reduction of CO_2 with H_2: GA characteristics and reaction mechanism. Journal of Physics D: Applied Physics. 2019;52:284001.

[102] Rusanov V, Fridman A, Sholin G. The physics of a chemically active plasma with nonequilibrium vibrational excitation of molecules. Soviet Physics Uspekhi. 1981;24:447.

[103] Heijkers S, Snoeckx R, Kozák Ts, Silva T, Godfroid T, Britun N, et al. CO_2 conversion in a microwave plasma reactor in the presence of N2: elucidating the role of vibrational levels. The Journal of Physical Chemistry C. 2015;119:12815-28.

[104] Chen G, Britun N, Godfroid T, Georgieva V, Snyders R, Delplancke-Ogletree M-P. An

overview of CO_2 conversion in a microwave discharge: the role of plasma-catalysis. Journal of Physics D: Applied Physics. 2017;50:084001.

[105] Silva T, Britun N, Godfroid T, Snyders R. Optical characterization of a microwave pulsed discharge used for dissociation of CO_2. Plasma Sources Science and Technology. 2014;23:025009.

[106] Fidalgo B, Domínguez A, Pis J, Menéndez J. Microwave-assisted dry reforming of methane. International Journal of Hydrogen Energy. 2008;33:4337-44.

[107] Ihara T, Ouro T, Ochiai T, Kiboku M, Iriyama Y. Formation of methanol by microwave-plasma reduction of CO_2 with H_2O. Bulletin of the Chemical Society of Japan. 1996;69:241-4.

[108] Snoeckx R, Heijkers S, Van Wesenbeeck K, Lenaerts S, Bogaerts A. CO_2 conversion in a dielectric barrier discharge plasma: N_2 in the mix as a helping hand or problematic impurity? Energy & Environmental Science. 2016;9:999-1011.

[109] Eliasson B, Kogelschatz U, Xue B, Zhou L-M. Hydrogenation of carbon dioxide to methanol with a discharge-activated catalyst. Industrial & engineering chemistry research. 1998;37:3350-7.

[110] Yu Q, Kong M, Liu T, Fei J, Zheng X. Characteristics of the decomposition of CO_2 in a dielectric packed-bed plasma reactor. Plasma Chemistry and Plasma Processing. 2012;32:153-63.

[111] Goujard V, Tatibouët J-M, Batiot-Dupeyrat C. Use of a non-thermal plasma for the production of synthesis gas from biogas. Applied Catalysis A: General. 2009;353:228-35.

[112] Mahammadunnisa S, Reddy EL, Ray D, Subrahmanyam C, Whitehead JC. CO_2 reduction to syngas and carbon nanofibres by plasma-assisted in situ decomposition of water. International Journal of Greenhouse Gas Control. 2013;16:361-3.

[113] Guo L, Ma X, Xia Y, Xiang X, Wu X. A novel method of production of ethanol by carbon dioxide with steam. Fuel. 2015;158:843-7.

[114] Chung W-C, Chang M-B. Dry reforming of methane by combined spark discharge with a ferroelectric. Energy Conversion and Management. 2016;124:305-14.

[115] Shapoval V, Marotta E. Investigation on Plasma-Driven Methane Dry Reforming in a Self-Triggered Spark Reactor. Plasma Processes and Polymers. 2015;12:808-16.

[116] Zhu B, Li X-S, Liu J-L, Zhu X, Zhu A-M. Kinetics study on carbon dioxide reforming of methane in kilohertz spark-discharge plasma. Chemical Engineering Journal. 2015;264:445-52.

[117] Li XS, Zhu B, Shi C, Xu Y, Zhu AM. Carbon dioxide reforming of methane in kilohertz spark-discharge plasma at atmospheric pressure. AIChE journal. 2011;57:2854-60.

[118] Kado S, Urasaki K, Sekine Y, Fujimoto K. Direct conversion of methane to acetylene or syngas at room temperature using non-equilibrium pulsed discharge☆. Fuel. 2003;82:1377-85.

[119] Zhu X, Li K, Liu J-L, Li X-S, Zhu A-M. Effect of CO_2/CH_4 ratio on biogas reforming with added O_2 through an unique spark-shade plasma. international journal of hydrogen energy. 2014;39:13902-8.

[120] Li D, Li X, Bai M, Tao X, Shang S, Dai X, et al. CO_2 reforming of CH_4 by atmospheric pressure glow discharge plasma: a high conversion ability. International Journal of Hydrogen Energy. 2009;34:308-13.

[121] Kogelschatz U, Eliasson B, Egli W. Plasma Chem. Plasma Process. 2003.

[122] Massines F, Gouda G. A comparison of polypropylene-surface treatment by filamentary, homogeneous and glow discharges in helium at atmospheric pressure. Journal of Physics D: Applied Physics. 1998;31:3411.

[123] Bogaerts A, Neyts E, Gijbels R, Van der Mullen J. Gas discharge plasmas and their applications. Spectrochimica Acta Part B: Atomic Spectroscopy. 2002;57:609-58.

[124] Fridman A, Chirokov A, Gutsol A. Non-thermal atmospheric pressure discharges. Journal of Physics D: Applied Physics. 2005;38:R1.

[125] Brandenburg R. Dielectric barrier discharges: progress on plasma sources and on the understanding of regimes and single filaments. Plasma Sources Science and Technology. 2017;26:053001.

[126] Bogaerts A, Wang W, Berthelot A, Guerra V. Modeling plasma-based CO_2 conversion: crucial role of the dissociation cross section. Plasma Sources Science and Technology. 2016;25:055016.

[127] Aerts R, Somers W, Bogaerts A. Carbon dioxide splitting in a dielectric barrier discharge plasma: a combined experimental and computational study. ChemSusChem. 2015;8:702-16.

[128] Nizio M, Albarazi A, Cavadias S, Amouroux J, Galvez ME, Da Costa P. Hybrid plasma-

catalytic methanation of CO_2 at low temperature over ceria zirconia supported Ni catalysts. International Journal of Hydrogen Energy. 2016;41:11584-92.

[129] Trinh HQ, Mok YS. Plasma-catalytic oxidation of acetone in annular porous monolithic ceramic-supported catalysts. Chemical Engineering Journal. 2014;251:199-206.

[130] Harling AM, Glover DJ, Whitehead JC, Zhang K. The role of ozone in the plasma-catalytic destruction of environmental pollutants. Applied Catalysis B: Environmental. 2009;90:157-61.

[131] Tu X, Whitehead J. Plasma-catalytic dry reforming of methane in an atmospheric dielectric barrier discharge: Understanding the synergistic effect at low temperature. Applied Catalysis B: Environmental. 2012;125:439-48.

[132] Schmidt-Szałowski K, Górska A, Młotek M. Plasma-catalytic conversion of methane by DBD and gliding discharges. Journal of Advanced Oxidation Technologies. 2006;9:215-9.

[133] Azzolina-Jury F, Thibault-Starzyk F. Mechanism of low pressure plasma-assisted CO_2 hydrogenation over Ni-USY by microsecond time-resolved FTIR spectroscopy. Topics in Catalysis. 2017;60:1709-21.

[134] Bacariza M, Biset-Peiró M, Graça I, Guilera J, Morante J, Lopes J, et al. DBD plasma-assisted CO_2 methanation using zeolite-based catalysts: Structure composition-reactivity approach and effect of Ce as promoter. Journal of CO_2 Utilization. 2018;26:202-11.

[135] Wierzbicki D, Moreno MV, Ognier S, Motak M, Grzybek T, Da Costa P, et al. Ni-Fe layered double hydroxide derived catalysts for non-plasma and DBD plasma-assisted CO_2 methanation. International Journal of Hydrogen Energy. 2019.

[136] Mikhail M, Wang B, Jalain R, Cavadias S, Tatoulian M, Ognier S, et al. Plasma-catalytic hybrid process for CO_2 methanation: optimization of operation parameters. Reaction Kinetics, Mechanisms and Catalysis. 2019;126:629-43.

[137] Hołub M. On the measurement of plasma power in atmospheric pressure DBD plasma reactors. International Journal of Applied Electromagnetics and Mechanics. 2012;39:81-7.

[138] Whitehead JC. Plasma catalysis: A solution for environmental problems. Pure and Applied Chemistry. 2010;82:1329-36.

[139] Mei D, Zhu X, Wu C, Ashford B, Williams PT, Tu X. Plasma-photocatalytic conversion

of CO_2 at low temperatures: Understanding the synergistic effect of plasma-catalysis. Applied Catalysis B: Environmental. 2016;182:525-32.

[140] Mei D, Ashford B, He YL, Tu X. Plasma-catalytic reforming of biogas over supported Ni catalysts in a dielectric barrier discharge reactor: Effect of catalyst supports. Plasma Processes and Polymers. 2017;14:1600076.

[141] Amouroux J, Cavadias S. Electrocatalytic reduction of carbon dioxide under plasma DBD process. Journal of Physics D: Applied Physics. 2017;50:465501.

[142] Whitehead JC. Plasma–catalysis: the known knowns, the known unknowns and the unknown unknowns. Journal of Physics D: Applied Physics. 2016;49:243001.

[143] Maria Mikhail PDC, Jacques Amouroux，Siméon Cavadias, Michael Tatoulian, Stéphanie Ognier， María Elena Gálvez. Electrocatalytic behaviour of CeZrOx-supported Ni catalysts in plasma assisted CO_2 methanation. Catalysis Science and Technology. 2020;https://doi.org/10.1039/D0CY00312C.

[144] Sun C, Świrk K, Wierzbicki D, Motak M, Grzybek T, Da Costa P. On the effect of yttrium promotion on Ni-layered double hydroxides-derived catalysts for hydrogenation of CO_2 to methane. International Journal of Hydrogen Energy. 2020.

[145] Pan Q, Peng J, Sun T, Wang S, Wang S. Insight into the reaction route of CO_2 methanation: Promotion effect of medium basic sites. Catalysis Communications. 2014;45:74-8.

[146] Benrabbah R, Cavaniol C, Liu H, Ognier S, Cavadias S, Gálvez ME, et al. Plasma DBD activated ceria-zirconia-promoted Ni-catalysts for plasma catalytic CO_2 hydrogenation at low temperature. Catalysis Communications. 2017;89:73-6.

[147] Wierzbicki D, Motak M, Grzybek T, Gálvez ME, Da Costa P. The influence of lanthanum incorporation method on the performance of nickel-containing hydrotalcite-derived catalysts in CO_2 methanation reaction. Catalysis Today. 2018;307:205-11.

[148] Rostrup-Nielsen J, Pedersen K, Sehested J. High temperature methanation: Sintering and structure sensitivity. Applied Catalysis A: General. 2007;330:134-8.

[149] Kesavan JK, Luisetto I, Tuti S, Meneghini C, Iucci G, Battocchio C, et al. Nickel supported on YSZ: The effect of Ni particle size on the catalytic activity for CO_2 methanation. Journal of CO_2 Utilization. 2018;23:200-11.

[150] https://www.engineeringtoolbox.com/relative-permittivity-d_1660.html.

RÉSUMÉ

Ce travail se focalise sur l'étude de la mise en oeuvre de la reaction de Sabatier dans un procédé catalytique plasma à décharge de barrière diélectrique (DBD) en présence d'un catalyseur hétérogène Ni/ $Ce_{0.58}Zr_{0.42}O_2$. Il a été montré que dans un réacteur hybride plasma DBD la température pour atteindre un rendement élevée en CO_2 est d'environ 220 °C, soit environ 130 °C de moins que celle en condition thermique. La température seuil de la réaction de Sabatier pendant le traitement au plasma a été déterminée aux environs de 116 °C sur la base des données expérimentales et de l'analyse de simulation par le logiciel COMSOL Multiphysics®. Ensuite, les rôles respectifs de la température et de la puissance plasma dans le processus catalytique plasma ont été étudié. Et la réaction a été effectuée dans un réacteur adiabatique à plasma pour démontrer que la consommation d'énergie du plasma pouvait être diminuée avec la réutilisation de la chaleur dégagée par la réaction. De plus, l'influence de paramètres tels que la taille des particules, le GHSV et la pression a été étudiée respectivement dans les processus thermiques et plasma. Un catalyseur avec une plus grande taille de particules s'est avéré avoir une conversion de CO_2 plus élevée dans les deux processus, peut être en raison d'une plus petite taille de particules métalliques Ni. L'influence du GHSV sur la conversion du CO_2 est similaire dans les deux processus. Concernant l'effet de la pression enfin, avec l'augmentation de la pression à l'intérieur du réacteur, il y a une légère augmentation de la conversion du CO_2 pour les deux processus étudiés et dans le cas du processus plasma la consommation d'énergie diminue lorsque la pression augmente.Enfin, une étude prospective de la méthanation du CO_2 est réalisée en milli-réacteur.

MOTS CLÉS

Méthanation du CO_2; Plasma-catalyse ; COMSOL ; Température; Puissance

ABSTRACT

This work focuses on the use of a heterogeneous catalyst Ni/$Ce_{0.58}Zr_{0.42}O_2$ in order to study the Sabatier reaction using a dielectric barrier discharges (DBD) plasma catalytic process. In plasma process, the temperature to achieved high CO_2 conversion and CH_4 selectivity was around 220°C, which was around 130°C lower than that in thermal condition. And the threshold temperature of the Sabatier reaction during plasma processing is assumed to be 116°C based on the experimental data and simulation analysis by COMSOL Multiphysics® software. Besides, the respective roles of temperature and plasma power in the plasma-catalytic process were investigated, and the reaction was perform in plasma adiabatic reactor to demonstrate that the plasma power consumption could be decreased with the reuse of the heat released from the reaction. Moreover, the influence of parameters, such as particle size, GHSV, and pressure was investigated in thermal and plasma process respectively. Catalyst with bigger particle size was found to have higher CO_2 conversion in both processes, maybe due to a smaller metallic Ni particle size. GHSV had a similar influence on CO_2 conversion in both process, and the temperature in plasma process increase with inlet flowrate. Concerning the effect of pressure, with the increase of pressure inside of the reactor, there is a slight increase of CO_2 conversion and the power consumption decreased in plasma process. Finally, prospective study of CO_2 methanation is milli-reactor was performed.

KEYWORDS

CO_2 methanation; Plasma-catalysis; COMSOL; Temperature; Power